9-2011

Role of Strongly Interacting Additives in Tuning the Structure and Properties of Polymer Systems

Vikram Kumar Daga
University of Massachusetts Amherst, vkdaga@gmail.com

ROLE OF STRONGLY INTERACTING ADDITIVES IN TUNING THE STRUCTURE AND PROPERTIES OF POLYMER SYSTEMS

A Dissertation Presented

by

VIKRAM KUMAR DAGA

Submitted to the Graduate School of the
University of Massachusetts Amherst in partial fulfillment
of the requirements for the degree of

DOCTOR OF PHILOSOPHY

September 2011

Department of Chemical Engineering

ROLE OF STRONGLY INTERACTING ADDITIVES IN TUNING THE STRUCTURE AND PROPERTIES OF POLYMER SYSTEMS

A Dissertation Presented

by

VIKRAM KUMAR DAGA

Approved as to style and content by:

_____
James J. Watkins, Chair

_____
Surita R. Bhatia, Member

_____
David M. Ford, Member

_____
Samuel P. Gido, Member

_____
T. J. Mountziaris, Department Head
Department of Chemical Engineering

ACKNOWLEDGMENTS

Graduate studies at UMass Amherst has positively affected me in a variety of ways. Being a part of the community, I have learnt many things but the most important gain is to have initiated the development of the ability to figure out merits or demerits of a particular proposed technical solution to a problem. I got a chance to work on multiple systems which enabled a broader understanding of applications involving polymeric sytems. Through this process, there have been many people who have been responsible in enhancing not only my scientific knowledge but also communication and organizational skills.

I thank my advisor, Prof. Jim Watkins for his constant support, keen interest and insightful feedback throughout my research work. His ability to foster creativity is commendable and it has been a source of immense motivation for me. My achievements are a direct result of his effectiveness as a leader. In addition, I learnt a lot by observing him passively.

I thank my dissertation committee members, Prof. Surita Bhatia, Prof. David Ford, and Prof. Sam Gido for their time and effort in providing useful insights that has helped me gain a better understanding and new perspectives on my research work.

Through this work, I collaborated with many people and some of the understanding delivered in this work was made possible due to these collaborations. I thank, Vijay Tirumala and Huagen Peng, former and current postdoctoral fellows at NIST for the many lengthy and insightful discussions. I also wish to thank them for hosting me at NIST on several occasions for conducting experiments together. I thank Evan Schwartz, a former graduate student at the Cornell University for the frank and fruitful discussions during his efforts on the synthesis of various molecular glass additives for the work on photo-induced ordering of block copolymers. I would also like to thank Ying Lin, a postdoctoral fellow at UMass Amherst for her efforts on the synthesis of the block copolymer employed for SANS studies as well as molecular glass additives employed for photoresists development. I would also like to thank Hua-Gen Peng, Wen-Li Wu and Chris Soles at NIST for their inputs on the fitting and

interpretation of the SANS results shown in Chapter 2 which has enabled a better understanding of the materials I worked with.

I wish to thank the collaborators for their time and effort through the work on additive-loaded EUV photoresists. I appreciate the useful insights and overall help provided by Uzodinma Okoroanyanwu at GlobalFoundaries. I thank Karen Petrillo, Dominic Ashworth, Emil Piscani and the RMDC team at SEMATECH for performing the photolithographic evaluations on our photoresist formulations. I also wish to thank Huagen Peng at NIST for the help with experiments conducted that were conducted at NIST. I am thankful to the Dow Electronic Materials group for supplying the ESCAP photoresist and in particular Jim Thackeray at Dow for providing valuable suggestions. The opportunity to go to Polymers Division at NIST for conducting the related experiments was a great learning experience and I thank Christopher Soles at NIST for making these visits possible. Help in synthesis of various additives by a prior post doctoral fellow and Prof. Todd Emrick is appreciated.

I thank the NSF's Center of Hierarchical Manufacturing at UMass Amherst and the Semiconductor Research Corporation for the financial support through my graduate studies as well as for the many resources made available due to these interactions. I would also like to acknowledge the Materials Research Science and Engineering Center (MRSEC) at the UMass Amherst for providing easy access and plentiful use of the various instruments. Not being limited by the instrument availability to conduct research helped me in working efficiently. I also appreciate the help from the scientists at NCNR and NSLS at BNL during my trips to perform experiments at the SANS and SAXS beamlines.

I would also like to take this opportunity to express my gratitude to the faculty members at the Department of Chemical Engineering, especially Prof. David Ford and Prof. Dimitrios Maroudas for doing an excellent job as instructors in the courses during the first year. I also enjoyed being closely associated with the Department of Polymer Science and Engineering as it was a great learning experience for me. My interest in polymers has only intensified as a result of this interaction.

I also appreciate the great companionship of the former and the present Watkins group members, the class of 2006 in Chemical Engineering and many others graduate students in both the departments. I appreciate the help from the staff members of both the departments. Their efforts in taking care of the issues beyond research allowed me to focus better on my work. I would specially like to thank Jo-Ann Bourguignon, Lisa Groth and Erin Mandeson for accommodating my needs and, at times, going out of the way to resolve certain issues.

There is a strong support system outside work that has largely influenced my performance at work. I would like to thank my family and friends who have always supported me in my pursuits and have made adjustments to accommodate my busy schedule. I would like to express my admiration towards my wife, Malvika, who has always supported me with ample patience and care. While I spent more time at work than at home, she took care of everything else and in addition brought joy and cheer to an otherwise routine lifestyle of mine. Being together with her most of my graduate life, I got to know many people and got ample help from her research group members. Of course, I must also acknowledge that being trained at the the Department of Polymer Science and Engineering, she has been a rich source of information for me. I would also like to express my gratitude to my in-laws who offered us their company and made our time spent quite interesting, enjoyable and memorable. Particular thanks to Menka for always being helpful and enlightening us with various tit-bits about things in general. It was also great to know Vishal, a classmate and a friend, who has been a source of inspiration and has always offered his help beyond my expectations. I would also like to express my appreciation for the good suggestions and support that my brother and sister-in-law have always provided.

Finally, I express my immense gratitude towards my parents who have always been a source of motivation, support and learning for me on many different levels that words fall short to describe. Their constant conviction in my abilities has always provided comfort in challenging times.

ABSTRACT

ROLE OF STRONGLY INTERACTING ADDITIVES IN TUNING THE STRUCTURE AND PROPERTIES OF POLYMER SYSTEMS

SEPTEMBER 2011

VIKRAM KUMAR DAGA, B. TECH., INDIAN INSTITUTE OF TECHNOLOGY, ROORKEE

M. CHE., UNIVERSITY OF DELAWARE

Ph.D., UNIVERSITY OF MASSACHUSETTS AMHERST

Directed by: Professor James J. Watkins

Block copolymer (BCP) nanocomposites are an important class of hybrid materials in which the BCP guides the spatial location and the periodic assembly of the additives. High loadings of well-dispersed nanofillers are generally important for many applications including mechanical reinforcing of polymers. In particular the composites shown in this work might find use as etch masks in nanolithography, or for enabling various phase selective reactions for new materials development.

This work explores the use of hydrogen bonding interactions between various additives (such as homopolymers and non-polymeric additives) and small, disordered BCPs to cause the formation of well-ordered morphologies with small domains. A detailed study of the organization of homopolymer chains and the evolution of structure during the process of ordering is performed. The results demonstrate that by tuning the selective interaction of the additive with the incorporating phase of the BCP, composites with significantly high loadings

of additives can be formed while maintaining order in the BCP morphology. The possibility of high and selective loading of additives in one of the phases of the ordered BCP composite opens new avenues due to high degree of functionalization and the proximity of the additives within the incorporating phase. This aspect is utilized in one case for the formation of a network structure between adjoining additive cores to derive mesoporous inorganic materials with their structures templated by the BCP.

The concept of additive-driven assembly is extended to formulate BCP-additive blends with an ability to undergo photo-induced ordering. Underlying this strategy is the ability to transition a weakly interacting additive to its strongly interacting form. This strategy provides an on-demand, non-intrusive route for formation of well-ordered nanostructures in arbitrarily defined regions of an otherwise disordered material.

The second area explored in this dissertation deals with the incorporation of additives into photoresists for next generation extreme ultra violet (EUV) photolithography applications. The concept of hydrogen bonding between the additives and the polymeric photoresist was utilized to cause formation of a physical network that is expected to slow down the diffusion of photoacid leading to better photolithographic performance (25-30 nm resolution obtained).

TABLE OF CONTENTS

Page

ACKNOWLEDGMENTS iv

ABSTRACT vii

LIST OF TABLES xii

LIST OF FIGURES xiii

CHAPTER 1

1. INTRODUCTION AND OVERVIEW 1

    1.1 Introduction 1
    1.2 Dissertation Overview 4

2. PHASE BEHAVIOR OF POLY(ETHYLENE OXIDE)-POLY(PROPYLENE OXIDE)-POLY(ETHYLENE OXIDE) TRI-BLOCK COPOLYMERS WITH POLY(ACRYLIC ACID) 6

    2.1 Introduction 6
    2.2 Experimental 11

        2.2.1 Materials 11
        2.2.2 Sample preparation 12
        2.2.3 Small-angle x-ray scattering 12
        2.2.4 Sample preparation for small angle neutron scattering 13
        2.2.5 Small angle neutron scattering 14

    2.3 Results and Discussion 15

        2.3.1 Phase behavior of blends of Pluronic BCPs and PAA homopolymers 15
        2.3.2 Organization of chains and the evolution of structure during ordering 19

    2.4 Conclusions 32

3. PHASE BEHAVIOR OF BLENDS OF POLY(ETHYLENE OXIDE) CONTAINING BLOCK COPOLYMERS WITH NON-POLYMERIC ADDITIVES 33

3.1 Introduction 33

3.2.1 Materials 39
3.2.2 Sample Preparation 40
3.2.3 Small-angle x-ray scattering 41
3.2.4 Differential Scanning Calorimetry 41
3.2.5 X-Ray Diffraction (XRD) 42
3.2.6 Procedure for the preparation of mesoporous silica 42
3.2.7 Transmission electron microscopy (TEM) 42
3.2.8 Fourier transform infrared spectroscopy (FTIR) 43

3.3 Results and Discussion 43
3.4 Conclusions 77

4. HYDROGEN-BOND-ASSISTED BLOCK COPOLYMER - BLOCK COPOLYMER COMPOSITES 81

4.1 Introduction 81
4.2 Experimental 84

4.2.1 Materials 84
4.2.2 Sample preparation 84
4.2.3 Small angle x-ray scattering 85

4.3 Results and discussion 85
4.4 Conclusions 100

5. PHOTO-INDUCED ORDERING OF BLOCK COPOLYMERS 102

5.1 Introduction 102
5.2 Experimental 108

5.2.1 Materials 108
5.2.2 Synthetic procedure for MG-TBCM 109
5.2.3 Sample preparation for small angle x-ray scattering and for differential scanning calorimetry 109
5.2.4 Small angle x-ray scattering 110
5.2.5 Differential scanning calorimetry 110
5.2.6 Sample preparation for scanning force microscopy 110
5.2.7 Scanning force microscopy 111

5.3 Results and Discussion 111
5.4 Conclusions 122

Appendix 5.1. Measurement of film thickness before and after deprotection 123

6. ADDITIVE-LOADED EUV PHOTORESISTS: PERFORMANCE ENHANCEMENT AND THE UNDERLYING PHYSICS 125

6.1 Introduction 125
6.2 Experimental 138

6.2.1 Materials 138
6.2.2 Description of photoresist formulations 139
6.2.3 Description of photolithographic characterization 139

6.3 Results and discussion 139

6.3.1 Determination of functionality desired on the additive molecules 139
6.3.2 Glass transition temperatures (T_gs) of candidate resist systems 142
6.3.3 EUV photolithographic performance 144
6.3.4 Characterization of acid diffusion length by bilayer experiments 149

6.4 Conclusions 152
Appendix 6.1. Incorporation of POSS based additives in model deprotected photoresist and the possibility of a negative photoresist with high etch resistance 154
Appendix 6.2. Derivation of the formula to convert electronic density to mass density 157

6. FINAL COMMENTS AND OUTLOOK 159

BIBLIOGRAPHY 162

LIST OF TABLES

Table Page

2.1. Neutron scattering length densities of various components.....22

2.2. Fitting results for 30 % PAA blends at varying molecular weights of PAA. The thickness t is in angstroms and the SLD is in A^{-2}.....26

2.3. Fitting results for 20 % PAA blends at varying molecular weights of PAA. The thickness t is in angstroms and the SLD is in A^{-2}. The first PAA 2k column shows the fitting results upon setting the SLD of PPO layer as that of pure PPO, however, it is not correct because the average SLD comes out to be significantly lower than that expected for the 20 % PAA blends.....28

3.1. Thermal characteristics of neat F108 and its blends with POSS-OAA and POSS-OAP at varying compositions.....73

4.1. Compositions of various blends of PS-PEO (9.5-5 kg/mol), PBd-PEO (5-2.3 kg/mol) and PAA of molecular weight 20 kg/mol. The weight ratio of the two BCPs is maintained at unity for all the blends while the percentage of PAA is increased starting from no PAA up to 55 % PAA.....89

2.2. Blends of PS-PEO (9.5-5 kg/mol) and PBd-PAA (5.8-4 kg/mol). The weights added to form the blends are shown and the corresponding volume fractions for the expected PBd, PS and PEO + PAA phases are shown. 95

4.3. Blends of P105 (PEO-PPO-PEO, ~6.5 kg/mol, 50 % PEO) and PBd-PAA (5.8-4 kg/mol). The weights added to form the blends are shown and the corresponding volume fractions for the expected PBd, PPO and PEO + PAA phases are shown. 99

6.1. Increase in density upon incorporation of HHB and BHCA at different mass fractions into PHOST. The error bars of the thickness t and Q_c^2 are from the Reflfit program. [11].....142

6.2. Results of acid diffusion length measurements for the ESCAP resist blended with MG1-tBCM and MG4-tBCM at 30 % loading. Top layer of the bilayer film was made from ESCAP resist (ES) with 8.5 % NonI and 1 % TEA loading while the bottom layers contained 1 % TEA as well.....151

6.3. Density of neat PHOST and its blend with POSS-OAA obtained by reflectivity.....155

LIST OF FIGURES

Figure Page

2.1. SAXS profiles of F108 and its blends with PAA (8.5 kg/mol) at varying compositions at 80 ^{o}C. 16

2.2. SAXS profiles of P105 and its blends with PAA (20 kg/mol) at varying compositions at 80 ^{o}C. 18

2.3. Phase behavior of blends of d-TB with various loadings of PAA. 22

2.4. SANS profiles obtained from the neat BCP (d-TB) and its blends at 20 % and 30 % PAA loading with varying PAA molecular weights from 2 kg/mol up to 88 kg/mol at 80 ^{o}C. 24

2.5. Model structure for blends of the BCP, d-TB with PAA. 25

2.6. Structure evolution in blends of Pluronic BCPs upon blending PAA. The initially disordered BCP orders as PAA is added. Even after ordering, some PEO chains are mixed within the PPO phase and is extracted upon addition of more PAA. Correspondingly, the number of junction points between PEO and PPO must increase continuously to reach a maximum when the PPO phase becomes pure. 32

3.1. Schematic representation of additive driven assembly of disordered F108 induced by blending with hydrogen bond-donating non-polymeric additives. PEO in green forms the matrix containing the dispersed small molecule additive. PPO in blue forms the minority domain, either cylinders or spheres. 39

3.2. Hydrogen bond-donating additives incorporated into the PEO phase of F108: (a) benzene-1,2,3,4,5,6-hexacarboxylic acid (BHCA), (b) benzene-1,2,3,4,5,6-hexol (HHB), (c) 5,5'-carbonylbis-(trimellitic acid) (CTMA), (d) 3,5-Bis(4-aminophenoxy)benzoic acid (BABA). 44

3.3. SAXS profiles of blends of F108 and benzene-1,2,3,4,5,6-hexacarboxylic acid (BHCA) as a function of composition at 80 ^{o}C. The disordered state and cylindrical and spherical morphologies of the blends are denoted by D, C and S, respectively. 46

3.4. SAXS profiles of (a) 10 % BHCA, (b) 20 % BHCA, (c) neat F108 at varying temperatures. 49

3.5. SAXS profiles of neat F108 and its blends with benzene-1,2,3,4,5,6-hexol (HHB) at 80 ^{o}C. The disordered state and the cylindrical morphology of the blends are denoted by D, and C, respectively. 50

3.6. SAXS profiles of neat F108 and its blends with 5,5'-carbonylbis-(trimellitic acid) (CTMA) as a function of composition at 80 ^{o}C. The disordered state and cylindrical and spherical morphologies of the blends are denoted by D, C and S, respectively. 52

3.7. SAXS profiles of neat F108 and its blend with 3,5-Bis(4-aminophenoxy)benzoic acid (BABA) at 80 ^{o}C. The disordered state and spherical morphologies of the blends are denoted by D, and C respectively. 53

3.8. Full width at half maximum (FWHM) of the primary scattering peaks for blends of F108 with BHCA, HHB and CTMA. 55

3.9. Comparison of behavior of BHCA, HHB and CTMA additives: (a) variation of position of primary peak for blends, (b) scaling of interplanar spacing with composition (ϕ_p) for blends that formed cylindrical morphologies. 56

3.10. DSC thermograms of neat F108 and its blend with (a) BHCA, (b) HHB, and (c) CTMA. The constants added to the heat flow values to shift the blend thermograms vertically upwards are shown in parenthesis. 59

3.11. Analysis of endotherm peaks obtained for blends with varying BHCA, HHB and CTMA compositions: (a) melting enthalpy normalized by the PEO concentration in the blends, (b) melting temperatures corresponding to the endotherms. 60

3.12. Schematic showing disorder-to-order transitions of poly(ethylene oxide) containing block copolymers induced by blending of polyhedral oligomeric silsesquioxanes functionalized with maleamic acid or aminophenyl groups. Strong and selective hydrogen bonding interaction of the additives with the poly(ethylene oxide) block (green chains) results microphase segregation of the PPO blocks (blue chains) to form well ordered BCP composites in which the additives are sequestered into the PEO (green) phase. 63

3.13. Structure of POSS octa maleamic acid (POSS-OAA, M_w= 1592 g/mol). 65

3.14. SAXS profiles of neat F108 and its blends with POSS-OAA at 80 ^{o}C. 67

3.15. SAXS profiles of composites containing 50% loading of POSS-OAA for various Pluronic BCPs at 80 ^{o}C: (a) F68, (b) F88, (c) F108 and (d) P105. 70

3.16. Scattering profiles of neat PS-PEO and its blend with POSS-OAA at 30% loading at 80 ^{o}C. 70

3.17. X-ray diffraction profiles of (a) neat F108, (b) 50 % POSS-OAA blend, (c) 70 % POSS-OAA blend and (d) neat POSS-OAA. 71

3.18. DSC thermograms of neat F108 and its blend with POSS-OAA and POSS-OAP (a) Neat F108, (b) 50/50 POSS-OAA/F108, (c) 70/30 POSS-OAA/F108. The thermograms for the blends were shifted vertically upwards to avoid overlap with the thermogram for neat F108. 73

3.19. Transmission electron micrographs of mesoporous silica obtained upon calcination of F108 composites containing a) 50 % POSS-OAA and b) 70 % POSS-OAA. 75

3.20. FTIR spectra: a) Neat POSS-OAA, b) Neat F108, c) 70 % POSS-OAA/F108 blend annealed to 75 ^{o}C, d) 70 % POSS-OAA/F108 blend annealed to 160 ^{o}C, e) 70 % POSS-OAA/F108 blend calcined to 650 ^{o}C. 77

4.1. Schematic showing two possible outcomes upon blending of PS-PEO, PBd-PEO and PAA. Either a composite morphology would result (top right), or two separate BCP + homopolymer morphologies would co-exist (bottom right) 86

4.2. SAXS profiles for neat (a) PS-PEO (9.5-5 kg/mol) and (b) neat PBd-PEO (5-2.3 kg/mol). 88

4.3. SAXS profiles of various blends (C1 to C6) of PS-PEO (9.5-5 kg/mol), PBd-PEO (5-2.3 kg/mol) and PAA of molecular weight 20 kg/mol. The weight ratio of the two BCPs is maintained at unity for all the blends while the percentage of PAA is increased starting from no PAA up to 55 % PAA. 91

4.4. SAXS profiles for neat PBd-PAA (5.8-4 kg/mol). 94

4.5. SAXS profiles of various blends (A1 to A6) of PS-PEO (9.5-5 kg/mol), PBd-PAA (5.8-4.0 kg/mol). 97

4.6. SAXS profiles of blends of P105 (PEO-PPO-PEO, ~6.5 kg/mol, 50 % PEO) and PBd-PAA (5.8-4 kg/mol). 99

4.7. Possible structure for the sample B2 that forms a hexagonally packed morphology. PBd is the majority phase and therefore should form the matrix. PPO is the minority phase and would form cores. Due to chain connectivity of PAA with PBd and PEO with PPO, the PEO + PAA phase should lie in between and therefore form a shell around the PPO cores. 100

5.1. Schematic representation of the photo-induced ordering process (left) and the underlying reaction (right). Upon spin coating a blend of F127, MG-TBCM and a photoacid generator, the film is disordered (green). Upon irradiation of the disordered film with UV light through a mask placed on top, a photo-generated acid is liberated in the exposed regions, which drives the chemical transformation of MG-TBCM to MG-COOH (reaction on right) upon baking while the unexposed regions remain unchanged. MG-COOH interacts strongly via hydrogen bonding with PEO resulting in spontaneous formation of microstructure due to disorder-to-order transition of F127 as PPO microphase separates as cylinders (orange) from the PEO + MG-COOH + photoacid phase which form the matrix (blue). 107

5.2. DSC thermograms of (a) neat F127, (b) 5/95 blend of PTSA/F127, (c) 40/60 blend of MG-TBCM/F127, (d) 40/60/5 blend of MG-TBCM/F127/PTSA (MG-TBCM here is actually converted to MG-COOH). The thermograms have been shifted vertically to avoid overlap. The melting temperature (^{o}C) and melting enthalpy *J*/(*g* of PEO) are mentioned beside each curve where melting was seen. 112

5.3. SAXS profiles of (a) neat F127 at 80 ^{o}C, (b) neat F127 at 22 ^{o}C, (c) 30/70 blend of CTMA/F127 at 80 ^{o}C, (d) 30/70 blend of CTMA/F127 at 22 ^{o}C 114

5.4. SAXS profiles of neat F127 and its blends with PTSA and/or MG-TBCM at varying compositions at 80 ^{o}C: (a) 20/80 MG-TBCM/F127, (b) 30/70 MG-TBCM/F127, (c) 40/60 MG-TBCM/F127, (d) 50/50 MG-TBCM/F127, (e) 20/80/5 MG-TBCM/F127/PTSA, (f) 30/70/5 MG-TBCM/F127/PTSA, (g) 40/60/5 MG-TBCM/F127/PTSA, (h) 50/50/5 MG-TBCM/F127/PTSA, (i) 5/95 PTSA/F127, (j) neat F127. Ratio of higher order peak positions with that of primary peaks indicate hexagonally packed cylindrical morphology for samples that contained both MG-TBCM and PTSA (e, f, g, and h). 116

5.5. SFM images of unexposed and exposed regions of the film. (a) Height image of the unexposed region (z range = 10 nm), (b) Phase image of the unexposed region (z range = 22^{o}), (c) Height image of the exposed region (z range = 4 nm), (d) phase image of the exposed region (z range = 9^{o}). Unexposed regions are rough due to formation of PEO crystallites while the exposed regions form well-ordered cylindrical morphology showing features in height and phase images thus indicating formation of chemical and topographical BCP pattern. Scale bars = 150 nm. 119

5.6. SAXS profiles of blends of various PEO containing block copolymers with MG-TBCM with and without PTSA: (a) 40/60 blend of MG-TBCM and F108, (b) 40/60 blend of MG-TBCM and P105, (c) 40/60 blend of MG-TBCM and PS-PEO, (d) 40/60/5 blend of MG-TBCM, F108 and PTSA, (e) 40/60/5 blend of MG-TBCM, P105 and PTSA, and (f) 40/60/5 blend of MG-TBCM, PS-PEO and PTSA. 121

6.1. Schematic showing photolithography (a) shows exposure of film to UV using a mask, (b) shows generation of photoacid in the exposed regions, (c) shows change in material in exposed region as a result of acid catalyzed reaction upon baking, (d) shows patterned photoresist film formed after developing positive photoresists, (e) shows patterned polymer film after developing negative photoresists 127

6.2. Scheme for ensuring compatibility of additives with the polymeric photoresist both before and after deprotection. Fully or partially protected additives are blended with protected photoresists. Upon deprotection of the polymer photoresist, the groups on the additives also undergo deprotection to form groups that can interact via strong hydrogen bonds with the polymer backbone and cause physical crosslinking. 130

6.3. (a) Plasticization upon addition of small additives, (b) Molecular mixing where additive blends well with the polymer and can obstruct photoacid diffusion (antiplasticization) (c) Molecular mixing but large additives do not pack efficiently in polymer matrix (d) Entropy driven phase separation of large additives 133

6.4. (a) and (b) depict the generation of jump volume due to segmental motion or side chain rearrangements of the photoresist polymer and the photoacid molecule diffusing through the created jump volume (shown by red arrows). (c) shows how additives can pack within the polymer matrix to obstruct the photoacid molecule, reducing its diffusivity. (d) and (e) depict the generation of strong interaction between the additive and the polymer segments due to the formation of hydrogen bonding groups on the additive upon deprotection. This strong interaction is expected to result in the formation of physical crosslinking which is expected to slow down the polymer dynamics and consequently the diffusion of photoacid. 137

6.5. Structures of the polymer resist and the MGs employed in this work: (a) ESCAP photoresist (molar ratio of HOST:PS:tBA = 65:20:15, weight average molecular mass M_w = 10 kg/mol), (b) MG1-tBCM, (c) MG2-tBCM, (d) MG3-tBCM, (e) MG4-tBCM 138

6.6. Structure of hydrogen bonding additives incorporated in PHOST: a) benzene-1,2,3,4,5,6-hexacarboxylic acid (BHCA)and b) benzene-1,2,3,4,5,6-hexol (HHB) 140

6.7. Glass transition temperatures (°C) of neat ESCAP (ES), neat molecular glasses, and their blends at a mass fraction of 30 % MGs in ESCAP. Comparison with estimates using the Fox equation is also shown for the blends. DSC thermograms were measured between -40 °C and 120 ^{o}C (at a ramp rate of 10 °C/min) and the T_g observed during the second heating cycle is reported. 144

6.8. a) Contrast curves (normalized thickness remaining vs. Log (dose, mJ/cm^2)) of ESCAP and its blends with MG3-tBCM and MG4-tBCM at various loadings in terms of mass ratio: A) ESCAP, B) 20/80 MG4-tBCM/ESCAP, C) 40/60 MG4-tBCM/ESCAP, D) 60/40 MG4-tBCM/ESCAP, E) 20/80 MG3-tBCM/ESCAP, F) 40/60 MG3-tBCM/ESCAP. Each formulation contained a mass percent of 5 % TPST (except B at 4%) and 0.15 % TOA based on the blend. b) SEM micrographs of patterns at 80 nm L/S obtained for the six formulations with films about 85 nm in thickness. The corresponding doses in mJ/cm^2 were A) 1.7, B) 2.2 C) 2.6, D) 3.3, E) 1.8, and F) 2.2. 146

6.9. SEM micrographs of patterns obtained from G) ESCAP at 60 nm L/S at a dose of 17.5 mJ/cm^2, H) 30/70 (mass ratio) MG1-tBCM/ESCAP at 40 nm L/S at a dose of 18.7 mJ/cm^2 with films of about 85 nm in thickness. 147

6.10. Left) Contrast curves (normalized thickness remaining vs. Log (dose, mJ/cm^2) and right) SEM micrographs of patterns obtained at 30 nm L/S: I) 30/70 (mass ratio) MG1-tBCM/ESCAP, NonI at a mass percent of 8.5 %, TEA at 0.63 %, dose = 6.6 mJ/cm^2, J) 30/70 (mass ratio) MG1-tBCM/ESCAP, NonI at a mass fraction of 8.5 %, TEA at 0.93 %, dose = 8.8 mJ/cm^2 at a film thickness of 60 nm, K) 30/70 (mass ratio) MG4-tBCM/ESCAP, NonI at a mass fraction of 8.5 %, TEA at 0.93 %, dose = 6.3 mJ/cm^2 at a film thickness of 60 nm. 148

6.11. Line width (μm, y-axis) at varying focus (μm, x-axis) for formulations I (top) and J (bottom) at various doses (the doses in the legend are per cm^2 area of the photoresist film). 149

6.12. The method of bilayer fabrication and processing for estimation of acid diffusion length for various photoresist formulations 151

6.13. Structures of POSS-based additives (a) diol functionalized POSS, (b) trisilanol POSS 154

6.14. Images showing systems where POSS molecules did not interact strongly enough and therefore phase separated from PHOST (a) AFM image (10x10 micron) of diol-POSS with PHOST, (b) Optical image of trisilanol-POSS with PHOST 155

6.15. Micron scale photolithography of blend of PHOST with POSS-OAA: PHOST (20 kg/mol): POSS-OAA=80:20, 20.7 % TMMGU, 10 % TPST. (a) Mask, (b) polymer film after developing in 0.1 N tetramethylammonium hydroxide solution. The exposure was carried out in a contact printing mode in which the mask was placed on the top of the photoresist film during exposure..... 156

CHAPTER 1

INTRODUCTION AND OVERVIEW

1.1 Introduction

Specific interactions in polymeric materials can lead to miscibility and significantly alter the physical properties of the materials obtained thereby bringing property enhancements to existing materials as well as opening up a range of new applications.[1,2] For example, Kevlar, one of the toughest man-made fiber, owes its toughness in part to the intermolecular hydrogen bonding.[3] Likewise, miscibility of poly(methyl methacrylate) and poly(ethylene oxide) is facilitated by dipole-dipole interactions.[4]

This work proposes to employ, understand and benefit from hydrogen bonding between components of a blended systems. In many cases discussed, an ability to employ hydrogen bonding leads to an ability to functionalize the polymers without a need for tedious synthetic procedures required in chemical grafting of similar additives on the polymer chains. Additionally, while blending is easily scalable, synthetic procedures can suffer difficulties in scalability due to stringent process requirements.

The first kind of systems explored in this dissertation is based on the formation block copolymers (BCP) composites including organic-inorganic hybrid materials by blending of polymeric and non-polymeric additives. One of the blocks of the block copolymers is chosen such that it's segments serve as hydrogen bond acceptors to the functional groups attached on the additive that serve as hydrogen bond donors. One advantage of employing hydrogen bond driven incorporation is that it enables

significantly high loadings of a wide range of additives by compensating for the various entropic penalties associated with such incorporation. Additionally, mostly, the BCPs chosen in this work are small and therefore disordered due to insufficient segregation strength, but an ordering is induced by selective interaction of the additive with one of the blocks. Thus, in the well-ordered structure that results, the additive is sequestered into one of the phases of the BCP nanostructure. Choice of small BCPs leads to formation of small domains at small spacings (d-spacings). The benefits of loading BCPs with additives ranges from simply tailoring the domain spacing and morphology, to more interesting applications where the incorporated additives bring in the functionalities desired for phase selective chemistries, or simply changes the physical properties of the hybrid material.

The phase behavior of the above blends of homopolymers and BCPs where the homopolymer interacts strongly with one of the blocks of the BCP is significantly different from the phase behavior of conventional blends of homopolymers and BCPs where no strong interactions are present. The origin of these differences were understood by performing detailed studies on blends of a particular BCP with strongly interacting homopolymers.

The learning about the hydrogen bonding capability was then applied to the concept of binding two different BCPs by having complementary hydrogen bonding blocks on two separate BCPs. Composite morphologies were formed as indicated by an increase in the domain spacing of the blends in comparison to the constituent BCPs.

As an extension to the additive-driven assembly approach, this dissertation also discusses a new approach to order a BCP-additive blend upon irradiation by ultra violet

(UV) light. The process is non-intrusive and depending upon the easy control of the regions in which the material is exposed, it is fairly easy to create ordered regions within an otherwise disordered material.

The second type of systems explored is based on incorporation of additives into polymeric photoresists for enhancing their photolithographic performance. Here, it must be ensured that the additives are miscible with the polymer to result in uniform dispersion and therefore uniform properties throughout the film made of such blends. Additionally, miscibility must be ensured both before deprotection and after deprotection during which the polymer undergoes a significant change in its polarity. Any additive aggregation would be detrimental to the utility of the additive-loaded photoresists. In this project, strategies were designed to cause good blending in the protected form and strong hydrogen bonding interaction in the deprotected form. Photolithography is a common technique used in semiconductor chip making industry to fabricate devices and integrated circuits on silicon wafers. In the process of photolithography, a photoresist film prepared by spin coating is exposed to an electromagnetic radiation of a certain wavelength - in the present case 13.5 nm (hence the name extreme UV (EUV) photolithography), to generate a photoacid in the exposed regions which masking of certain desired regions where no photoacid is generated. Following exposure, a baking step is employed in which the photoresist film is heated to cause a chemical deprotection reaction in which the polarity of the photoresist changes in the exposed regions rendering the material soluble in a developer solution while the unexposed material remains undissolved. Ideally, it is desired that no photoacid diffuses from the exposed portion to the unexposed portion of the film but at the interface, the

photoacid diffuses from exposed regions to unexposed regions. The goal of this work is to tailor the polymer properties such that this undesired diffusion is reduced, thus enabling better photolithographic performance of the additive-loaded EUV photoresists.

Fundamentally, this work would aid in establishing design rules that enable efficient blending of polymers and additives. Such guidelines should ultimately enable new avenues for creation of highly loaded hybrid nanocomposite materials for a variety of applications. While, the two broad research areas, additive-loaded BCPs and additive-loaded EUV photoresists, target largely different applications, they share common principles and therefore allow an exchange of ideas to create new opportunities in materials development.

1.2 Dissertation Overview

This dissertation consists of seven Chapters. Chapter 1 (present) provides an introduction and overview of the dissertation. In Chapter 2 the phase behavior of blends of BCPs with strongly interacting homopolymer is presented followed by a detailed study on the organization of chains and evolution of structure as strongly interacting homopolymers are blended into disordered BCPs. Certain unique aspects about this type of phase behavior is discussed. Chapter 3 explores the requirements of structure and functionality of additive molecules that lead to efficient incorporation within the BCP by choosing a variety of non-polymeric additives. Suitable functionalities resulted in highly-loaded BCP nanocomposites. Chapter 4 considers a special case of hydrogen bonding additives in which the additive itself is a BCP. Thus, different BCPs were blended to form structures that are more complex than the constituent block copolymers.

Chapter 5 explores another special case in which the additive molecule can transition chemically from a weakly interacting to a strongly interacting form which causes the disorder-to-order transition of the host block copolymer. The concept is then extended to provide a new route to creating nanostructures in polymeric materials simply by exposure to light in a non-intrusive manner. Chapter 6 focuses on additive-loaded photoresists for next generation photoresist applications. Finally, Chapter 7 concludes the work done, and provides some future work and outlook.

CHAPTER 2

PHASE BEHAVIOR OF POLY(ETHYLENE OXIDE)-POLY(PROPYLENE OXIDE)-POLY(ETHYLENE OXIDE) TRI-BLOCK COPOLYMERS WITH POLY(ACRYLIC ACID)

2.1 Introduction

Self assembly of block copolymers (BCPs) can yield nanostructured polymeric materials containing periodically arranged nanoscale domains.[5-7] Many applications of BCPs could emerge due to differences in the chemical and/or physical properties of the various phases present in a self assembled BCP material or BCP-templated composite. For example, BCPs have attracted attention as low line edge roughness resists for nanoscale electronics[8] and as templates for the fabrication of nanoscale microelectronic structures including high density data storage media.[9-11] BCPs have also been used as templates to carry out phase selective reactions for the fabrication of inorganic mesostructured materials,[12-14] and phase selective treatments of BCPs have been performed to remove the minority phase, or a component of it, to form nanoporous polymeric materials.[15-17] BCPs have been used to direct the organization of hybrid materials, including polymer/nanoparticle composites.[18,19] These materials have generated significant interest due to their potential in emerging areas such as photovoltaics[20-22] and photonics.[23-25] A recent review summarizes the advances in employing BCP nanostructures in electronics.[26] Incorporation of additives such as homopolymers, nanoparticles and small molecules selectively into BCP domains is advantageous as it not only imparts a desired functionality, but can also be used to

gradually alter morphology and domain spacing without a need for synthesis of new BCPs for each of the states obtained. Thomas et al. discuss the avenues for BCP nanocomposites in their review paper.[27]

Microphase separation BCPs is thermodynamically governed by the product χN where χ is the Flory-Huggins interaction parameter between the segments of the dissimilar blocks and N is the total number of repeat units. When the segregation strength is high, BCPs containing two chemically dissimilar blocks (i.e. A-B, A-B-A, A-B-A-B and so on) form spherical, cylindrical and lamellar morphologies as determined mainly by the relative volume fractions of A and B phases.[5,6] For a particular volume fraction, the critical segregation strength required for microphase separation increases as the number of blocks increase. For example, for symmetric BCPs, i.e., for BCPs with equal volume fraction of A and B blocks, phase segregation of A and B blocks of A-B diblock copolymer occurs when segregation strength exceeds 10.5^{6} while A-B-A type triblock copolymer requires a segregation strength of greater than 18 for microphase separation.[28,29] When these critical values are not met due to a small χ and/or N, the BCP remains disordered. This is the case for most of the neat BCP employed in this work. As BCPs become increasingly asymmetric with respect to the relative volume fraction of the blocks, the critical segregation strength for microphase separation increases rapidly as evidenced by a steep shift in the phase boundary.

For many proposed applications of BCPs small domain sizes and domain spacings are desired. These include the use of BCPs for nanofabrication in which each domain serves as a device feature which is desired to be maximized in a given area. Smaller domain sizes and d-spacings corresponds to a higher number density of

domains and therefore there has been a continued research focus on obtained well-ordered BCP materials with smaller domains. One example of the use of BCPs in nanofabrication where small domain sizes are preferable is the proposed use of BCP thin films to fabricate magnetic data storage media in which each domain could serve as a single bit and therefore smaller domain spacings would result in higher bit density. Likewise, the use of small BCPs domains to fabricate devices such as field effect transistors,[30] capacitors,[31,32] and contact holes[33,34] on semiconductor chips has been explored. Other applications such as formation of inorganic materials within the BCP material by selective reaction of appropriate precursors and reagents would also benefit from the small domain spacings and sizes as they would provide creation of smaller pores in the material obtained.[12-14] For example, well-ordered mesoporous silica made by selective condensation of a silica precursor in the poly(ethylene oxide) (PEO) domains of Pluronic surfactants has been explored as size selective porous media for gold nanoparticles.[35]

The main challenge for achieving small domain sizes is that decreases in molar mass required to decrease the inter-domain spacing also weaken the segregation strength. Therefore, BCPs with a high χ is therefore preferable for maintaining order even at low molecular weights. However, even with large χ upon there is still a lower value of N for which the BCP cannot order. Enhancing the segregation strength to cause ordering of BCPs is another way to achieve smaller domain spacings. Most Pluronic BCPs (poly(ethylene oxide)-poly(propylene oxide)-poly(ethylene oxide) = PEO-PPO-PEO) tri-block copolymers lack the sufficient segregation strength to microphase separate into an ordered morphology at practical temperatures. However, it was found

by Watkins and co-workers that ordering of Pluronic BCPs can be induced by blending of hydrogen bond donating homopolymers that can interact selectively with PEO blocks. Thus, well-ordered morphologies were reported by addition of a variety of homopolymer additives.[36] The enhanced propensity of the blocks to phase segregate upon addition of additives is due to selective favorable interaction of the additive with the incorporating block. Likewise, blending of lithium[37-40] and gold[9] salts in PEO containing BCPs is known to enhance the segregation strength and induce ordering.

Several studies have focused on incorporation of homopolymers into BCPs in which the observed phase behavior of the blend was found to vary gradually depending upon the composition and chain length of homopolymers. For example, Hashimoto and coworkers examined polystyrene-polyisoprene BCPs with polystyrene and/or polyisoprene homopolymers as additives.[41,42] Because the interaction between the homopolymer additive and the incorporating block is athermal in this case, the phase behavior of such blends is governed primarily by entropic factors. Thus, low molecular weight homopolymers mix homogeneously with the incorporating block because of favorable entropy of mixing but larger homopolymers localize towards the center of the incorporating block to minimize the loss in entropy caused by stretching of the BCP and homopolymer chains. Due to homogenous mixing, as the loading of small homopolymer additives is increased a smaller change in domain spacing occurs but the system undergoes order-to-order transitions (OOT) upon increasing the homopolymer loading, while due to localized mixing, sufficiently large homopolymers cause a larger change in domain spacing but do not cause OOT.[41] The lack of strong interaction between the homopolymer and the incorporating block also sets a low limit on the size of

homopolymers above which they macrophase separate from the BCP. For example, macrophase separation of poly (methyl methacrylate) homopolymer occurs from polystyrene-poly(methyl methacrylate) block copolymer when the ratio of chain lengths of the homopolymer to the molecular weight of BCP exceeds about 1.0.[43]

In contrast, strong interactions between the additive homopolymer and incorporating block can facilitate incorporation of high loadings of even large homopolymers as the favorable enthalpic interactions can offset the entropic penalty associated with stretching of large homopolymers.[43] Watkins and co-workers recently reported that the addition of homopolymers that selectively associate through hydrogen bonding with the PEO blocks of disordered Pluronic triblock copolymer surfactants (poly(ethylene oxide)-poly(propylene oxide)-poly(ethylene oxide)) (PEO-PPO-PEO) induces microphase segregation and strong order.[13,36] Phase segregation in the blends is driven by the strong attractive interactions of the homopolymers with the PEO blocks and the system assembles to maximize the energetically favorable interactions between PEO and homopolymer, which results in exclusion of PPO from the PEO-homopolymer phase and ultimately leads to the formation of well ordered BCP morphologies. The use of hydrogen bonding as a means to mediate interactions of polymers and additives is advantageous because the strength of interaction and hence the structure and properties of such blends can be controlled by varying the nature of the functional groups placed on the additive molecules as well as by varying the temperature.

In this chapter, the effects of molecular weight and composition of poly(acrylic acid) (PAA) upon the phase behavior of Pluronic surfactants is studied systematically. Through detailed studies with Pluronic-PAA system, this study will explore the

morphologies and domain spacings that result upon addition of PAA of varying chain lengths at varying compositions with respect to the Pluronic surfactants. To generalize the results, these studies are carried out with two Pluronic surfactants namely F108 (EO_{127}-PO_{48}-EO_{127}, 14.6 kg/mol) and P105 (EO_{37}-PO_{56}-EO_{37} ~ 6.5 kg/mol). The data for blends containing P105 along with detailed explanations is published elsewhere.[44]

As explained later, many differences (some counterintuitive) were observed in the behavior of blends of Pluronic BCPs with PAA in light of the vast literature on the behavior of typical BCP-homopolymer blend systems in which only weak interaction existed. To explain these differences and to gain and insight into the phase behavior, a detailed study was performed based on small angle neutron scattering (SANS) measurements of blends of a specially synthesized, partially deuterated PEO-PPO-PEO tri-block copolymer with PAA of various chain lengths and loading.

2.2 Experimental

2.2.1 Materials

Pluronic F108 (EO_{127}-PO_{48}-EO_{127}, 14.6 kg/mol, EO = 80 % by weight) and P105 (EO_{37}-PO_{56}-EO_{37}, 6.5 kg/mol, EO = 50 % by weight) are commercially available commodity surfactants and were donated by BASF. Using gel permeation chromatography the polydispersity index (PDI) of F108 and P105 were found to be 1.18 and 1.27 respectively. Ethanol, water and 1-propanoic acid were purchased from Fisher Scientific. All the materials and solvents were used as received. Poly(acrylic acid) (PAA) of different molecular weights, M_n = 8.5, 20, 44, and 88 kg/mol, with

corresponding PDIs = 1.07, 1.09, 1.08, and 1.12, respectively were purchased from Polymer Source. The 2 kg/mol (high PDI) PAA was purchased from Sigma Aldrich. For small angle neutron scattering (SANS) experiments, a PEO-PPO-PEO tri-block copolymer (Mw = 10.7 kg/mol, polydispersity index (PDI) = 1.1) with PEO = 55.6 wt. %, PPO deuterated to 65 wt. % was synthesized as described elsewhere.[45] This BCP is referred to as d-TB and was synthesized by Ying Lin at the University of Massachusetts at Amherst.

2.2.2 Sample preparation

Appropriate amounts of F108 or P105 and PAA were dissolved in ethanol and slight amount of water to form a homogenous solution by stirring at 65 ^{o}C. The solutions were drop casted on glass slides and kept inside a vacuum oven maintained at 75 ^{o}C for ~24 hours. Solvent mass losses were tracked to confirm that the resulting samples did not contain any residual solvent. In this work, a 30 % loading of an additive implies its composition in the blend equals 30 % by weight while the rest 70 % is the BCP. This is also represented in other places as a 30/70 blend of additive/BCP. In all cases, weight percentages are used.

2.2.3 Small-angle x-ray scattering

The dried samples were placed in the center of 1 mm thick metal washers and sealed on both sides with Kapton film. The filled metal washers were maintained at 80 ^{o}C on a heating stage from Linkam equipped with TMS94 temperature controller. A 30 minute equilibration time at 80 ^{o}C was employed before the measurements which were

conducted for each sample for 1 hour. Small angle x-ray scattering (SAXS) was performed using an instrument from Molecular Metrology Inc. (presently sold as Rigaku S-Max3000) using 0.1542 nm (CuK_α radiation) and an incident beam of 0.4 mm diameter. The sample to detector distance was calibrated using silver behenate standard peak at 1.076 nm^{-1}. The setup employs a two-dimensional gas-filled wire detector for collection of scattered x-ray and allows measurements in wave vector (q) range of $0.06<q<1.6$ nm^{-1} in which $q=(4\pi/\lambda)\sin\theta$, where 2θ is the scattering angle. The raw scattering data was circularly averaged and plotted as intensity (I) vs. q where intensity was used in arbitrary units. For data presentation, the profiles are shifted vertically by multiplying intensity values with constant factors to avoid overlap of the profiles.

2.2.4 Sample preparation for small angle neutron scattering

Solutions of required quantities the BCP and PAA of molecular weights, 2, 8.5, 20, 44 and 88 kg/mol were made by dissolving in ethanol. The solutions were casted on silicon wafers placed on a hotplate at 60 ^oC. To estimate the thickness of the samples, it is necessary that the samples are free of any bubbles that may form as ethanol evaporates from the viscous polymer solution being casted. To avoid the formation of bubbles, the solvent casting was performed slowly by dropping the solutions on the wafers over an extended period of time. Following this, the samples were heated for another 24 h in which ethanol dried slowly. To remove the residual ethanol, the samples were placed in a vacuum oven set to 60 ^oC and the vacuum was raised gently to evaporate the remaining ethanol. Here again, care was taken to avoid rapid evaporation as it would result in the formation of bubbles. Therefore partial vacuum was applied

with several purge cycles in between. Gradually, as the ethanol evaporated, the vacuum was raised and the temperature was increased to 75 ^{o}C and the samples were dried for 48 hours.

2.2.5 Small angle neutron scattering

The samples were placed on heated blocks with beam apertures of 1/2" in diameter, to define the incoming beam. Another aperture of 3/8" in diameter was placed just before the samples. Neutron scattering was performed on these samples while maintaining them at 70 ^{o}C on the NG7 30 m small angle neutron scattering (SANS) beam line at the NIST Center for Neutron Research at Gaithersburg, MD, USA. The wavelength of the neutron beam was set to 6 A. The data was collected at three sample to detector distances (SDD) of 1 m, 4.5 m, and 13.5 m. These SDDs cover the high q range from 0.04 1/A to 0.5 1/A, the mid q range between 0.007 1/A to 0.1 1/A, and the low q range from 0.003 1/A to 0.032 1/A. The NCNR SANS reduction and analysis package, "Reduction and Analysis of SANS and USANS Data using Igor Pro" was used to reduce the data into I vs. q form.[46] For data reduction, the transmission (the ratio between the transmission count rate of the sample and the transmission count rate of the silicon substrate) was used to calculate the sample thickness. The obtained intensities were normalized by the sample thickness to estimate the absolute scattering intensity. These absolute intensities allow comparison of peak heights to provide a comparison of the scattering intensity from different samples. The obtained absolute intensity was plotted as a function of q. In the plots, the intensity values were shifted vertically for

clarity in data presentation. The absolute intensity data were fitted based on a 4-layer model in the q range of 0.02 1/A to 0.25 1/A which is the region of interest.

2.3 Results and Discussion

2.3.1 Phase behavior of blends of Pluronic BCPs and PAA homopolymers

First, the phase behavior of blends of Pluronic BCPs with poly(acrylic acid) is considered. Two different Pluronic BCPs, F108 and P105 were blended with PAA of various molecular weights at varying compositions and the phase behavior of the blends was observed using SAXS. While F108 is a PEO majority copolymer with 80 % PEO, P105 is symmetric with 50 % PEO. Therefore different morphologies are expected from blends of these two BCPs.

Figure 2.1 shows the scattering profiles for blends of F108 with 8.5 kg/mol PAA. The SAXS profile of F108 shows a broad peak which is due to the correlation hole effect observed for disordered BCPs.[6,47] This is expected as F108 should be disordered at the measurement temperature of 80 ^{o}C.[48] When PAA is blended, the correlation hole peak sharpens into a primary peak and higher orders of reflection appear at 30 % loading, indicating the formation of a well-ordered morphology. The peak position ratios of 1:√3:√4:√7 indicate formation of a hexagonally-packed cylindrical morphology. When more PAA is incorporated into the PEO phase an order-to-order transition (OOT) occurs because as the PEO phase is enriched, its relative volume fraction is increased. The blend containing 40 % PAA shows a scattering profile with peak position ratios of 1:√2:√3:√4..., indicating the formation of a spherical

morphology on a body-centered cubic lattice. Here, since PPO is the minority component, the cylinders and spheres are formed with the PPO middle blocks. Thus, PAA induces phase segregation of F108 by interacting selectively with the PEO chains while secluding PPO that form the cylinders and spheres. The interplanar spacing (d-spacing) between 110 and 100 planes of the cylindrical morphology and spherical morphology at 30 % and 40 % PAA loading is 13.9 and 14.6 nm (calculated as $d = 2\pi/q^*$, where q^* is the primary peak position).

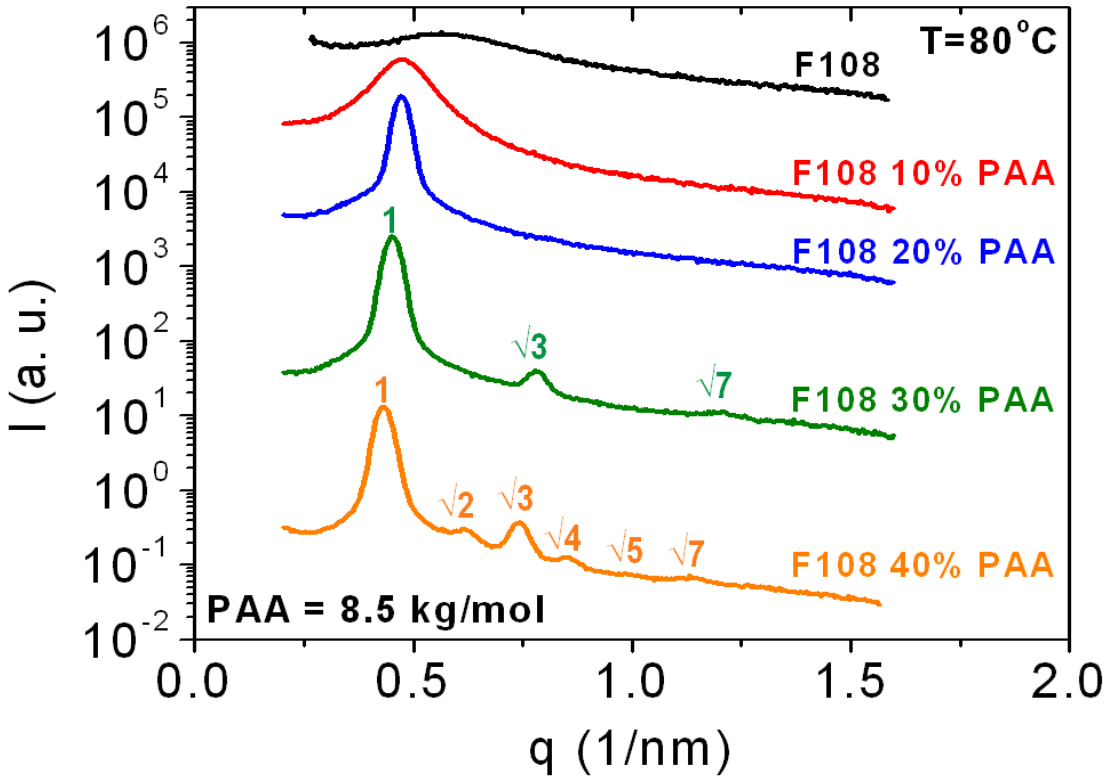

Figure 2.1. SAXS profiles of F108 and its blends with PAA (8.5 kg/mol) at varying compositions at 80 °C.

Thus, in comparison to the case of blends of weakly interacting homopolymers and BCPs, the phase behavior observed here is different in that the primary peak

position remains nearly invariant and the homopolymer's molecular weight does not seem to vary the phase behavior. The origin for these differences are later explored using small angle neutron scattering with blends of PAA and another partially deuterated BCP. The SAXS profiles for blends of F108 with other PAA (20, 44 and 88 kg/mol) were found to be similar in the morphologies obtained and the domain spacings formed.

Figure 2.2 shows the scattering profiles of P105 with 20 kg/mol PAA. Here again, addition of PAA induces order in the blends formed. At 30 % loading, a lamellar morphology is formed as indicated by the peak position ratios of 1:2:3…. Since P105 is symmetric with respect to the amount of PEO and PPO, it forms alternating lamellae of PPO and PEO + PAA. Upon increasing the PAA loading, the PEO phase is enriched to result in a transition from a lamellar morphology to a hexagonally packed cylindrical morphology where PPO forms cylinders. The position of primary peak represents an interplanar spacing ranging between 10.5 to 11 nm.

For the case of Pluronic BCP surfactant, P105 (EO_{37}-PO_{56}-EO_{37}, 6.5 kg/mol) blending of 20 % to 50 % poly(acrylic acid) (PAA) of molecular weights ranging between 2 to 88 kg/mol caused ordering and OOT in all cases.[44] Thus, in contrast to the above mentioned chain ratio limit of about 1.0 for achieving incorporation of a weakly interacting homopolymer, homopolymer chains significantly larger than the BCP could be incorporated in this case. However when 1-propanoic acid, a small molecule analogous to a single repeat unit of PAA was blended with P105, the system remained disordered. This problem of the inability of a small molecule to induce a disorder-to-order transition (DOT) of Pluronic BCPs is focused on in the next Chapter where the

architecture and chemical functionalities of non-polymeric additives that can cause a DOT of Pluronic BCPs are elaborated.

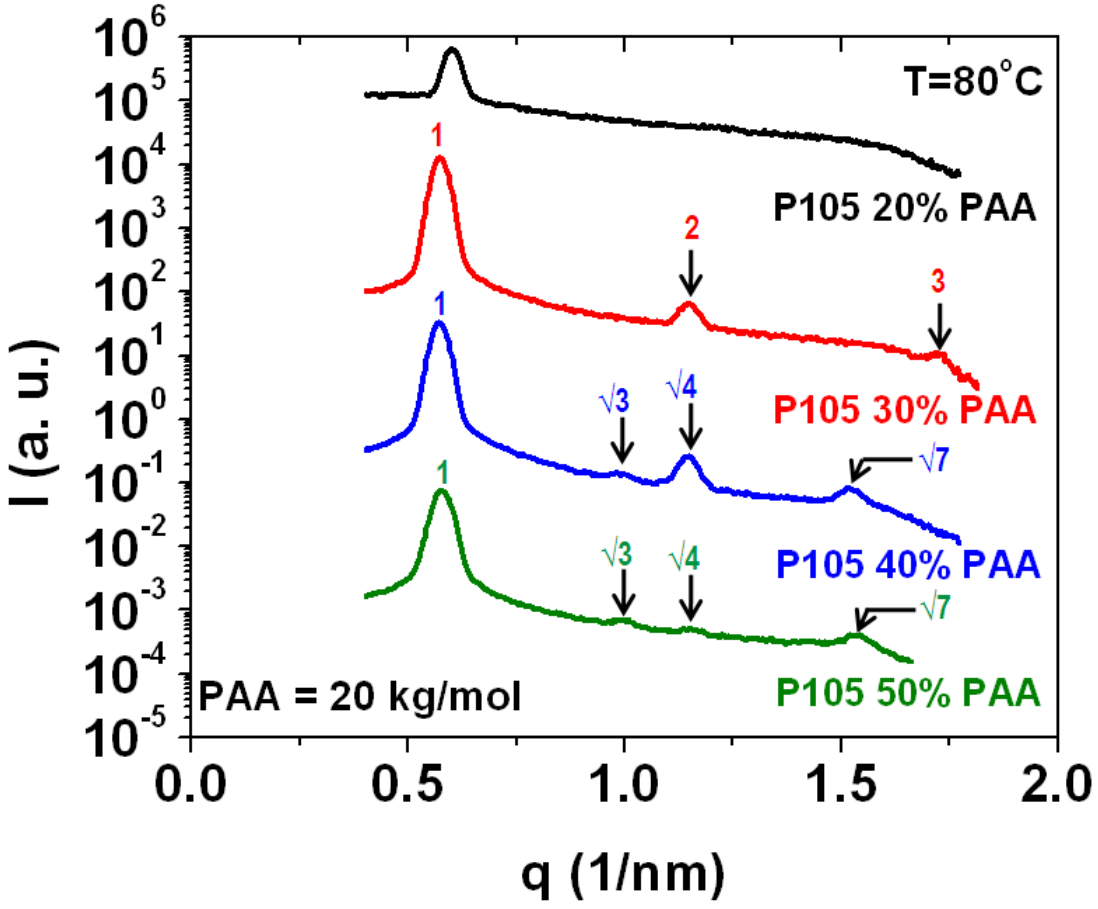

Figure 2.2. SAXS profiles of P105 and its blends with PAA (20 kg/mol) at varying compositions at 80 °C.

As in the case of blends of F108 and PAA, the blends of P105 and PAA did not show significant differences as the PAA molecular weight was varied between 8.5 to 88 kg/mol: the domain spacing and the morphologies obtained do not seem to be affected significantly by the molecular weight of the PAA chains as well as loading of the PAA chains which is counterintuitive from the stand point of the behavior of typical BCP-

homopolymer systems in which domain spacing increases with the homopolymer loading as well as its molecular weight. Here again, it is found that a significantly large PAA (88 kg/mol) as compared to P105 (6.5 kg/mol) is still incorporated in the BCP and is not macrophase separated. For the case of weak interaction between homopolymers and the incorporating block of the BCP, such long homopolymers cannot be incorporated as they macrophase separate as described above. Thus, it is observed that the chain length of homopolymer does not matter much for the case of a strongly interacting BCP-homopolymer system and consequently a sample of homopolymer with a high PDI would not affect the morphology. The details of phase behavior with blends of P105 with PAA of various chain lengths are discussed elsewhere.[44]

2.3.2 Organization of chains and the evolution of structure during ordering

Having observed the phase behavior of Pluronic BCPs with PAA, we now focus our attention on understanding the organization of chains and structure evolution during the process of ordering as PAA is blended with PEO-PPO-PEO triblock copolymers. For blends of Pluronic BCPs with PAA, although high loadings of PAA can be incorporated - as evidenced by the systematically varying scattering profiles which represents molecular incorporation of PAA into PEO phases – the system deviates from the behavior for weakly interacting BCP-homopolymer blends in that even as high loadings of PAA is added, the primary peaks of the scattering profiles do not shift as much implying that the d-spacing remains nearly invariant with the incorporation of PAA into the PEO phase. This is counterintuitive because normally it is expected that the homopolymer would swell the incorporating phase and increase the domain spacing.

Second unique aspect of this system is that molecular weight of the added homopolymer, PAA, does not seem to affect the domain spacing or the morphology in the range of 8.5 to 88 kg/mol. Again, this is surprising because for weakly interacting systems a strong dependence of the molecular weight of the incorporated homopolymers on the domain spacing and the morphology has been observed. The ability to incorporate PAA chains that are very large as compared to the PEO blocks of P105, raises another important question: is all of the PAA chain is restricted to the PEO phase or does it, occasionally, loop or bridge across the PPO phase as well? The concern here is that large PAA chains would have to stretch significantly to remain in the small PEO domains and this perturbation from the gaussian coil shape is associated with an entropic penalty of stretching and is therefore unfavorable. So, the question is, does PAA chains relax their stretching by looping or bridging across the PPO domains at times or is the enthalpic interaction of PAA chains with PEO chains enough to offset this entropic loss? These aspects are explained in this part of the chapter by performing SANS on blends of PAA with specially designed and synthesized triblock copolymer (PEO-PPO-PEO, Total M_w = 10.7 kg/mol, polydispersity index = 1.1, PEO = 55.6 wt. %, PPO deuterated to 65 wt. %) similar to Pluronic P105 but larger in size. This BCP is referred to as the deuterated triblock copolymer (or d-TB) in this chapter. The consequent fitting of the scattering profiles obtained provide insights into the structure evolution as PAA is added. Measurements were performed for blends with two different loadings of PAA which provides snapshots of the phase behavior as a function of increasing PAA loading. This study has lead to an understanding of the causes for

various differences in the phase behavior of the present system with those of weakly interacting systems.

First, using SAXS, the blend compositions that lead to the formation of a lamellar morphology were determined. Figure 2.3 shows the SAXS profiles of the neat d-TB with PAA from which it is seen blends of the d-TB with 20 % and 30 % PAA form lamellar morphology. At 40 % loading of PAA, the morphology transitioned into a cylindrical morphology. While this behavior is similar to P105 as expected, here we explore the 20 % and 30 % blends in detail to study the governing physics underlying the phase behavior of such blends. This work was done in collaboration with Hua-Gen Peng, Wen-Li Wu and Christopher Soles at the Polymers Division at National Institute of Standards and Technology (NIST), Gaithersburg, MD, USA. In particular, the fitting of SANS profiles along with interpretation of the results was a majorly an effort of Hua-Gen Peng.

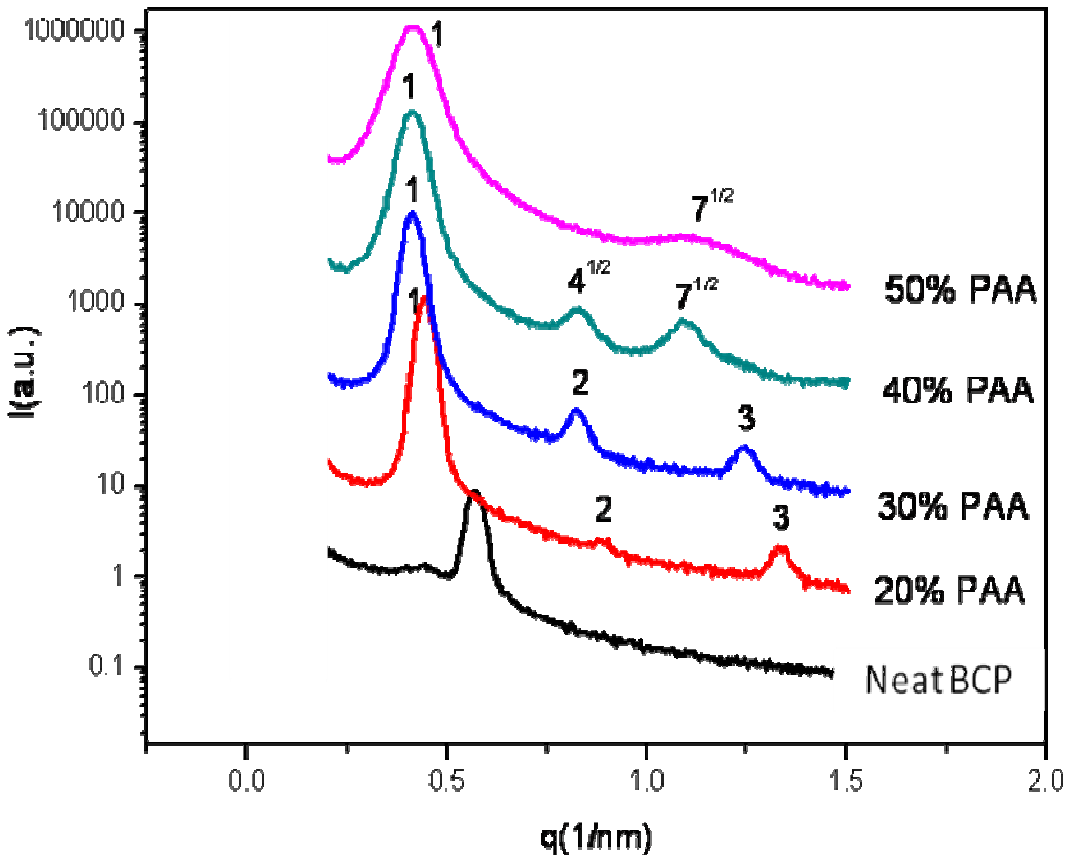

Figure 2.3. Phase behavior of blends of d-TB with various loadings of PAA.

The neutron scattering length densities (SLD) for the PEO block, PPO block and PAA are tabulated in Table 2.1. Also shown is the average SLD for 20 % and 30 % PAA blends. These average values are later used as checks to make sure that the results from the fitting of the SANS profiles are correct.

Table 2.1. Neutron scattering length densities of various components.

	(SLD, 10^{-6} A^{-2})	
PEO completely deuterated	6.77	**Average SLDs of blends** 20% PAA = 4.90 30% PAA = 4.52
PPO 65 % deuterated	4.42	
PAA (hydrogenated)	1.66	

Figure 2.4 shows the SANS profiles obtained from the neat BCP (d-TB) and its blends at 20 % and 30 % PAA loading with varying PAA molecular weights from 2 kg/mol up to 88 kg/mol. The primary and the secondary structure factor peaks corresponding to the lamellar morphology is observed for all the blends. The primary peak is more intense than the secondary peak for all the 20 % PAA blends, however, the reverse is true for 30 % PAA blends. A scattering profile in which primary peak is smaller than the secondary peak is an indication of the formation of a more complex structure than a simple two-layer lamellar morphology. Also, the SLDs were designed such that at 30 % loading of PAA, the lamellae would have been very close to contrast matched. However, the structure factor peaks corresponding to the lamellar morphology are still observed. This is another indication that PAA must not be distributed uniformly in the PEO domains.

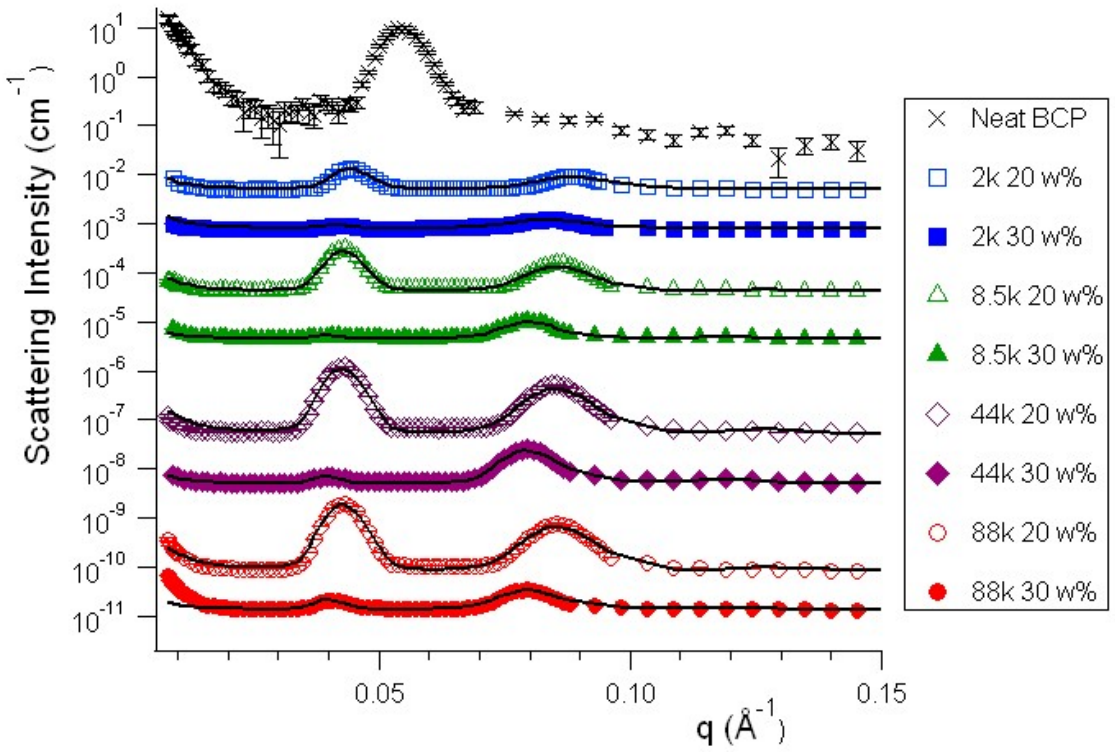

Figure 2.4. SANS profiles obtained from the neat BCP (d-TB) and its blends at 20 % and 30 % PAA loading with varying PAA molecular weights from 2 kg/mol up to 88 kg/mol at 80 ^{o}C.

To accommodate for a gradient in the concentration of PAA in the PEO phase, a model as shown in Figure 2.5 was chosen. Here, PPO layer separates from PEO + PAA layers. The PEO + PAA layers are split into a central PAA-rich region and two PEO-rich regions on the PPO domain interface. The results of fitting the SANS profiles with this model is shown by lines in the Figure 2.4 where it is seen that a good fitting resulted. However, it must be noted that in reality there would be a gradient in the concentration of PAA in the PEO + PAA phase instead of a step change. However, as described later, the goodness of fit and the corresponding thicknesses and SLDs

obtained for the individual layers indicate that the gradient in PAA concentration must not be high.

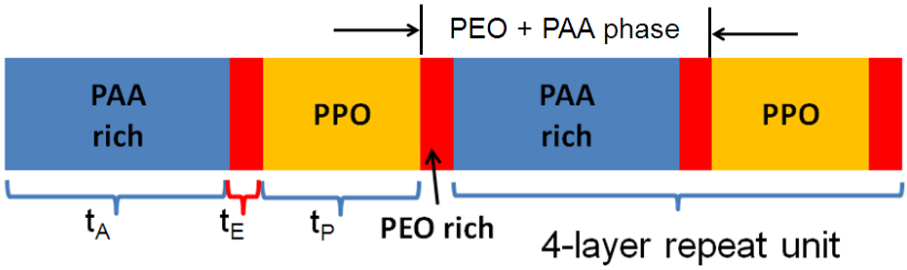

Figure 2.5. Model structure for blends of the BCP, d-TB with PAA.

The case of 30 % PAA blend is simpler and is therefore explained first. Table 2.2 shows the resulting thicknesses and SLDs of the various layers. In this fitting, the SLD of PPO layer was set to 4.42 x 10^{-6} A^{-2} which equals that of pure PPO (see Table 2.1), while the rest of the parameters (thickness (t), thickness fluctuations and SLD of the various layers) and were fitted. The average SLD based on the thickness of various layers and the SLDs obtained are also shown. It can be seen that these average values for the SLDs match closely with that expected for the 30 % PAA blend (see Table 2.1) and therefore the fitting results must be reasonably accurate.

Table 2.2 brings forth a number of insights into the phase behavior of the PEO-PPO-PEO tri-block copolymers when blended with PAA (and possibly other hydrogen bonding homopolymers). It can be seen from Table 2.2 that the thickness of the PEO-rich layer is just over 10 angstroms and the PAA-rich layer spans almost all the PEO + PAA phase. This is true for even 88 kg/mol PAA which is significantly larger than the

BCP, d-TB. Therefore, the favorable enthalpic interaction offsets the entropic factors that direct long homopolymer chains towards the center of the incorporating block.

Table 2.2. Fitting results for 30 % PAA blends at varying molecular weights of PAA. The thickness t is in angstroms and the SLD is in A^{-2}.

	PAA 2 kg/mol	PAA 8.5 kg/mol	PAA 44 kg/mol	PAA 88 kg/mol
$t_{PAA\text{-}rich}$	75.1	80.4	78.5	78.1
$t_{PEO\text{-}rich}$	11.6	11.7	12.8	12.8
t_{PPO}	50.6	53.4	53.6	53.3
d-spacing (4-layer)	148.8	157.1	157.7	157.1
$SLD_{PAA\text{-}rich}$	4.46	4.46	4.48	4.47
$SLD_{PEO\text{-}rich}$	4.62	4.65	4.75	4.65
SLD_{PPO}	4.42	4.42	4.42	4.42
SLD_{Ave}	4.48	4.47	4.47	4.50

The SLD of PEO-rich and PAA-rich layers correspond to a 41 % and 45 % PAA in the PEO phase which are not too different. This implies that the gradient in PAA concentration in the PEO + PAA phase is not high except just near the interface where PAA might not like to situate itself due to unfavorable interaction with PPO. The SLD of PPO layer being equal to that of the pure PPO implies that PAA is selectively incorporated into the PEO phase.

The d-spacing (4-layer) for blends with PAA from 8.5 to 88 kg/mol are almost the same. Thus, as observed before, the d-spacing does not vary with the molecular weight of PAA homopolymer except at very low PAA chain lengths. Blends with PAA with molecular weight 2 kg/mol shows a slightly smaller d-spacing which could be due to the ability of this small molecular weight PAA to locate itself closer to the PEO-PPO domain interface. This stagnancy in the d-spacing for PAA from 8.5 to 88 kg/mol persists even at 20 % PAA loading. The reason for an invariant domain spacing with the molecular weight of PAA is that regardless of the molecular weight, the PAA chains are almost uniformly mixed in the PEO phase and the entropic factors that result in dependence of d-spacing on the molecular weight of the added homopolymer (localization of longer homopolymers towards the center of the incorporating domain) is offset by favorable enthalpic interactions.

Table 2.3 shows the fitting results obtained for 20 % PAA blends at varying molecular weights of PAA. The first column for PAA of molecular weight 2 kg/mol shows the fitting results upon setting the SLD of PPO layer as that of pure PPO. However, it is not correct to do so because the average SLD comes out to be significantly lower than that expected for the 20 % PAA blends (see Table 2.1). To match the average SLD to the SLD expected for this blend, the SLD of PPO layers must be increased. The rest of the columns show the fitting results for all the PAA molecular weights in which the SLD of the PPO layer is increased. The close match between the average SLDs obtained with that expected for this blend (see Table 2.1) validates the correctness of the results.

Table 2.3. Fitting results for 20 % PAA blends at varying molecular weights of PAA. The thickness t is in angstroms and the SLD is in A^{-2}. The first PAA 2k column shows the fitting results upon setting the SLD of PPO layer as that of pure PPO, however, it is not correct because the average SLD comes out to be significantly lower than that expected for the 20 % PAA blends.

	PAA 2 kg/mol	PAA 2 kg/mol	PAA 8.5 kg/mol	PAA 44 kg/mol	PAA 88 kg/mol
$t_{PAA\text{-}rich}$	57.3	47.6	52.8	53.8	53.0
$t_{PEO\text{-}rich}$	12.2	12.9	12.9	13.7	14.3
t_{PPO}	59.0	68.0	67.5	66	65
d-spacing (4-layer)	**140.6**	**141.3**	**146.1**	**147.2**	**146.6**
$SLD_{PAA\text{-}rich}$	4.47	4.85	4.85	4.85	4.86
$SLD_{PEO\text{-}rich}$	4.66	5.06	5.14	5.26	5.26
SLD_{PPO}	4.42	4.83	4.8	4.74	4.74
SLD_{Ave}	4.48	4.87	4.87	4.88	4.88

Among the constituents in the blend, only PEO has a higher SLD than PPO (see Table 2.1) and therefore a higher SLD of the PPO layer can only be possible if some PEO would mixed with it. This is a very important point and one reason why the d-

spacing remains invariant with the PAA loading. When, PAA is added, it interacts with PEO but at a 20 % loading, it is insufficient to extract all the PEO from the PPO layers. Thus, although an ordered structure forms, some PEO chains are still mixed within PPO layers. The remaining PEO chains are extracted from PPO layers when more PAA is added and at 30 % loading, the PPO layer is left nearly pure. The SAXS profile for the neat d-TB BCP shows a sharp peak corresponding to the microphase separated lamellae but also shows a broader correlation hole peak at a smaller q value. This SAXS profile is in agreement with the presence of PEO within the PPO phase even after the initial ordering of the BCP. While the BCP is segregated to form a lamellar morphology, some PEO is still present in the PPO phase and that represents a disordered BCP and would show a broad correlation hole peak in the SAXS profile just like any other disordered BCP does. It must be noted that this behavior is different from typical systems in which a DOT proceeds with segregation of all the dissimilar chains so that they lie on different sides of the domain interface and their junction point lies at the domain interface. Thus, in typical BCP systems, the number of junction points at the domain interface is fixed when DOT occurs as well as when additives are incorporated. However, here a new kind of phase behavior occurs: even after an ordered structure has formed, chemically different blocks can be situated on the same side of the domain interface (20 % PAA blends). The junction points between the PEO lying in the PPO layer and the PPO connected to those PEO chains need not be situated at the domain interface. However, since at 30 % PAA loading, all the PEO chains are extracted out of the PPO layers, the PEO chains that were extracted out must contribute to additional junction points at the domain interface. To accommodate the additional junction points, there would be a

lateral stretching of the domain interface. Therefore, between 20 % and 30 % PAA loading, an increase in the thickness of the PEO phase due to incorporation of PAA and due to transfer of some PEO chains from PPO layers to the microphase separated PEO phase, must be offset by a decrease in the PPO thickness due to a mass loss as PEO leaves this layer as well as decreases in the thicknesses of all layers due to an additional spreading of the interface as additional junction points are placed at the interface. Additionally, favorable interaction between the PEO and PAA is also expected to cause a slight reduction in the thickness of the PEO + PAA phase. The net result of this offsetting is that the change in d-spacing between 20 % and 30 % PAA loading is just ~7 % as opposed to ~11 % for the case of typical systems.[41]

It must be noted that in the case of blends of d-TB with PAA, the d-spacing increases as the PAA loading is increased from 20 % to 30 %. However, for Pluronic surfactants the d-spacing does not increase. This difference in the dependence of d-spacing on the loading of PAA might be due to the high PDI of the Pluronic surfactants as well as presence of other impurities in the commercial materials used. However, the above study indicates the underlying mechanism for the various unique aspects about the phase behavior of blends of Pluronic BCPs with PAA of various molecular weights at varying loadings.

The schematic shown in Figure 2.6 represents the structure evolution for the case of Pluronic surfactants upon blending PAA. Upon blending PAA into Pluronic surfactants, the PAA associates with some but not all the PEO chains. Since PAA is incompatible with PPO, the PEO + PAA phase segregates resulting in the formation of an ordered structure. However, even when ordered, some PEO is still mixed within the

PPO phase. In samples to which higher amounts of PAA is added, more PEO can interact with the available PEO and therefore less PEO would remain within the PPO phase. This process of reduction of PEO from the PPO phase is expected to continue until the entire PEO is segregated out of the PPO phase. This unique feature about the structure evolution of two different types of blocks present on the same side of the domain interface even after ordering results in the unique aspects of the phase behavior. As explained before, as PAA loading is increased, the number of junction points at the interface would increase. This would cause a lateral swelling that would offset the increase in the domain spacing as PAA is added to the PEO phase. Additionally, strong enthalpic interactions offset the entropic factors which influence and dominate the observations in the phase behavior of weakly interacing BCP-homopolymer blends. Thus, in this case, the entropic factors related to the molecular weight of the PAA homopolymer are not able to influence the phase behavior and little effect of molecular weight of the homopolymer on the phase behavior is observed.

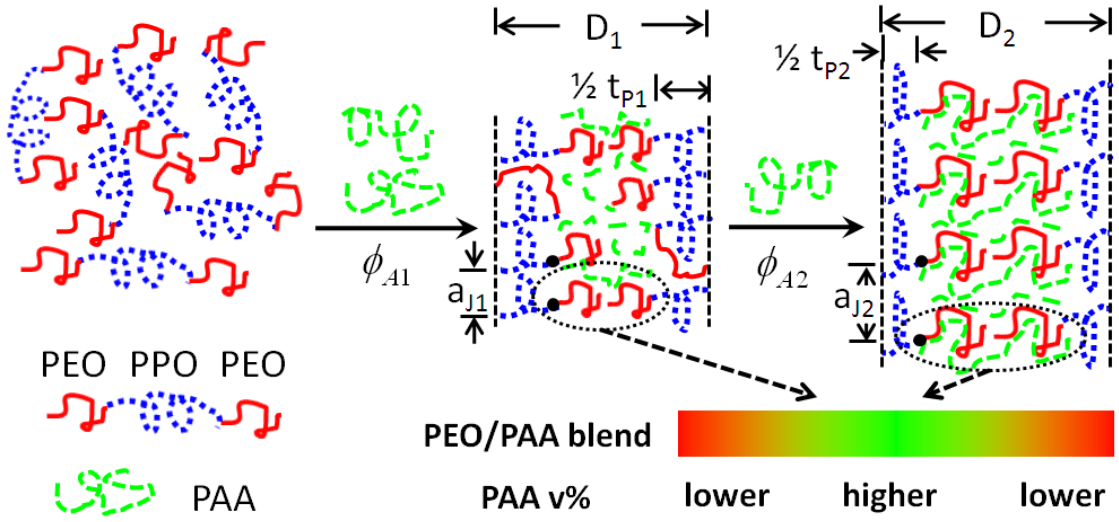

Figure 2.6. Structure evolution in blends of Pluronic BCPs upon blending PAA. The initially disordered BCP orders as PAA is added. Even after ordering, some PEO chains are mixed within the PPO phase and is extracted upon addition of more PAA. Correspondingly, the number of junction points between PEO and PPO must increase continuously to reach a maximum when the PPO phase becomes pure.

2.4 Conclusions

This chapter dealt with the phase behavior of blends of PAA with PEO-PPO-PEO tri-block copolymers. First the phase behavior of blends of commercially available Pluronic BCPs with PAA was studied using SAXS. Upon closer look, several counterintuitive features were observed in the phase behavior, the most important ones being that the domain spacing did not vary much with the loading as well as molecular weight of PAA. On the other hand, OOT transitions were observed upon increasing PAA loadings which implies a molecular level incorporation of PAA into the Pluronic BCPs. To explain these unusual aspects of the phase behavior, a specially synthesized, partially deuterated PEO-PPO-PEO tri-block copolymer was studied upon blending with PAA of various molecular weights at 20 % and 30 % loading . Partial deuteration of PPO blocks and complete dueteration of PEO chains allowed for enhancing the contrast and this amplified the differences between the various phases. The SANS profiles for these blends were obtained and fitted based on a 4-layer model to obtain important insights into the phase behavior which explains the reason for the unusual aspects of the phase behavior observed for blends of PEO-PPO-PEO tri-block copolymers with PAA (and possibly other homopolymers capable of hydrogen bonding with the PEO blocks).

CHAPTER 3

PHASE BEHAVIOR OF BLENDS OF POLY(ETHYLENE OXIDE) CONTAINING BLOCK COPOLYMERS WITH NON-POLYMERIC ADDITIVES

3.1 Introduction

As mentioned in Chapter 2, when the critical segregation strength for microphase separation is not met, either due to a small χ and/or a small N, the BCPs remain disordered as is the case for the BCPs employed in this work.[6 28,29] The segregation strength of such disordered BCPs can be enhanced by blending a selectively interacting homopolymer (Chapter 2) or by blending selectively interacting non-polymeric additives. For example, the blending of lithium[37-40] and gold[9] salts in PEO containing BCPs results in an enhanced segregation strength and are known to also induce ordering of otherwise disordered BCPs.[9] In these examples, the salts complex with the PEO blocks and enhance the segregation of the BCPs. This approach of additive-driven assembly is advantageous as it results in the formation of an ordered structure from small BCPs and thus results in smaller domain sizes and d-spacings. In Chapter 2, it was found that favorable hydrogen bonding enthalpic interactions can offset the entropic penalties associated with the incorporation of large homopolymers that results in macrophase separation in weakly interacting BCP-homopolymer blends.[41,42 43] In this chapter, BCP composites with non-polymeric hydrogen bonding additives is considered.

In the case of hybrid materials, high and selective loading of additives is desired as that would serve a number of functions. Firstly, by varying the loading of additives the domain spacing and domain sizes can be caused to change continuously. The loading of additives can also allow access to different morphologies as the BCP system undergoes OOT at particular additive loadings. As mentioned in Chapter 2, the addition of additives is also known to affect the domain orientation and alignment which are desired attributes for many applications. The physicochemical properties of the additives can be largely different from the BCP and therefore their selective incorporation can result in a change in the properties of the incorporating phase while the other phase of the BCP remains unchanged in its properties. Thus phase selective incorporation of functional additives may provide BCP templates an additional versatility for different phase selective treatments such as phase selective reactions or phase selective etch. For example, incorporation of PAA in the PEO phase of a Pluronic BCP can be seen as a means to functionalize the PEO phase with carboxylic acid functionality. Since carboxylic acid functionality is reactive, such selective functionalization of the PEO phase might open new avenues for phase selective reactions.

As mentioned in Chapter 2, although PAA induced a DOT of Pluronic BCPs, 1-propanoic acid, a small, non-polymeric molecule analogous to a single repeat unit of PAA was unable to induce a similar ordering of the Pluronic BCPs. In this chapter, we first explore the structures and the kinds of non-polymeric additives capable of hydrogen bonding with PEO that can induce ordering in Pluronic and other PEO containing BCPs just like PAA does. The aim of this study is to provide design rules of

the molecular architecture and functionalities of non-polymeric additives that allow high loadings and also induce order of disordered BCPs. While such rules are applied to BCPs, such rules is likely be applicable also to homopolymers-additive hybrid materials for cases in which the homopolymer is capable of hydrogen bonding with the additives. It is also important to note that the range of physicochemical properties that can be accessed is increased by making use of non-polymeric additives as illustrated later in this chapter. The use of non-polymeric additives reduces the need for polymerizing the additives before incorporation.

For hybrid materials, it is further desirable to maintain strong phase segregation and order upon the selective addition of additives to one domain of microphase segregated BCP templates. Unfortunately the amount of additives, especially nanoparticles, that can be incorporated into BCPs can be limited as high loadings can disrupt the ordered BCP structure due to entropic penalties associated with polymer chain stretching required to accommodate the additives.[49] In contrast, in this work, additives that have favorable interaction with the incorporating block of the BCPs are used such that the entropic losses are offset by favorable interactions and thus blending is efficient. A poor interaction of the additive with the BCP can allow aggregation or crystallization of the additives which could disrupt the BCP morphology and could lead to macrophase separation.[50] This problem can also be avoided by ensuring a stronger interaction between the additive and the BCP than between the additives themselves so that the chance of additive aggregation or crystallization is reduced.

Hydrogen bond interactions have recently attracted a great deal of attention as a tool for manipulating polymer self-assembly as they can be utilized quite generally due

to many available choices of complementary donor – acceptor functionalities. A rich phase behavior has been observed when selectively associating small molecule additives are blended into microphase segregated BCPs. As described in a recent literature,[51, 52] order-to-order transitions (OOT) and disorder-to-order transitions occur upon addition of small molecules like 3-n-pentadecylphenol to polystyrene-polyvinyl pyridine (PS-PVP) and polyisoprene-polyvinyl pyridine BCPs to obtain well ordered morphologies in bulk as well as in thin films.[53,54] Such additive molecules exhibit phenol groups at one end which enable their supramolecular association with the PVP block through hydrogen bonding interactions.[51] These additive molecules also exhibit long non-interacting alkyl chains that provide access to a complex and varied phase behavior. For example, within a temperature window, microphase separation of alkyl chains from the other phases causes formation of separate domains within the block copolymer domains.[55,56] In contrast, here we focus on non-polymeric additives in which the non-interacting cores are functionalized around their periphery with groups that can form hydrogen bonds to a particular block of the copolymer. This design strategy should enable incorporation of the additive within one domain as the aromatic core is "shielded" from unfavorable interactions with the host domain. As shown here, such a strategy can preserve the native morphologies of block copolymers (i.e. no hierarchical structures would form) while allowing high additive loadings. Ability to functionalize a phase uniformly without formation of hierarchical structures are important to many applications such as block copolymer electrolytes[57] in which well-defined ion conduction pathways are desired or block copolymer lithography[58] which relies on the difference in etch contrast of the different BCP phases. Non-polymeric additives that do

not lead to formation of substructures within BCP domains have also been demonstrated to affect BCP morphology. One example of such an additive is 2-(4′-hydroxybenzeneazo)benzoic acid, which has been used with PS-PVP to control domain orientation and as a means to generate porous structures by subsequent removal of the additive.[17,59-62]

In this chapter an important extension of the phenomenon ordering of Pluronic surfactants with associating homopolymers is reported. First, the incorporation of small, non-polymeric additives that contain multiple hydrogen bonding sites such as phenol or carboxylic acid groups at their periphery is shown to induce order in PEO containing BCPs resulting in formation of well ordered materials at additive loadings up to 40 % (Figure 3.1). This concept is then extended to the incorporation of large non-polymeric molecules at loadings up to 80 % while maintaining the BCP morphology. The highest additive loading while maintaining the order in the BCP composite obtained is found to depend on various factors such as the molecular architecture, number of interacting sites and the ratio of the interacting portion (hydrogen bonding groups) to the non-interacting (cores) portion. Further, while some additives macrophase separate beyond their saturation level in the BCP, certain other additives do not macrophase separate but cause a loss in correlations of the domains formed from the other block as evidenced by disappearance of structure factor peaks in the SAXS profiles.

In comparison to homopolymer additives, non-polymeric additives offer more structural, chemical and functional flexibility in functionalization of BCPs. A vast array of small molecules bearing such hydrogen bonding groups exist and the ones employed here only represent a few possible structures. Since small molecules are monodisperse

in their size and structure they also allow a systematic study by providing a precise control on the size of additive molecules and the number and type of functional groups. It is expect that the principles established here will be of general utility for the design and preparation of well-ordered BCP composites (as well as homopolymer-composites). Indeed, the concept was extended recently Ying Lin at University of Massachusetts Amherst to incorporate similarly functionalized nanoparticles into the PEO phase of PEO containing BCPs to form highly-loaded, well-ordered BCP nanocomposites.[45] A part of this chapter on incorporation of small molecule additives was recently published[63] while the later part on incorporation of large non-polymeric molecules is planned for a separate publication to appear.[45]

In most examples in the literature on BCP composites, the maximum loading of additives is limited. Depending upon the nature of interaction and the size of additives, loadings from a few percent to as high as ~40 % (in a few cases) has been observed. Usually, near neutral interactions between the ligands of the additives and the host polymer has been attempted which requires the ligands to be a large part of the nanoparticle additives. Thus, on the basis of the nanoparticle cores, just a few percent loadings are generally observed. The polymeric part contributed by the BCP and the ligands are still the majority in the blend. However, if the interaction between the ligands and the host polymer was stronger, for example hydrogen bonding, it would lead to higher levels of incorporation of the additives with smaller ligands. Thus on a ligand free basis, higher additive loadings could be envisaged. There is one example, where significantly high loadings of Pt nanoparticles were facilitated by interaction of ionic liquid ligands with suitably designed BCP.[64] Due to high and selective loading, the Pt

nanoparticles bridged together within the incorporating BCP phase upon pyrolysis and mesoporous Pt were obtained upon removal of the remaining carbon. Here, simpler chemistries based on hydrogen bonding are employed to form highly-filled BCP composites with readily available materials. In one case, shown later in detail, the ability to incorporate high loadings of an additive with inorganic cores selectively into the PEO phase is then utilized to form mesoporous silica network by calcination of the ordered blends. This network formation can only occur when the additive cores are situated in close proximity in the PEO phase.

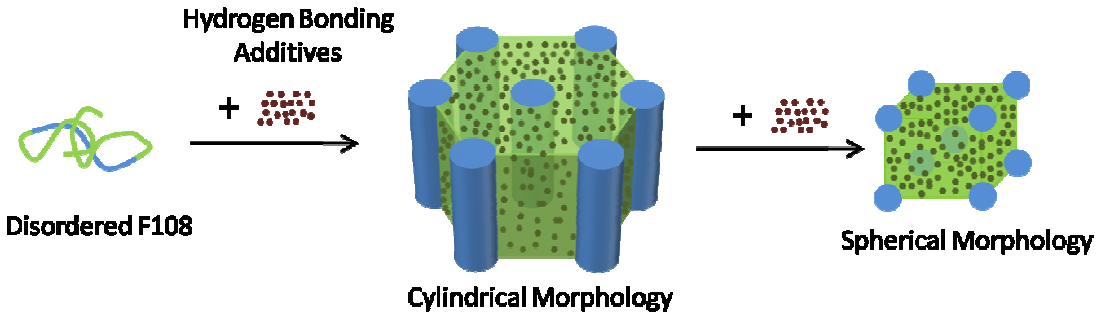

Figure 3.1. Schematic representation of additive driven assembly of disordered F108 induced by blending with hydrogen bond-donating non-polymeric additives. PEO in green forms the matrix containing the dispersed small molecule additive. PPO in blue forms the minority domain, either cylinders or spheres.

3.2 Experimental

3.2.1 Materials

Pluronic BCPs, F108 and P105 that were used are described in Chapter 2. Pluronic F88 (PEO_{109}-PPO_{41}-PEO_{109}, 11.4 kg mol^{-1}), and F68 (PEO_{82}-PPO_{31}-PEO_{82}, 8.4

kg mol^{-1}) each containing about 80% PEO were also donated by BASF. Polystyrene-poly(ethylene oxide) (PS-PEO) of molecular weight 3.8 kg/mol – 4.8 kg/mol was purchased from Sigma Aldrich. Benzene-1,2,3,4,5,6-hexacarboxylic acid (BHCA, M_w= 342 g/mol), benzene-1,2,3,4,5,6-hexol (HHB, M_w= 174 g/mol) and 3,5-Bis(4-aminophenoxy)benzoic acid (BABA, M_w= 336 g/mol) were purchased from TCI America. 5,5'-carbonylbis-(trimellitic acid) (CTMA, M_w= 446 g/mol) was purchased from Sigma Aldrich. Polyhedral oligomeric silsesquioxane (POSS) octa maleamic acid (POSS-OAA, M_w= 1592 g mol^{-1}) and octa aminophenyl POSS (POSS-OAP, M_w= 1154 g mol^{-1}) were purchased from Hybrid Plastics. N,N-dimethylformamide (DMF) and water were purchased from Fisher Scientific. All the materials and solvents were used as received.

3.2.2 Sample Preparation

Appropriate amounts of the required BCP and additives were dissolved in DMF to form 10 wt. % solids solutions on a hot plate set to 65 ^{o}C with occasional gentle stirring. For the case of blends of F108 and BHCA, a 1:1 ratio by weight water-DMF mixture was used as the solvent. The solutions were drop casted on glass slides and kept inside a vacuum oven maintained at 75 ^{o}C for 36 to 48 hours. Solvent mass losses were tracked to confirm that the resulting samples did not contain any residual solvent. The samples made with PS-PEO BCP were also dissolved in DMF, followed by drying at 75 ^{o}C for 6 hours. Following this, they were annealed at 100 ^{o}C for 30 h in a vacuum oven. In this work, compositions are reported as weight ratios of additive to BCP. For

example, a blend referred to as 30/70 contains 30% additive and 70% F108 by weight. This blend is also referred to a 30 % additive blend.

3.2.3 Small-angle x-ray scattering

The setup described and the data processing method described in Chapter 2 was used for the work shown in this chapter as well.

3.2.4 Differential Scanning Calorimetry

The blends prepared for small angle x-ray scattering (SAXS) were also used for differential scanning calorimetry (DSC) to obtain complementary data. Sample masses of 10 to 15 mg were filled into aluminum pans and hermetically sealed. DSC thermograms were measured using a TA Instruments Q100 DSC equipped with an RCS cooling system and nitrogen gas purge with a flow rate of 50 mL/min. All measurements were conducted in the temperature range of -90 ^{o}C to 80 ^{o}C at a constant heating and cooling rate of 10 °C/min under nitrogen atmosphere. Temperature calibration was carried out using Indium as a standard (T_m = 156.6 °C) and the Indium heat of fusion (28.6 J/g) was used to calibrate the heat flow. The reported DSC thermograms were measured during second heating cycle. With the exception of neat F108 the thermograms of the samples are shifted vertically for data presentation. The constants added for this vertical shifting are reported. Universal analysis software was used to calculate the melting enthalpy and the melting temperature associated with the PEO melting endotherm. The calculated melting enthalpies were normalized with respect to the weight of PEO in the blend.

3.2.5 X-Ray Diffraction (XRD)

The samples were prepared freshly and were kept at room temperature for about 30 to 45 minutes after taking out of a vacuum oven heated to 80 ^{o}C following which XRD was performed in the 2θ range of 5 to 35 degrees at room temperature using PANalytical x-ray diffraction system with divergence slit of 1/16″ and X'Celerator detector.

3.2.6 Procedure for the preparation of mesoporous silica

The 50 % and 70 % blends of POSS-OAA and F108 were heated to 70 ^{o}C in a vacuum oven. The temperature was raised slowly to 120 ^{o}C in a period of about 10 hours and then maintained at 120 ^{o}C for one day. Following this, the temperature was raised in a period of 8 hours to 135 ^{o}C and maintained for one day. The temperature was then raised in a period of 8 hours to 160 ^{o}C at which the samples were maintained for 4 hours after which heating was switched off to let the sample cool down to room temperature. These samples were then calcined in the presence of air by ramping up the temperature to 650 ^{o}C in 10 hours, maintaining the temperature at 650 ^{o}C for 8 hours and then ramping down to room temperature in the 10 hours. White mesoporous silica was obtained and characterized using transmission electron microscopy.

3.2.7 Transmission electron microscopy (TEM)

The mesoporous silica samples obtained after calcination were ground to a fine powder and suspended in ethanol. Carbon coated copper grids were dipped into the suspensions to collect the particles on the grid. Ethanol was dried off the grid and TEM

was performed using a JEOL 100CX transmission electron microscope operated at 100 kV. No staining of the samples was performed.

3.2.8 Fourier transform infrared spectroscopy (FTIR)

FTIR of neat F108, neat POSS-OAA and 70 % POSS-OAA blend with F108 were performed using Perkin Elmer 100 infrared spectrometer. Spectra were obtained from 4000 cm^{-1} to 400 cm^{-1}, and were averaged over 32 scans with a 2 cm^{-1} resolution. For all samples, solid material was crushed and placed directly onto the diamond crystal.

3.3 Results and Discussion

The small molecule additives blended with Pluronic BCP F108 are shown in Figure 3.2. This set of molecules allows study of the phase behavior as a function of the identities of the hydrogen bond-donating groups and of the size of the non-interacting cores at progressive additive loadings. BHCA and HHB allow comparison of the behavior of carboxylic acid groups vs. phenol groups in ordering F108 as they both have the same core and the same number of hydrogen bonding groups. Comparison between BHCA and CTMA illustrates the differences occurring due to varying the core size while maintaining the same number of carboxylic acid groups on additive molecules. The incorporation of BABA into F108 establishes the ability of additives bearing different kinds of hydrogen bonding groups (here carboxylic acid and amine) to induce ordering of PEO containing BCPs. The carboxylic acid and amine groups can react together to form an imide upon heating. This imidization would lead to the formation of

a crosslinked network within the PEO phase and is later described in this chapter with another additive, POSS octa maleamic acid (POSS-OAA).

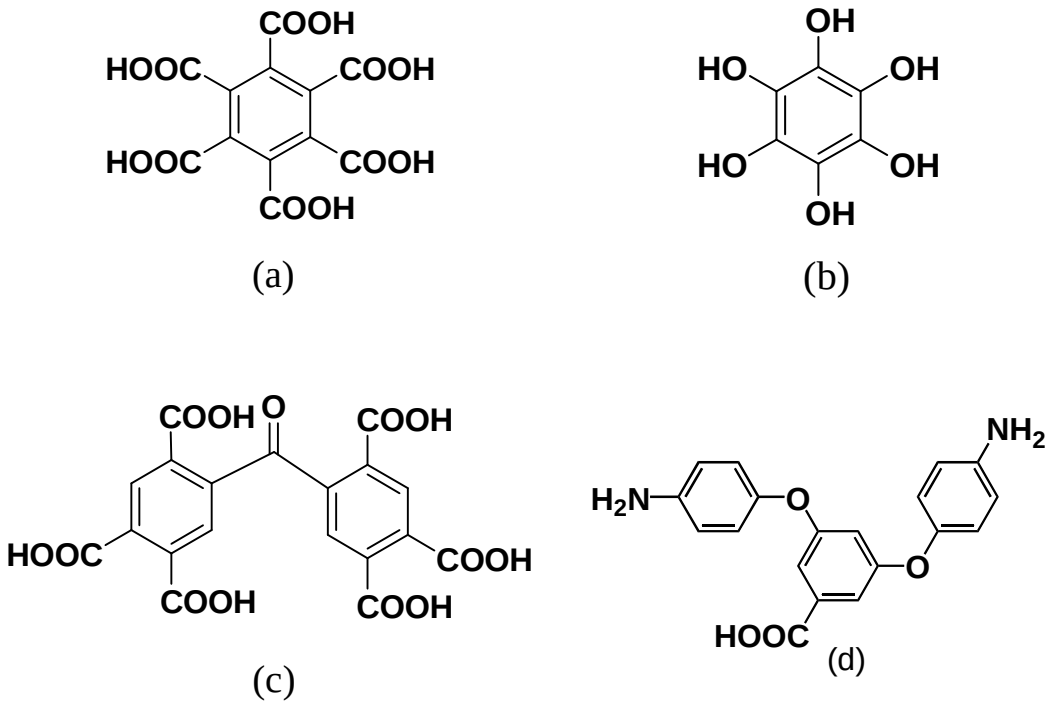

Figure 3.2. Hydrogen bond-donating additives incorporated into the PEO phase of F108: (a) benzene-1,2,3,4,5,6-hexacarboxylic acid (BHCA), (b) benzene-1,2,3,4,5,6-hexol (HHB), (c) 5,5'-carbonylbis-(trimellitic acid) (CTMA), (d) 3,5-Bis(4-aminophenoxy)benzoic acid (BABA).

In order to test the capability of the additives to induce ordering of F108, the phase behavior of their blends was assessed using SAXS. Figure 3.3 shows the SAXS profiles for neat F108 and its blends with BHCA at varying compositions ranging up to 40 % in which the disordered state and cylindrical and spherical morphologies are denoted by letters D, C and S in parenthesis beside the respective profiles. The SAXS profile of F108 shows a broad peak which is due to the correlation hole effect observed

for disordered BCPs.[6,47] This is expected as F108 is expected to be disordered at the measurement temperature of 80 ^{o}C.[48] As BHCA is blended, the peak gradually sharpens indicating an apparent increase in the segregation strength, χN, between the PEO and PPO blocks. At 10 % loading of BHCA the blend is ordered as indicated by a sharp primary peak together with appearance of a higher order peak. Multiple higher order peaks at 30 % BHCA loading indicate formation of well ordered cylindrical morphology. Thus loadings of BHCA from 10 % to 30 % resulted in formation of cylindrical morphology. Since F108 is PEO rich, PEO + BHCA form the matrix whereas PPO forms the cylindrical domains. As more BHCA was incorporated, the morphology of the blend transitioned into well ordered spherical morphology at 40% loading. On a BCP phase diagram, the state of blends of F108 and BHCA may be visualized to traverse from disordered to cylindrical morphology to spherical morphology regions as the loading of BHCA increases progressively.

While neat F108 is disordered at 80 ^{o}C, the favorable enthalpic interactions created by maximizing the number of contacts between the additive and the PEO chains drive the disorder-to-order transition for blends of F108 with BHCA, resulting in an increase in the ODT temperature. The effect of weakening the hydrogen bond strength by increasing the temperature was explored for blends containing 10 % and 20 % BHCA between 60 ^{o}C and 120 ^{o}C as shown in Figures 3.4 (a) and 3.4 (b). The 10 % BHCA blend was found to be ordered at 100 ^{o}C but disordered at 120 ^{o}C indicating that the ODT temperature of this blend falls between 100 ^{o}C and 120 ^{o}C. The 20 % BHCA blend remained ordered up to 120 ^{o}C indicating that the ODT should be higher than 120 ^{o}C. For the case of 20 % BHCA blend since there are more additive molecules present, a

larger number of hydrogen bond associations are possible for PEO chains which are sufficient to maintain order up to 120 ^{o}C. It is expected that blends containing 20 % or more BHCA would disorder at an even higher temperature but we did not identify the ODT temperatures in these cases as experiments at greater than 120 ^{o}C are complicated by reaction of the carboxylic acid groups to produce anhydrides.[65] In comparison, as expected, the neat F108 is disordered between 60 ^{o}C and 120 ^{o}C as shown in Figure 3.4 (c).

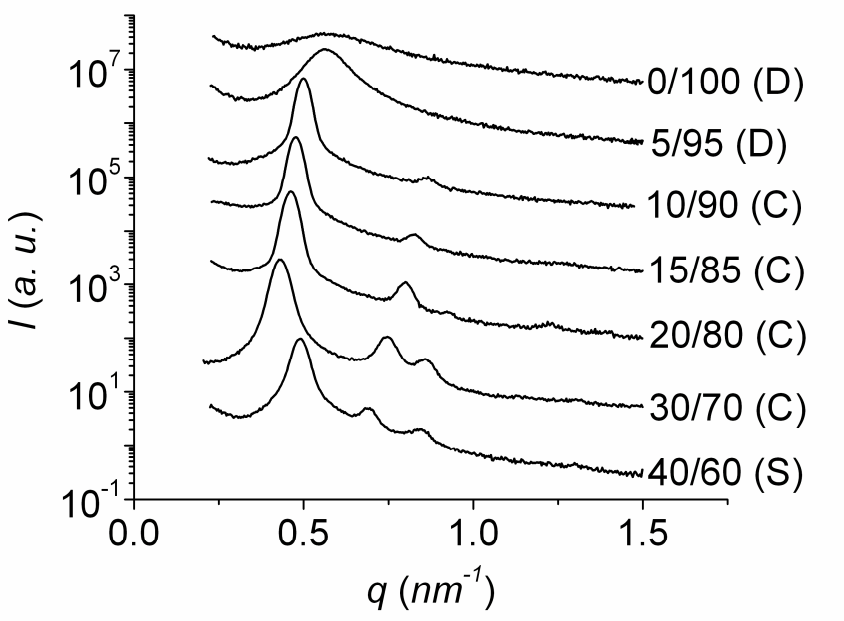

Figure 3.3. SAXS profiles of blends of F108 and benzene-1,2,3,4,5,6-hexacarboxylic acid (BHCA) as a function of composition at 80 ^{o}C. The disordered state and cylindrical and spherical morphologies of the blends are denoted by D, C and S, respectively.

A closer look at the scattering profiles with increasing BHCA (Figure 3.3) loading reveals some important features of the phase behavior of the composite. The continuous progression in the location of the primary peak (d-spacing of the composite) and the appearance of an OOT from cylindrical to spherical morphology is consistent

with molecular level incorporation of BHCA in F108. The analysis of the data also suggests that BHCA exhibits limited compatibility with the PEO domains at high additive loadings. The SAXS data suggest that the maximum BHCA loading is about 40 % as the SAXS profile for 50 % loading of BHCA matched in peak positions and morphology to that obtained for 40 % loading, suggesting that addition of BHCA above this point leads to macrophase segregation. This system was therefore studied up to 40 % loading of BHCA. Furthermore, in addition to indicating molecular level incorporation of BHCA, occurrence of OOT from cylindrical to spherical morphology between 30 % and 40 % loading of BHCA indicates qualitatively that the incorporation of BHCA must be selective towards PEO thereby causing a reduction in the relative volume fraction of the PPO phase leading to formation of spherical morphology. Scaling of interplanar spacing with composition as discussed later further suggests that this indeed is the case.

We next explore the effect of the nature of hydrogen bond-donating group (i.e. carboxylic acid vs. phenol groups) of the additive molecules on the ordering of F108 by comparing the behavior of the BHCA and HHB additives. Since the interaction of additive molecules with PEO chains drives the ordering of F108, a change in the functional group must affect the strength of interaction, which should affect the incorporation of additives and the consequent phase behavior. Figure 3.5 shows the scattering profiles of blends of F108 with HHB loaded up to 30 %. Qualitatively, the phase behavior of HHB blends is similar to that observed with BHCA. The broad correlation hole peak of neat F108 sharpens into a primary peak and higher order peaks appear as HHB composition increases, indicating disorder-to-order transition due to

enhanced segregation strength between PEO and PPO chains. However, the change in segregation strength upon addition of HHB to F108 is found to be less than that with BHCA. This can be seen by comparing the SAXS profiles at 10 % loading in both cases. While 10 % BHCA caused formation of well ordered morphology, 10 % HHB blend is not ordered even though the number of carboxylic acid groups contributed by BHCA per equivalent volume fraction of additive is less because of its higher molecular weight than HHB. Thus, carboxylic acid groups are found to be more efficient at causing ordering of F108 than phenol groups which seems to indicate that as compared to phenol groups, carboxylic acid groups interact more strongly with the ether oxygen of PEO. Upon addition of 15 % to 30 % loading of HHB, an ordered cylindrical morphology appears similar to that seen for BHCA at same loadings. The scattering profiles of blends with loadings higher than 30 % did not show variation in position of primary peak or OOT and therefore the saturation level of HHB in F108 must be close to 30 %. Thus, by comparison, the carboxylic acid functionality was slightly more effective for achieving high additive loading as compared to phenol functionality.

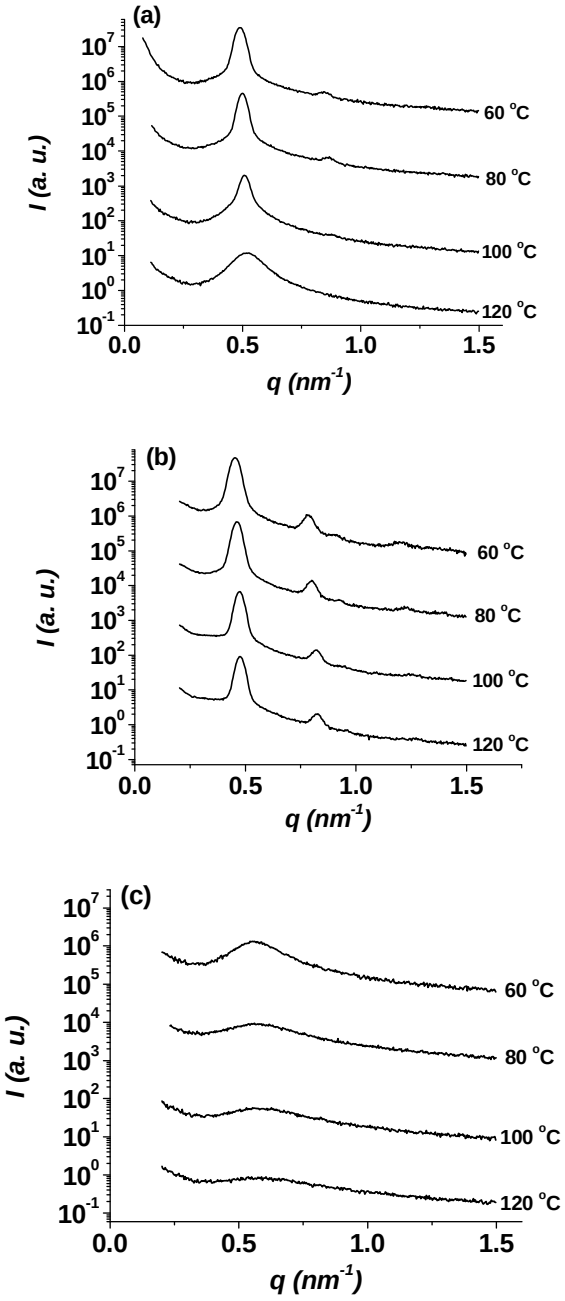

Figure 3.4. SAXS profiles of (a) 10 % BHCA, (b) 20 % BHCA, (c) neat F108 at varying temperatures.

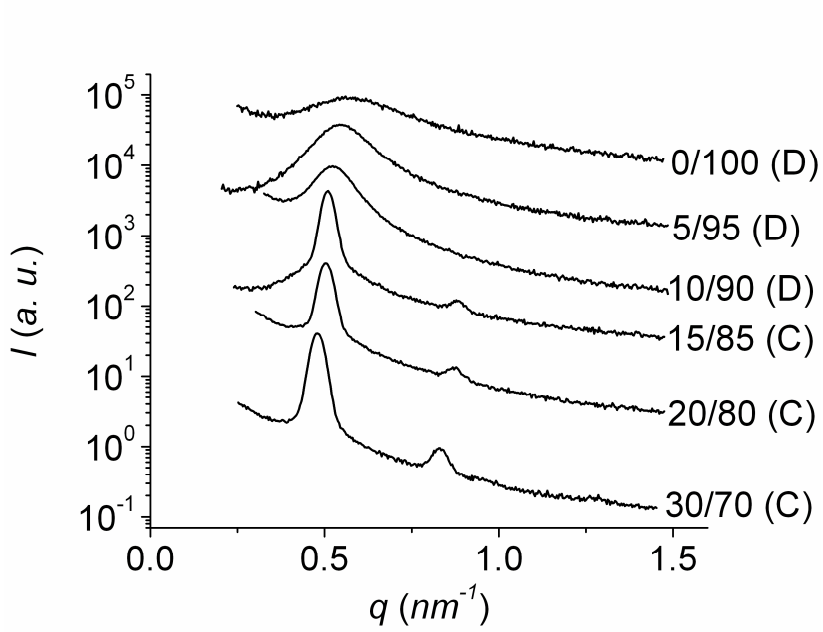

Figure 3.5. SAXS profiles of neat F108 and its blends with benzene-1,2,3,4,5,6-hexol (HHB) at 80 ^{o}C. The disordered state and the cylindrical morphology of the blends are denoted by D, and C, respectively.

Next, the effect of increasing core size of additive molecule while maintaining the same number of hydrogen bonding interaction sites on each molecule was explored by comparing the behavior of BHCA and CTMA for which the core size is about double that of BHCA. The SAXS profiles obtained for blends of F108 with CTMA are shown in Figure 3.6. As the size of the core is increased while maintaining the same number of carboxylic acid groups, the number of available carboxylic acid groups added is decreased at a particular additive loading. This impacts segregation strength and at a 10 % loading, while BHCA blend is ordered, CTMA blend is not yet ordered. By comparison to BHCA, the range of composition within which CTMA blends form cylindrical morphology is smaller. While 30 % BHCA blend shows cylindrical morphology, 30 % CTMA blend showed spherical morphology. This implies that simply by varying the molecular structure of the additives the resulting blend

morphology may be varied at the same additive loading, i.e., at the same relative volume fraction of the two phases formed. A transition from cylindrical to spherical morphology should occur at a point when the entropic penalty of stretching the PEO and PPO chains away from the interface exceeds the entropic penalty in causing additional interfacial curvature in transitioning from cylindrical to spherical morphology.[42] The OOT occurs at a lower composition of CTMA than BHCA, which may imply a larger capacity of CTMA to affect chain density at the interface and thus the chain stretching. This in turn may imply that CTMA is present closer to the PEO-PPO interface than BHCA. CTMA blends showed systematically varying scattering profiles up to 45 % loading which was the maximum loading explored without any signs of macrophase separation. In contrast, as described earlier, the saturation level for BHCA and HHB was found to be 40 % and 30 % respectively. At 45 % loading a loss in structural correlation of the PPO spheres occurs as seen from the broadening of the primary peak and the disappearance of the higher order structure factor peaks.

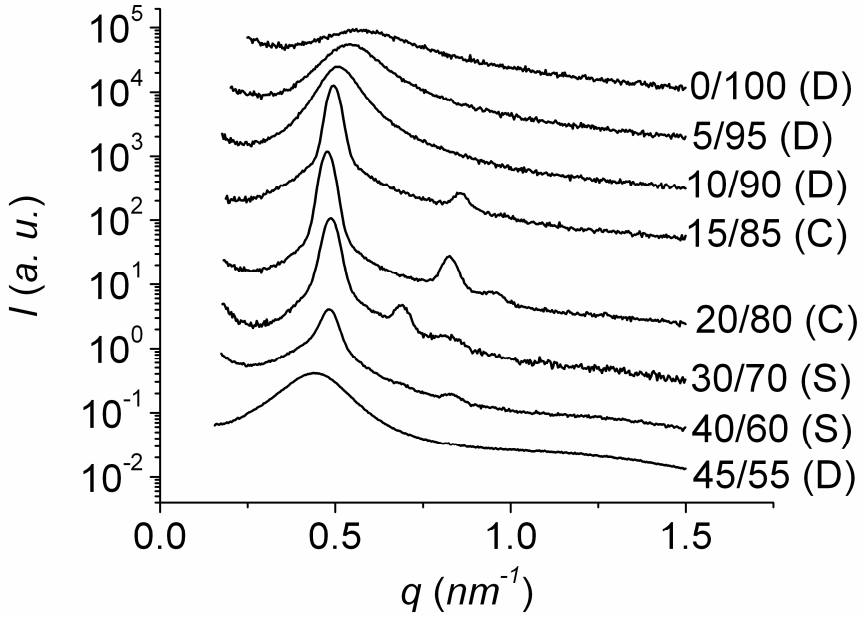

Figure 3.6. SAXS profiles of neat F108 and its blends with 5,5'-carbonylbis-(trimellitic acid) (CTMA) as a function of composition at 80 ^{o}C. The disordered state and cylindrical and spherical morphologies of the blends are denoted by D, C and S, respectively.

The SAXS profiles of blends of F108 with 3,5-Bis(4-aminophenoxy)benzoic acid (BABA) are shown in Figure 3.7. It is seen that while at 20 % loading the primary peak is a little narrower than that of neat F108 indicating an increase in the segregation strength, at 25 % loading, a well-ordered spherical morphology formed. This behavior is different from the other additives in that an intermediate cylindrical morphology is not observed. Thus the range of composition of this blend in which the blends remain ordered is smaller than the other additives. This highlights the need for optimization of the structure and the chemical functionalities on the additives to achieve high loadings. While it requires a further detailed study to systematically characterize the trends, it is noted here that at the same loading of different additives the morphology formed can be

different. These differences often arise from the organization of the additives and their ability to affect the chains at the domain interface. For example, for the case of homopolymer additives it is well known that when the additives are situated closer to the interface, they tend to cause an OOT at lower concentrations but a smaller change in domain spacing than the case when additives are situated farther away from the domain interface.[41,42] Since the range of compositions of blends with BABA at which an ordered morphology forms is quite narrow, this molecule was not investigated further and in the following, only BHCA, HHB and CTMA are studied in further detail.

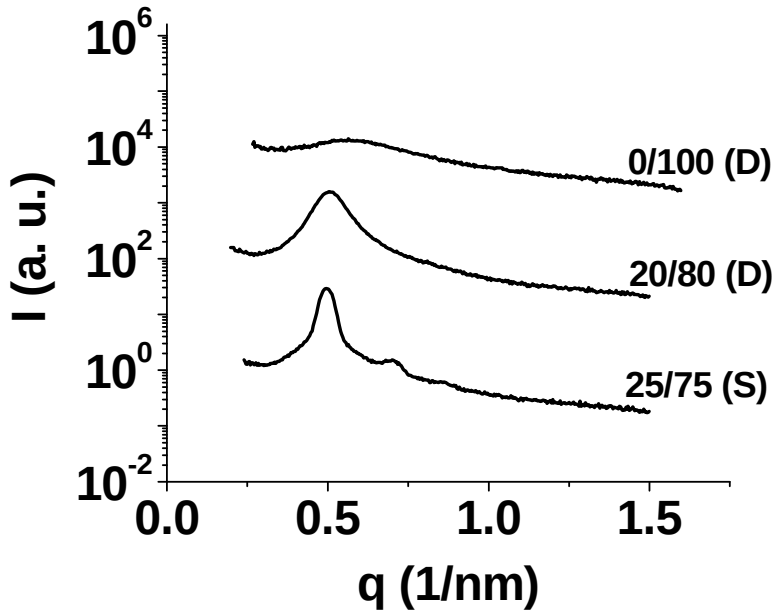

Figure 3.7. SAXS profiles of neat F108 and its blend with 3,5-Bis(4-aminophenoxy)benzoic acid (BABA) at 80 ^{o}C. The disordered state and spherical morphologies of the blends are denoted by D, and C respectively.

Comparison of the full width at half maximum (FWHM) of the primary peaks of the SAXS profiles provides a comparison of the degree of order in BCP systems.[36,62] Smaller FWHM corresponds to a higher degree of segregation and overall order. The

primary peaks for all blends were fitted to a Gaussian curve and the values of FWHM obtained were plotted against blend compositions as shown in Figure 3.8.[66] For all additives, the FWHM value decreases from that of neat F108 indicating an increase in segregation strength upon addition of additives. At lower loadings, BHCA blends show the largest drop in FWHM which indicates that BHCA has the highest tendency to cause phase segregation of F108. The FWHM values of CTMA and HHB blends are larger than BHCA with that of CTMA being slightly lesser than that of HHB. The FWHM values decreases rapidly initially with loading of additives indicating a sudden jump as disorder-to-order transition occurs and then follows a slowly increasing trend with further increase in the loading of additives. After the initial dramatic reduction in FWHM, the FWHM for blends with different additives are comparable in the intermediate composition range (probably due to detector resolution limit) and preclude any comparison. Even so, as seen next, the primary peak positions provide a comparison between segregation strengths induced by various additives. The FWHM of CTMA covered the entire range of behavior, i.e., initial rapid decrease, followed by a gradual increase in the ordered region and then a rapid increase at high loadings implying order-to-disorder transition.

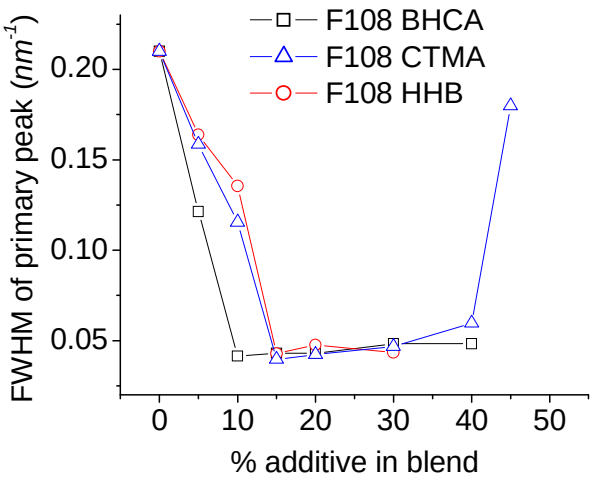

Figure 3.8. Full width at half maximum (FWHM) of the primary scattering peaks for blends of F108 with BHCA, HHB and CTMA.

Figure 3.9 (a) compares the variation of primary peak position, q* for all blends. The value of q* is the smallest for BHCA and largest for HHB within a particular morphology with CTMA falling in between. A sudden increase in the q* value at 40% for BHCA and at 30% for CTMA is due to OOT from cylindrical to spherical morphology while HHB blends remained cylindrical in the composition range explored. The interplanar spacing between 100 planes of blends forming cylindrical morphology was estimated as $2\pi/q^*$ and plotted against the weight fraction of F108 on a log-log scale in Figure 3.9 (b). The value of scaling exponent β in the relation $d \sim \phi_p^{-\beta}$ of interplanar spacing (d) vs. volume fraction of BCP (ϕ_p) can be useful in identifying the selectivity of the additives.[67] Positive value of β indicates selectively of additives towards one of the phases. In this work, assuming that the density of additives is the same as the density of F108 the interplanar spacing vs. volume fraction for the blends formed with the three additives have been fitted as shown in Figure 3.9 (b) according to

the relation, $d = A\phi_p^{-\beta}$, where the prefactor A represents a hypothetical interplanar spacing of neat F108 had it been ordered. The value of A was set to 11.852 nm and the d vs. ϕ_p data was fitted to estimate the β exponents. This value of A was found to minimize the sum of squares of residuals for all the three fittings.[68] The values of scaling exponent, β, for the case of BHCA, HHB and CTMA were found to be 0.595, 0.264, and 0.455 respectively.

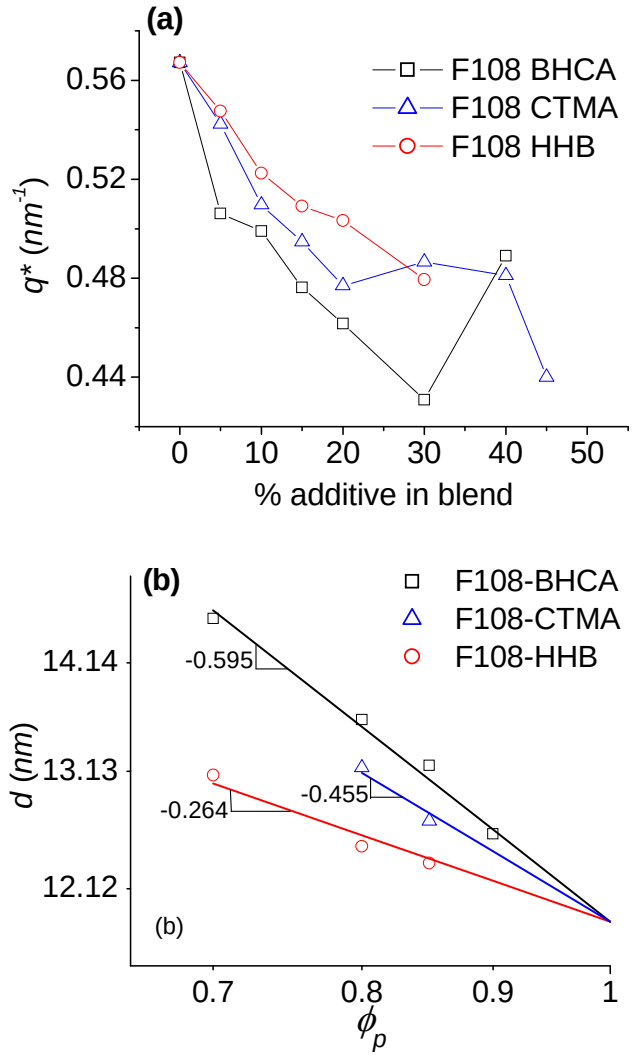

Figure 3.9. Comparison of behavior of BHCA, HHB and CTMA additives: (a) variation of position of primary peak for blends, (b) scaling of interplanar spacing with composition (ϕ_p) for blends that formed cylindrical morphologies.

Compared to values in literature for other systems,[67] such positive and high values indicate strong selectivity of the additives towards PEO phase as the systems order. Although these values are estimated assuming that the density of additive molecules are the same as that of F108, the scaling exponents could be estimated more precisely by using liquid-like densities as the density of additives. However, such values are not reported in part because BHCA and CTMA contain carboxylic acid groups which undergo dehydration below melting temperature. Since additive molecules interact favorably among themselves via hydrogen bonding, the liquid-like densities of additives are expected to be at least as small as F108 if not higher. If the densities of the additives were higher than that of F108, even higher β exponents would result. Therefore the values estimated above represent the lower bounds of the scaling exponents. Although all the three additives are strongly selective towards the PEO phase, their blends differ in the domain spacings formed at the same loadings. This is attributed to the differences in the capacity of the additives to enhance the segregation strength. As segregation strength increases, the domain interface becomes narrower and the polymer chains stretch farther away from the domain interface leading to larger domain spacing. Such a behavior is commonly observed in other BCP systems in which temperature dependent variations in segregation strength shift the domain spacing.[69-71] Similar behavior is observed for the 10% and 20% BHCA blends (see supporting information). Among the three additives employed in this work, the SAXS data indicates that BHCA enhances the segregation strength most effectively followed by CTMA and then HHB. Therefore, BHCA blends form the highest domain spacing followed by CTMA and then HHB.

The strength of interaction of the additives with PEO chain segments and consequently their miscibility with PEO phase can be compared by comparing the DSC thermograms of neat F108 with that of various blends.[13] The DSC thermograms obtained between -60 ^{o}C to 75 ^{o}C for neat F108 and its blend with the additives BHCA, HHB, and CTMA are shown in Figure 3.10. The thermograms for the blends were shifted vertically by adding constant values to heat flow. The values of the shifts are given in parenthesis beside the thermograms. Neat F108 is characterized by a melting endotherm associated entirely with the melting of PEO crystallites because PPO does not crystallize and therefore shows no melting. As the additives are blended they associate with the PEO segments, impede their crystallization and cause a lowering of the PEO melting temperature. The general trend observed upon blending additives is that the melting endotherm peak becomes smaller and its peak position shifts systematically to lower temperatures, which indicates molecular scale interaction and of the additives with PEO chains. The behavior of the three additives can be better compared by comparing the melting enthalpies normalized by the weight of PEO in the blends and the melting temperatures represented by the endotherm peak positions. These comparisons are plotted in Figure 3.11 as a function of the blend compositions. BHCA caused maximum changes in these values from neat F108 indicating the strongest interaction with PEO which is consistent with the earlier mentioned observations of least FWHM of the primary scattering peaks and largest domain spacing for BHCA blends. The interaction of HHB with PEO is the weakest out of the three additives while CTMA ranges in between BHCA and HHB. It is clear from this data that while all the three additives showed favorable enthalpic interaction with PEO,

carboxylic acid groups promote stronger interaction with PEO chains than phenol groups.

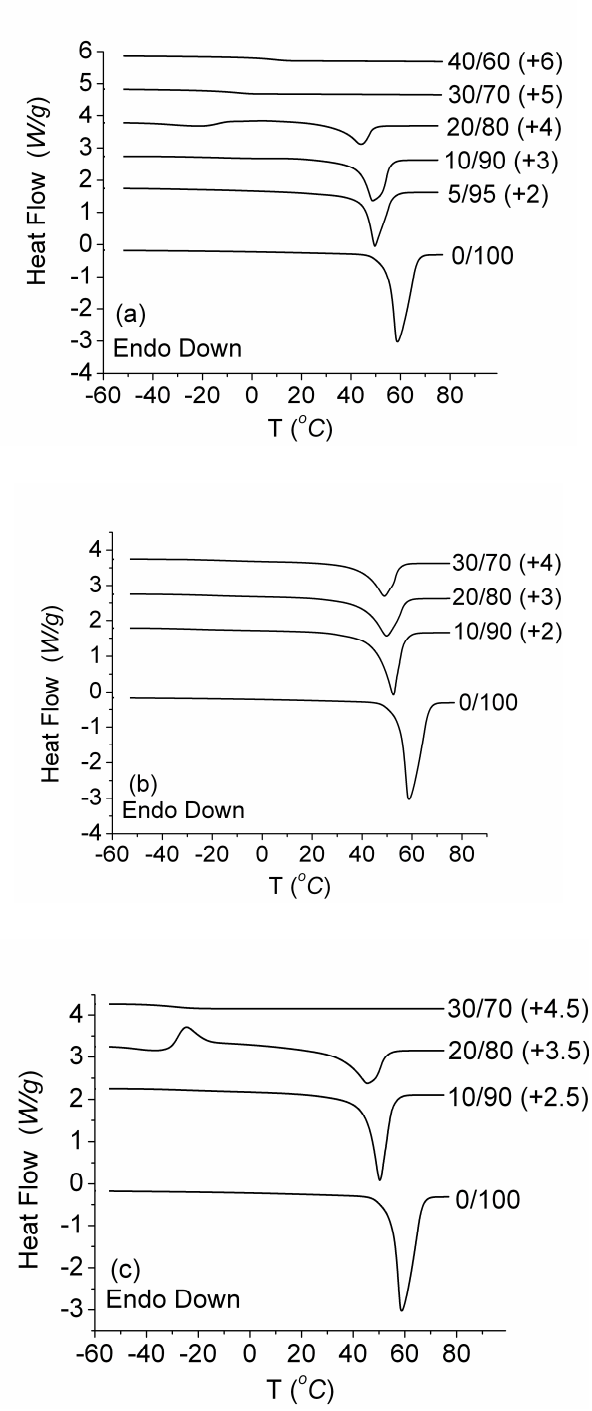

Figure 3.10. DSC thermograms of neat F108 and its blend with (a) BHCA, (b) HHB, and (c) CTMA. The constants added to the heat flow values to shift the blend thermograms vertically upwards are shown in parenthesis.

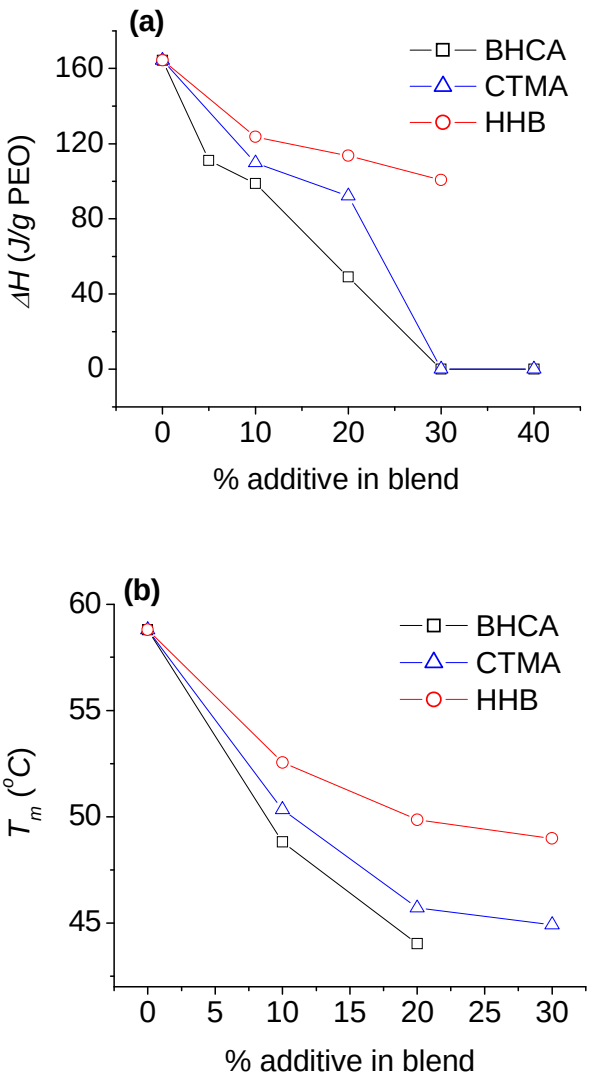

Figure 3.11. Analysis of endotherm peaks obtained for blends with varying BHCA, HHB and CTMA compositions: (a) melting enthalpy normalized by the PEO concentration in the blends, (b) melting temperatures corresponding to the endotherms.

A smaller change in melting enthalpy for HHB blends also supports the finding from SAXS that hydrogen bond strength between HHB and PEO is less than the hydrogen bond strength between BHCA and PEO. Since PEO has a strong tendency to

crystallize, weaker interaction energy of PEO with HHB allows more PEO segments to crystallize.

Having characterized the behavior of small molecules as additives to BCPs, in the following, the possibility of incorporation of larger non-polymeric additives is explored. Blends of rigid nanoscale fillers and polymers are of interest for a wide range of applications. Among these, block copolymer (BCP) nanocomposites[27] are an important class of materials in which the block copolymer guides the spatial location and periodic assembly of the additives governed by the nanostructured periodic morphologies that BCPs can form.[5-7] The difference between the chemical nature of the constituent blocks can be utilized to direct the organization of additives such as small molecules, homopolymers and nanoparticles.[18,19,36,44,51,72, 52,63] Certain nanoparticles have been formed in-situ in pre-organized BCP thin film templates by phase selective reactions, however, the method is limited due to the need for specific functionality in the incorporating block as well as other synthetic and mass transport challenges.[73-77] The incorporation of additives within one of the phases can create functional materials or enhance differences in the chemical and/or physical characteristics of the domains, which can be exploited in many applications. In block copolymer lithography the etch resistance of one of the phases can be enhanced by selective incorporation of materials with higher etch resistance[78,79]. BCP composites can also find use as low line edge roughness resists for nanoscale electronics[8] and as templates for the fabrication of nanoscale microelectronic structures including high density data storage media.[9-11] BCP composites materials are also of interest as materials in devices such as photovoltaics[20-22] and photonics.[23-25] The other area where BCP composites might find applications is

their use as templates for the fabrication of inorganic mesostructured materials via phase selective reactions[12-14] or the formation of nanoporous polymeric materials by treating the BCP composites to phase selective treatments to remove the minority phase[15-17] in which the phase selective functionalization might provide new avenues in phase selective reactions. In some cases, the additives have been used to influence domain orientation and cause the domains of the BCP to orient perpendicular to the substrate[80-83] which is desired for many applications mentioned above.

In the rest of this chapter, it is demonstrated that by tuning the interaction of the additive with the incorporating block, additives with large cores can be incorporated at very high loadings (up to 80 %) while maintaining the block copolymer morphology (Figure 3.12**)**. We chose polyhedral oligomeric silsesquioxanes (POSS) cages, which are about 1 nm in size, as the core. The POSS cages are functionalized on all eight silicons with maleamic acid ligands that bear carboxylic acid and secondary amines as the hydrogen bonding sites. This additive is referred to as POSS-OAA in this chapter. As explained in more detail later, choosing these functionalities not only assists in the formation of highly-filled BCP nanocomposites but also allows phase selective crosslinking. Two block copolymers containing PEO as one of the blocks are chosen as templates, namely Pluronic tri-block copolymer surfactants (PEO-PPO-PEO) and polystyrene-poly(ethylene oxide) (PS-PEO).

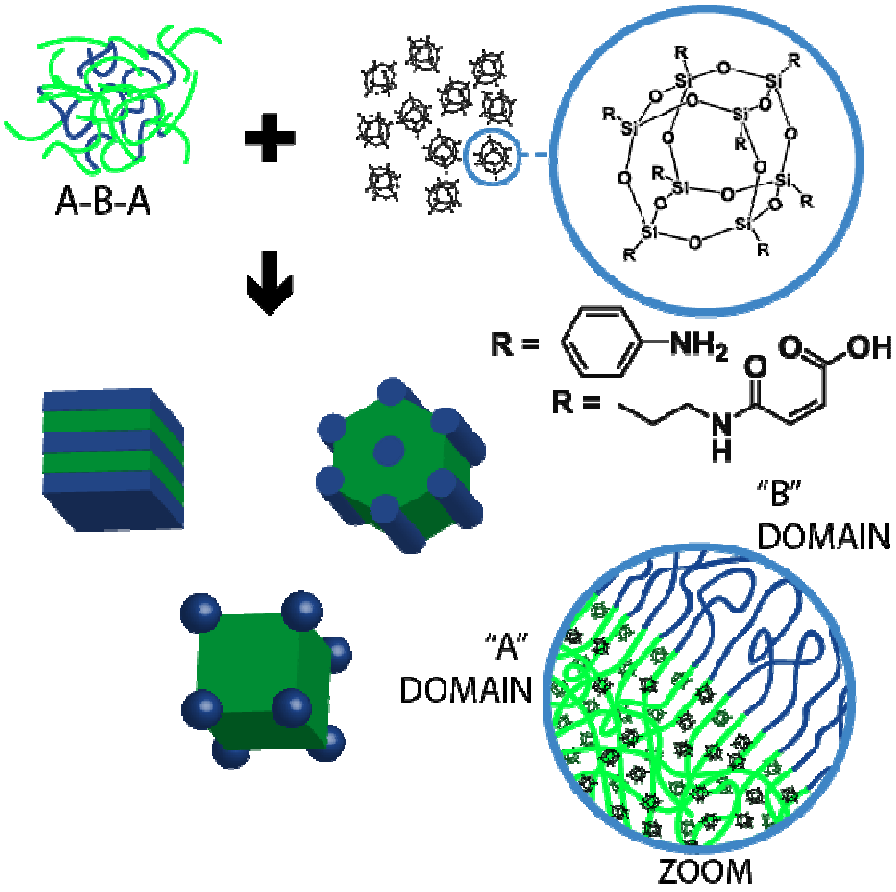

Figure 3.12. Schematic showing disorder-to-order transitions of poly(ethylene oxide) containing block copolymers induced by blending of polyhedral oligomeric silsesquioxanes functionalized with maleamic acid or aminophenyl groups. Strong and selective hydrogen bonding interaction of the additives with the poly(ethylene oxide) block (green chains) results microphase segregation of the PPO blocks (blue chains) to form well ordered BCP composites in which the additives are sequestered into the PEO (green) phase.

The choice of PEO containing disordered BCPs is motivated by the fact that PEO can act as a good hydrogen bond acceptor and therefore selectively interacts with hydrogen bond donating additives. This results in the formation of BCP nanocomposites with high and selective additive loadings as well as small d-spacings. Hydrogen bond interaction between the additive and PEO blocks leads to a strong segregation of the PPO chains and excellent local order even at high additive loadings. Thus, the favorable

enthalpic interaction between the additive and the incorporating block overcomes the entropic penalties, including chain stretching around the nanoscopic additives, that result from incorporation of the additives.[49] The strong interaction between the additive and block copolymer also serve to suppress additive aggregation. Additive aggregation is not only often undesirable in terms of materials properties, but large aggregates can also disrupt the BCP structure.[50] As is discussed later, the neat POSS-OAA additive tends to crystallize but when blended in the PEO phase, its crystallization is quenched which implies the presence of strong favorable interaction with the PEO chain segments.

The choice of POSS as the additive core is useful for a variety of applications. In general, high loadings of well-dispersed rigid nanofillers are important to mechanical reinforcing of polymers and POSS is often used for this purpose. Specifically, POSS cages, tightly bound within an organic matrix can condense to form silica upon calcination.[84] We utilize this attribute to show that at high loadings, the BCP/POSS composites can yield well-ordered mesoporous silica films directly upon heating in the presence of air. In another application, self-assembled BCP templates with etch resistant POSS cages chemically grafted to one of the block were demonstrated useful in block copolymer lithography.[78] The strategy of simply blending the POSS cages rather than incorporation by chemical grafting is advantageous not only because of reduction in the synthetic inputs but also because the BCP may be varied independently to access the desired morphologies and d-spacings.

The structure of POSS-OAA is shown in Figure 3.13. We compare the two additives in terms of their interaction with the PEO chains and the corresponding phase

behavior of their blends and the morphologies obtained. We express loadings in terms of weight percent of the additive. Thus it should be noted that because the mass of the ligands on POSS-OAA is larger than that of the ligands on POSS-OAP, the POSS cage loading in the PEO phase on a ligand free basis is greater for the POSS-OAP blends at equivalent additive loadings.

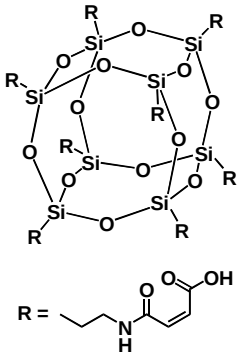

Figure 3.13. Structure of POSS octa maleamic acid (POSS-OAA, M_w= 1592 g/mol).

First the phase behavior of blends of POSS-OAA with F108 is presented. SAXS was performed at 80 ^oC to avoid complications from PEO crystallization. As shown in Figure 3.14 while the neat F108 shows a correlation hole peak that is a characteristic signature of disordered BCPs,[6] incorporation of POSS-OAA induced microphase segregation to form well-ordered morphologies as indicated by sharpening of the primary peak and presence of multiple higher order reflections. In this system, PPO forms the minority phase and PEO + POSS-OAA form the matrix. Selective incorporation of POSS-OAA in the PEO rich domain is confirmed by XRD, DSC and TEM characterization as discussed later. At 50 % loading of POSS-OAA a blend with well-ordered hexagonally packed cylindrical morphology was obtained with a d-spacing

(= $2\pi/q^*$) of ~16 nm. Upon increasing the loading of POSS-OAA to 55 %, the well-defined structure factor peaks disappeared implying an ill-defined morphology as an order-to-order transition (OOT) from cylindrical to spherical morphology is traversed. At 65 % loading the structure of the blend transitioned into a well-ordered body centered cubic spherical morphology with a d-spacing of 14.5 nm. This transition from cylindrical to spherical morphology also indicates the selective incorporation of POSS-OAA in the PEO phase which causes the volume fraction of PPO to decrease until OOT occurs. The spherical morphology persisted at 70 % loading but at 80 % loading, the peaks began to broaden implying a weakening of structural correlations. These samples were found to be optically clear at all compositions and the SAXS profiles varied systematically as a function of composition indicating that macrophase separation of POSS-OAA from F108 did not occur.

One unique feature of these composites is that the fraction of minority phase (PPO) at which the OOT from cylindrical to spherical morphology occurs is significantly lower than the expected volume fraction of 0.2. For instance, for the blend containing 60 % POSS-OAA which is nearly the concentration of POSS-OAA at which the OOT occurs, the weight fraction of the PPO phase is just 0.08. This weight fraction of PPO corresponds to a volume fraction of 0.09 (assuming density of PEO, PPO and POSS-OAA = 1.18, 1.04, and 1.25 g/cm^3 respectively) which is significantly smaller than 0.2. This deviation might be due to the high PDI of the F108 BCP as explained by Hillmyer and coworkers[85] or (as seen in Chapter 2) could be due to a thin PEO layer at the PPO interface in which the POSS loading is not very high in which case the

tendency for stretching of PEO and PPO chains away from the domain interface would be lowered.[86]

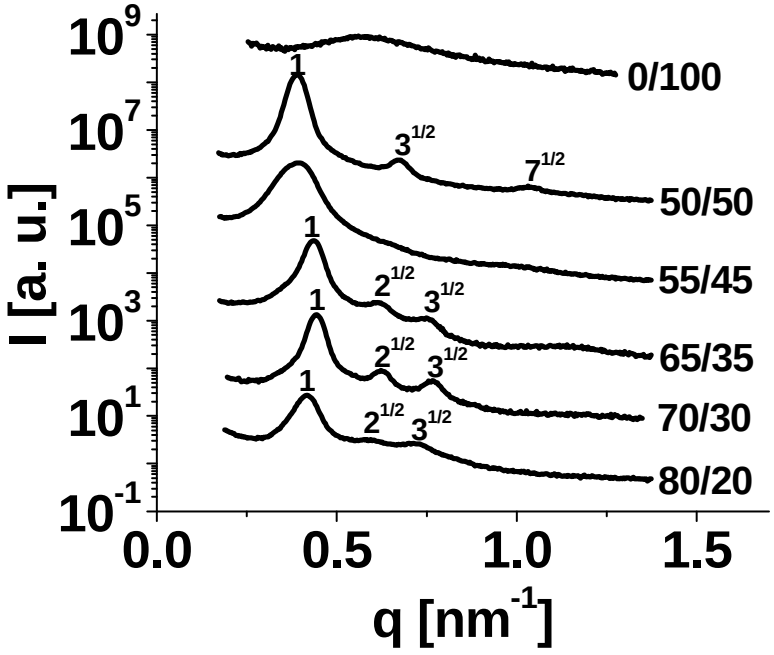

Figure 3.14. SAXS profiles of neat F108 and its blends with POSS-OAA at 80 °C.

The mass of the POSS cage is 26.2 % of the entire POSS-OAA molecule and therefore a loading of 80 % POSS-OAA translates to 21 % loading of the inorganic cores. The formation of such highly-loaded and well-ordered composites is promising because it shows how suitable chemical functionalities can lead to high levels of incorporation of additives thereby significantly altering the properties of the host polymer. It is also interesting to find that just a little F108 can guide the spatial assembly of a large quantity of POSS-OAA while maintaining the block copolymer morphology. This is a particularly interesting finding in light of the literature, which suggests that the entropic penalty associated with polymer chain stretching around the

additives tends to cause macrophase separation of the additive from the polymer and thus sets a limit to the maximum loading.[49] Thus, this method of providing the system with enthalpically favorable interactions to offset entropic penalties of polymer chain stretching around the additive molecules as well as stretching away from the domain interface, holds promise for incorporation of a variety of cores into PEO containing block copolymers. It is interesting to note that the concentration of POSS-OAA in the PEO phase of the ordered composite can be as high as 83 % by weight with only ~17% PEO. This is in contrast to the other BCP-additive systems in which the BCP has to remain the major component.

In typical BCP systems it is expected that as the additive molecules are incorporated selectively into one of the phases, they should cause domain swelling and thus an increase in d-spacing and increases up to a factor of 2 has also been reported in other systems.[41,42] While a similar increase in the d-spacing was observed for blends of F108 with small molecule additives such as BHCA, HHB and CTMA (see Figure 3.9) for the blends of F108 with POSS-OAA the d-spacing is nearly invariant even at very high loadings of additives. Likewise, for the case of poly(acrylic acid) homopolymers as additives, the d-spacing of its blends with Pluronic BCPs was found not to vary significantly (see chapter 2).[44] One could argue that perhaps the POSS additives macrophase separate above a certain loading, but the systematic variation in the SAXS profiles as explained earlier (OOT from cylindrical to spherical morphology) indicates molecular level changes which cannot occur if the POSS additives were to macrophase separate.

Blends of POSS-OAA with other Pluronic BCPs resulted in the formation of smaller d-spacings as well as lamellar morphology for the case of a symmetric Pluronic BCP. POSS-OAA was blended at 50 % loading with various Pluronic BCPs namely, F88 (PEO_{109}-PPO_{41}-PEO_{109}, 12 kg mol^{-1}), F68 (PEO_{82}-PPO_{31}-PEO_{82}, 9 kg mol^{-1}) and P105 (PEO_{34}-PPO_{52}-PEO_{34}, 6 kg mol^{-1}) and the SAXS profiles of the blends obtained are shown in Figure 3.15. Both F88 and F68 contain 80 % PEO like F108 and therefore the effect of changing N can be observed by comparing the behavior of F108, F88 and F68. Like F108, F88 also forms cylindrical morphology at 50 % loading of POSS-OAA, but at a slightly smaller d-spacing of 14 nm. In the case of F68, the scattering profile had a broad first peak without any higher order peaks indicating that the segregation of F68 was not sufficient to form an ordered morphology. Pluronic P105 is symmetric and formed lamellar morphology at a d-spacing of 13.4 nm.

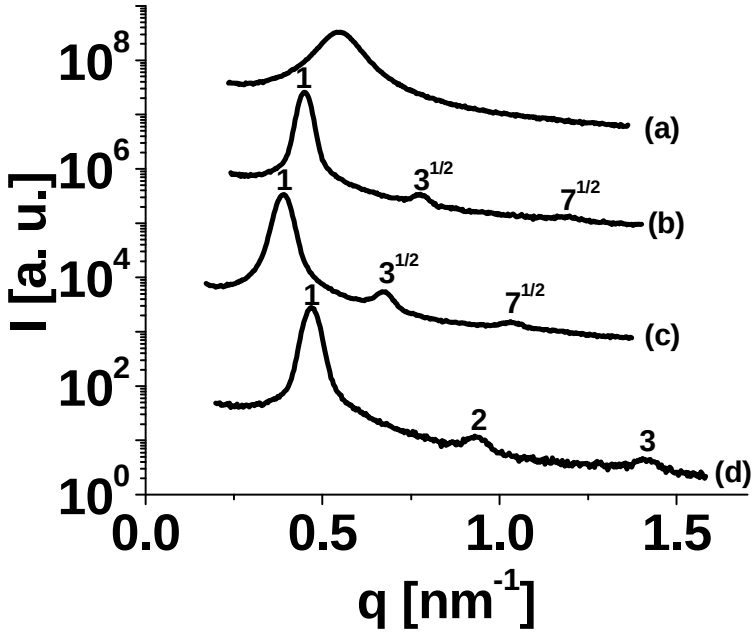

Figure 3.15. SAXS profiles of composites containing 50% loading of POSS-OAA for various Pluronic BCPs at 80 ^{o}C: (a) F68, (b) F88, (c) F108 and (d) P105.

To test the generality of this additive-driven assembly of PEO containing BCPs, the ability to incorporate POSS-OAA into a PS-PEO block copolymer was also determined as shown in the Supporting Information. A low molecular weight poly(styrene-b-etheylene oxide) diblock copolymer (PS-PEO. 3.8 kg/mol - 4.8 kg/mol) was chosen as the BCP and the SAXS profiles were measured for the neat BCP and its blend containing 30 % loading of POSS-OAA. Figure 3.16 shows that while the neat PS-PEO is disordered, its blend with 30% loading of POSS-OAA formed a well-ordered lamellar morphology. Thus a behavior similar to that observed for Pluronic BCPs is observed for the PS-PEO BCP.

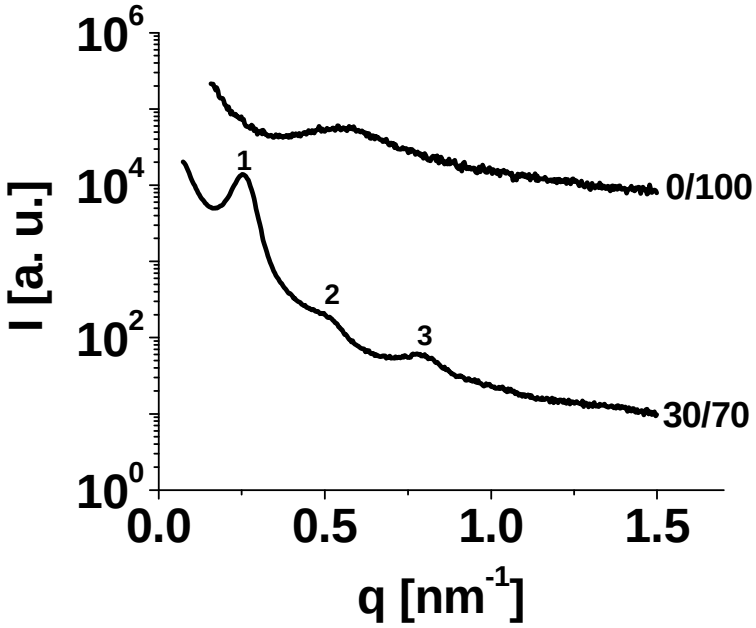

Figure 3.16. Scattering profiles of neat PS-PEO and its blend with POSS-OAA at 30% loading at 80 ^{o}C.

The molecular mixing of POSS-OAA with PEO phase of F108 was confirmed observed using XRD at high angles. Figure 3.17 compares the XRD profiles of neat

F108 and neat POSS-OAA with blends of F108 and POSS-OAA at 50 % and 70 % loading. Neat F108 shows a crystalline structure due to formation of PEO crystallites[87] and neat POSS-OAA shows multiple peaks showing that it is also crystalline. Upon blending POSS-OAA and F108, the peaks corresponding to neat POSS-OAA disappeared completely, indicating molecular dispersion of POSS-OAA in the PEO phase. At 50 % loading, the intensity of the peaks corresponding to PEO crystallites of neat F108 diminishes significantly in intensity although a faint peak is still visible at a 2θ value of ~18. The peaks disappear completely at 70 % loading indicating complete inhibition of crystallization of PEO. This implies good mixing such that PEO and POSS-OAA inhibit each other's crystallization and prefer to associate by hydrogen bonding instead of self-association by means of crystallization. These results of slight crystallanity of PEO at 50 % loading while total inhibition of crystallanity at 70 % loading is consistent with the DSC results discussed next.

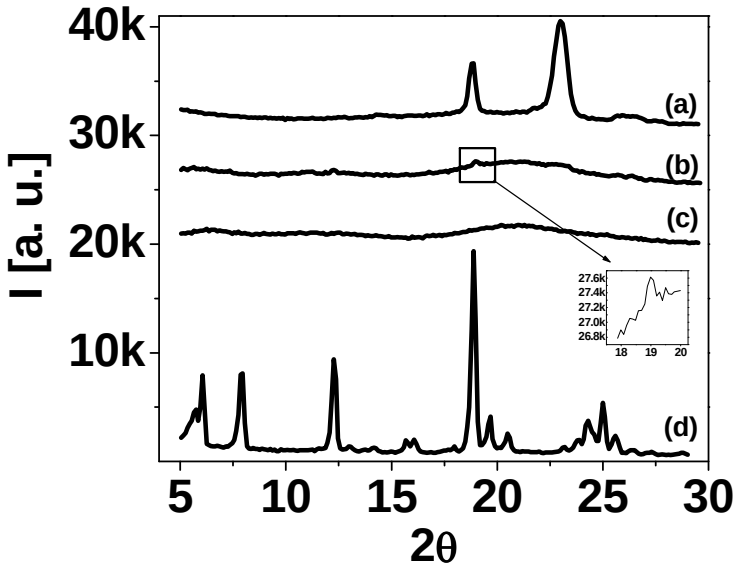

Figure 3.17. X-ray diffraction profiles of (a) neat F108, (b) 50 % POSS-OAA blend, (c) 70 % POSS-OAA blend and (d) neat POSS-OAA.

DSC was performed to further explore the nature of interaction of POSS-OAA with the PEO chain segments and to assess their compatibility.[13,72] Figure 3.18 shows the DSC thermograms of neat F108 and its blend with POSS-OAA between -60 ^{o}C to 75 ^{o}C. For clarity in data presentation, the thermograms for the blends were shifted vertically upwards by adding constant values to heat flow as given in parenthesis beside each thermogram. The melting endotherms observed correspond to the melting of the PEO crystallites because PPO does not crystallize and therefore shows no melting endotherm. The corresponding melting temperatures, denoted by the peak position of the endotherm, and the melting enthalpy normalized by the fraction of PEO present in the blends are tabulated in Table 3.1. Upon incorporation of POSS-OAA, the melting temperature and the normalized melting enthalpy decrease which is consistent with the interaction of these additives with the PEO chain segments. POSS-OAA and PEO interact strongly with each other and therefore their crystallization is no more favorable. At 70 % POSS-OAA loading, the crystallization of PEO was completely inhibited and no melting endotherm was observed. The systematic variation of the DSC thermograms obtained is consistent with compatibility and strong interaction of POSS-OAA with PEO.

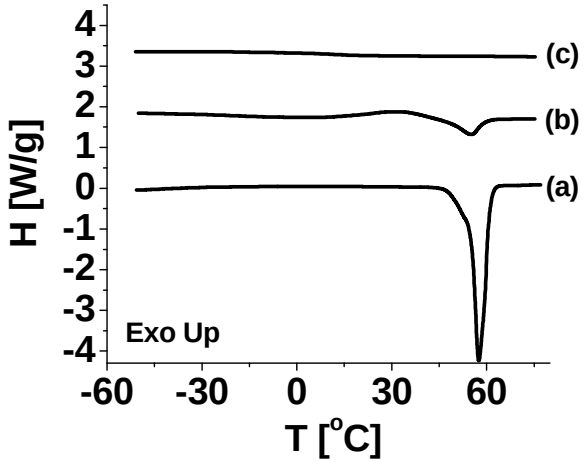

Figure 3.18. DSC thermograms of neat F108 and its blend with POSS-OAA and POSS-OAP (a) Neat F108, (b) 50/50 POSS-OAA/F108, (c) 70/30 POSS-OAA/F108. The thermograms for the blends were shifted vertically upwards to avoid overlap with the thermogram for neat F108.

Table 3.1. Thermal characteristics of neat F108 and its blends with POSS-OAA and POSS-OAP at varying compositions.

Sample	Melting Temperature [^{o}C]	Normalized Melting Enthalpy [J (g PEO)$^{-1}$]
F108	57.5	162.3
50% POSS-OAP	52.7	60.7
50% POSS-OAA	55.0	47.3
70% POSS-OAA*	-	-

* 70% POSS-OAA blend did not show any melting indicating inhibition of PEO crystallization

It is known that POSS cages can be oxidized into a silica network upon calcination.[84,88] However, the cages must be tightly held within the organic matrix to prevent their volatilization before they begin to crosslink.[88,89] Additionally, a high composition of POSS cages is desired so that they are situated in close proximity for mutual condensation upon calcination to form a large network of SiO_2. Since POSS-OAA can be incorporated selectively into the PEO phase of F108 at high loadings, the

close proximity of cages is ensured. The maleamic acid groups bear carboxylic acid and secondary amine groups which can be crosslinked by heating to 160 ^{o}C by the formation of imides and formation of anhydrides.[65] Blends of F108 with 50 % or 70 % POSS-OAA were heated by gradually raising the temperature to 160 ^{o}C which was found sufficient to form a crosslinked network of POSS-OAA within the PEO phase. This thermal treatment caused the blends to transform from a sticky paste to a flexible self-supporting non-sticky and insoluble solid indicating qualitatively that crosslinking occurred. The FTIR measurements discussed next track the reactions that occurred at different stages of the processing for the F108 composite. The crosslinked samples were then placed in a calcination oven where, in the presence of air, the temperature was gradually raised to 650 ^{o}C over a period of 10 hours, maintained at 650 ^{o}C for 8 hours and then ramped down to room temperature over a period of 10 hours. During calcinations, the yellow colored crosslinked samples were converted to white mesoporous silica powder and flakes, which were then characterized by TEM. Figure 3.19 shows the TEM micrographs obtained for the mesoporous silica obtained from the two blends which confirms that the cylindrical and spherical morphologies of the original blends were preserved upon calcination. One advantage of this method is that the silica precursor is contained within the composite material and therefore bulk amount of materials can be transformed to mesoporous silica without any concern of diffusion limited infusion of silica precursors in thick polymeric films. Using other methods, more silica precursors may be infused to densify the mesoporous silica obtained.[12,13] Another advantage is that the process of the formation of well-ordered composite materials is independent of the step in which they are converted to

mesoporous silica. Thus, well-ordered crosslinked composites may be prepared separately and calcined when mesoporous silica is desired.

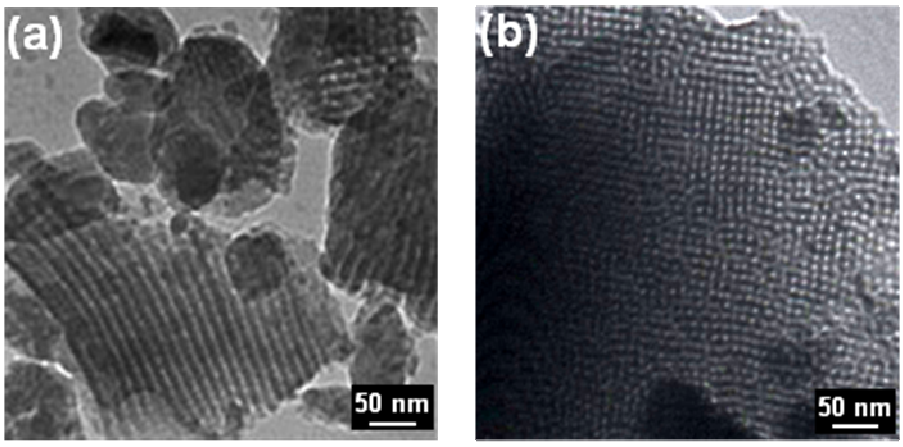

Figure 3.19. Transmission electron micrographs of mesoporous silica obtained upon calcination of F108 composites containing a) 50 % POSS-OAA and b) 70 % POSS-OAA.

FTIR spectra were obtained for the 70% POSS-OAA/F108 blend after vacuum drying at 75 ^{o}C and after annealing at 160 ^{o}C as shown in Figure 3.20. For comparison, the spectra of neat F108 and neat POSS-OAA are also shown. Changes in the spectra obtained at 75 ^{o}C and 160 ^{o}C indicate reaction of carboxylic acid groups with the secondary amine groups as is known to occur in similar systems.[90,91] Carboxylic acid groups can also react among themselves to form anhydrides. The peaks between 3420 cm^{-1} and 2775 cm^{-1} in the spectrum of 70% POSS-OAA/F108 blend after annealing at 75 ^{o}C, match exactly in their positions with the peaks in this region for the case of neat POSS-OAA. More specifically, the peaks at 3261 cm^{-1} and 3072 cm^{-1} can be attributed to the presence of secondary amine and hydroxyl groups on carboxylic acid respectively. However, both these peaks disappear after annealing at 160 ^{o}C indicating imide

formation by reaction between carboxylic acid groups and the secondary amine groups. The appearance of a peak at 1780 cm^{-1} corresponds to carbonyl group of the imide formed.[92] Additionally, the disappearance of the N-H stretching peak at 3261 cm^{-1}, and the secondary N-H bending peak at 1560 cm^{-1}, also confirms the crosslinking between the secondary amine and the carboxylic acid groups. The peak at 1707 cm^{-1} contributed from POSS-OAA can be attributed to the carbonyl groups of the carboxylic acid. This peak shifts to 1700 cm^{-1} upon annealing to 160 ^{o}C, and might be linked to a change in the response of carbonyl group upon reaction of carboxylic acid groups. FTIR spectrum of the mesoporous silica formed from the 70 % POSS-OAA/F108 blend was also obtained to explore the changes upon calcination to 650 ^{o}C. Most peaks corresponding to the organic components disappear which implies that most organic material was removed upon calcinations which is expected at such a high calcination temperature. The broad hump between 1100 cm^{-1} and 1000 cm^{-1} and the shoulder around 1210 cm^{-1} correspond to the stretching Si-O-Si bonds.[93] The peak at 800 cm^{-1} indicates the formation of Si-C which could form as the first carbon on the ligand is covalently bound to the Si on the POSS cage.[94] The presence of some carbonaceous material is indicated by the CH_2 and CH_3 stretching peaks around 3000 cm^{-1} which could arise from some trapping of impurities during the calcinations process.[94]

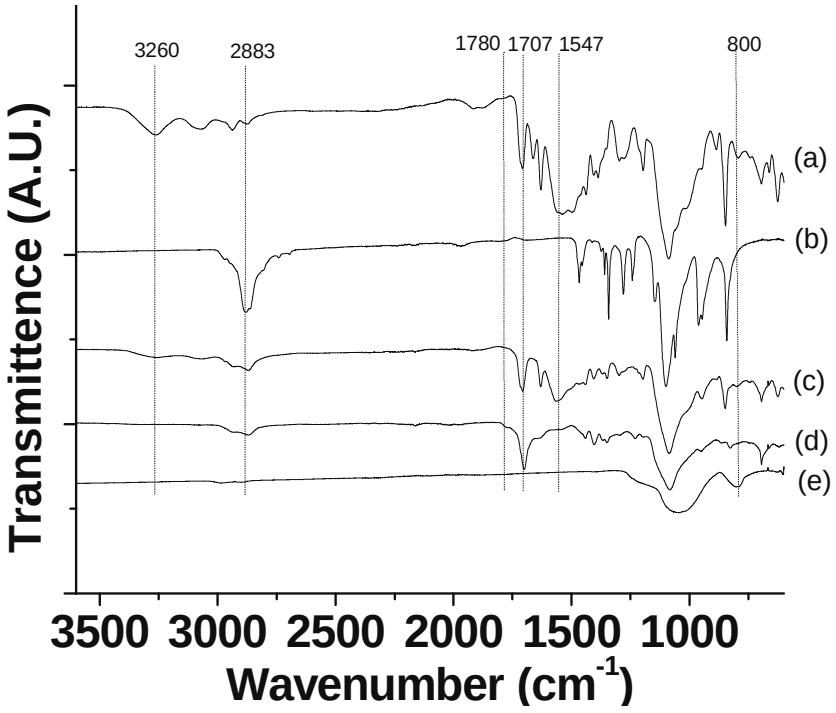

Figure 3.20. FTIR spectra: a) Neat POSS-OAA, b) Neat F108, c) 70 % POSS-OAA/F108 blend annealed to 75 ^{o}C, d) 70 % POSS-OAA/F108 blend annealed to 160 ^{o}C, e) 70 % POSS-OAA/F108 blend calcined to 650 ^{o}C.

3.4 Conclusions

It was found that blending of small molecule additives that bear hydrogen bonding sites for PEO at multiple locations can induce order in otherwise disordered Pluronic surfactants due to strong association with the PEO chains. Favorable hydrogen bonding interaction between the additive molecules and PEO blocks causes selective incorporation of high loadings of the additives into the PEO phase. With increasing amount of additives in the blends OOT from cylindrical to spherical morphology occurred and in the case of CTMA, this was followed by a loss in structural correlations as hexagonally-packed arrangement of PPO spheres was perturbed.

The presence of multiple hydrogen bonding groups as well as the amount of such additives is important factors that lead to ordering of PEO containing BCPs. For instance, a 10 % loading of BHCA induces ordering. However this does not translate to a 20 % loading of 1,3,5-benzenetricarboxylic acid which contains only 3 carboxylic acid groups instead of 6 carboxylic acid groups on BHCA molecules. Attempts to blend 1,3,5-benzenetricarboxylic acid resulted in macrophase separation.

The availability of Pluronic surfactants with a wide range of relative volume fractions of PEO and PPO and the possibility of enriching them with a wide variety of readily available additives having various chemical attributes and molecular structures provide a rather general route to formation of BCP templates with phase selective functionalization with different morphologies and continuously range of domain spacings. Judicious choice of the additive allows formation of BCP templates selectively functionalized with different chemical groups which might allow various phase selective chemistries. Moreover, variation of the core structure will enable the design of functional or structural materials. For example, as shown next, this strategy is extended to phase selective assembly of inorganic cores including polyhederal oligomeric silsesquioxanes (discussed next in this chapter) and large aromatic molecules (discussed in Chapter 5). This strategy is also well-applicable to incorporation of nanoparticles functionalized with multiple hydrogen bonding sites to form highly loaded and well ordered polymer nanocomposites. For the study on nanoparticles, the nanoparticles were synthesized by Ying Lin at University of Massachusetts Amherst and is discussed elsewhere.[45] While the assembly described here should be generally applicable to block copolymer / additive systems containing complementary hydrogen

bond donors and acceptors, the realization of well-ordered materials that are templated entirely from commercially available BCP surfactants offer advantages to traditional BCPs in terms of availability, scalability and cost.

It is observed that when sufficient amount of additives that are capable of interacting with PEO are added, in addition to the phase segregation to form ordered morphologies, the crystallization of PEO is also suppressed. In addition, the blends studied were solid-like even at 80 ^{o}C whereas F108 is liquid at this temperature. Reduction in crystallanity of PEO while maintaining solid-like consistency is important for application of PEO and PEO based block copolymers towards polymer electrolytes in rechargeable lithium ion batteries. For example, significant efforts have been made to reduce the crystallanity of PEO thereby increasing its ionic conductivity by incorporation of salts and nanofillers.[95-98] In addition, the need for high mechanical integrity has been addressed by employing PEO containing BCPs in which the other block provides the necessary mechanical strength as well as constraints by which the ion conduction paths become well-defined.[57,99,100] The present work hints at the design rules for additives in terms of their molecular architecture and chemical functionality which can be effective in altering the properties of PEO based polymers.

POSS cages fully functionalized with maleamic acid or aminophenyl ligands capable of hydrogen bonding with the PEO blocks of low molecular weight BCPs can induce order in the otherwise disordered BCP melts producing well-ordered and highly-filled composites with small domains. The phase behavior of the composites depends significantly upon the choice of hydrogen bonding ligands, however, blends with both additives with F108 formed well-ordered cylindrical and spherical morphologies.

Lamellar morphologies were accessible using Pluronic P105 as the template. Between the two ligands, maleamic acid was found to result in higher levels of incorporation than aminophenyl while maintaining the well-ordered BCP morphology. The possibility of such high loadings of POSS cages suggests that this design of using hydrogen bonding interactions and of uniform functionalization of the additive could be employed generally for other cores. Strong order in the BCP nanostructure was maintained up to 80 % loading of POSS-OAA and up to 40 % loading of POSS-OAP in F108. In comparison to POSS-OAP, POSS-OAA interacts more strongly with PEO which allows higher levels of incorporation. XRD and DSC measurements indicated miscibility and compatibility of both the additives with PEO.

Crosslinking upon heating to 160 ^{o}C followed by calcination at 650 ^{o}C of the POSS-OAA - F108 composite at 50 % and 70 % additive loadings yielded mesoporous silica with cylindrical and spherical morphologies that were templated by the presence of the BCP. This is consistent with phase selective incorporation of the POSS additive into the PEO phase.

CHAPTER 4

HYDROGEN-BOND-ASSISTED BLOCK COPOLYMER – BLOCK COPOLYMER COMPOSITES

4.1 Introduction

Tri-block copolymers of the type A-B-C in which A, B and C denote chemically different and phase separating blocks can result in various complex structures comprising of three different phases which cannot be formed by A-B or A-B-A type block copolymers.[5] However, synthesis of such triblock copolymers is often tedious due to the stringent requirements for anionic polymerization. The goal of this chapter is to build upon the concept of hydrogen bond assisted incorporation of additives discussed in the previous two chapters by employing this favorable interaction to bind two different BCPs. The constituent BCPs would contain two dissimilar blocks (i.e. would be of the type A-B or A-B-A) and their molecular binding would result in the formation of morphology more complex than formed with A-B and A-B-A type BCPs. As described in the previous chapters, the A-B or A-B-A block copolymers can only form the classical BCP morphologies like lamellar, cylindrical and spherical morphologies at high segregation strength and form bicontinuous morphologies in a narrow range of composition and when the segregation strength is not too high. Since in certain cases, three-phase morphologies can be obtained and the synthesis of tri-block copolymers to obtain those morphologies could be avoided. Additionally, simply by varying the composition of the constituents of the composite morphology, a variation in the

morphology and d-spacing would be possible and therefore the need for synthesizing various tri-block copolymers to access different structures could be avoided.

In this work, two strategies for blending two BCPs have been explored. In the first strategy, two BCPs, A-B and B-C were blended with a homopolymer D such that D interacts via hydrogen bonding with both the B blocks on the two different diblock copolymers. The hypothesis for this strategy is that the homopolymer D would bridge between the B blocks of the two different BCPs and result in binding the two BCPs to form a composite structure. The blocks A and C are chosen such that they are non-interacting and therefore would phase separate forming two of the three phases while the two B blocks and the homopolymer D are expected to form the third phase. A possible challenge for this strategy to work is that the homopolymer might bind separately with each of the diblock copolymers but might not bridge between the two different BCPs. Thus, instead of a single composite morphology, two different BCP morphologies might co-exist in the blends obtained. The SAXS profiles would then show peaks corresponding to the individual BCPs blended with the homopolymer D.

In the second strategy the above mentioned complexity is addressed and simplified. Here, two different BCPs, A-B and C-D (or C-D-C) have been employed such that the block B interacts via hydrogen bonding with the block C. No homopolymer is added to cause binding. In this case, the degrees of freedom in tuning the blend composition are less than the previous strategy because of the absence of the homopolymer: only the BCP compositions can be varied in the blends to vary the structure of the resulting blends and the homopolymer concentration or chain length is not available to be varied. However, this strategy is easier to implement and

straightforward to analyze. For instance, if a blend shows d-spacing that is significantly larger than the constituent BCPs, then it must be true that binding occurred because there is no other way the d-spacing could increase. Thus, when binding occurs, the blocks B and C would form a single phase while the non-interacting blocks A and D would form the other two phases of the composite morphology obtained. A challenge in this strategy is that the blocks A and D are designed in such that they would phase separate if the other blocks were not present to prevent them from doing so by associating with each other. Therefore, as the size of the BCPs increase, especially with large A and D blocks, at some point the hydrogen bonding interaction between the B and C blocks might not be strong enough to prevent the A blocks to macrophase separate from the D blocks. In such situations, binding of the two BCPs would not occur and macrophase separation would result and the two BCPs would two co-existing in the mixtures made. The SAXS profiles would then show peaks corresponding to the individual BCPs.

Previously, binding of different blocks via hydrogen bonding has been explored using other hydrogen bonding blocks, for example, poly(hydroxystyrene) and poly(vinyl pyridine) to form similar composite morphologies.[101] A similar method based on hydrogen bonding interaction between the different blocks was utilized to obtain a BCP blend system which could form domains arranged on a square lattice.[102] Here we explore the use of hydrogen bonding interaction between PEO and PAA blocks for forming composite morphologies. One benefit of employing PEO and PAA as the interacting blocks is that these do not require high annealing temperatures. The annealing temperature would depend on the glass transition temperatures of the other

blocks. Therefore, using PEO and PAA as the interacting blocks, the need for high temperatures in thermal annealing could be avoided which might become important for the case of temperature sensitive non-interacting blocks.

4.2 Experimental

4.2.1 Materials

The BCPs and the homopolymers purchased from Polymer Source Inc. are as follows: Polystyrene-poly(ethylene oxide) (PS-PEO) BCPs with molecular weights 9.5-5 kg/mol and 16-5 kg/mol, polybutadiene-poly(ethylene oxide) (PBd-PEO) BCPs with molecular weights 5-2.3 kg/mol and 11.8-2.9 kg/mol, polybutadiene-poly(acrylic acid) (PBd-PAA) of molecular weight 5.8-4 kg/mol, and PAA homopolymers with molecular weights 8.5 kg/mol, 20 kg/mol and 44 kg/mol. The solvents tetrahydrofuran (THF) and ethanol (EtOH) were purchased from Fisher Scientific.

4.2.2 Sample preparation

Required amounts of BCPs and PAA were dissolved either in pure THF or a 80:20 by weight mixture of THF and EtOH. The solutions were dissolved at 45 ^{o}C on a hot plate with occasional stirring. These solutions were casted either at room temperature or on a hotplate at a range of temperatures. After drying for ~5 hours, the samples were then annealed in a vacuum oven at different temperatures for different times. The dried samples were put between metal washers between kapton films and SAXS was performed on them.

4.2.3 Small angle x-ray scattering

One of the SAXS results shown was obtained on a setup described in Chapter 2. The rest of the SAXS data was measured at the Advanced Polymers Beamline (X27C), located at the National Synchrotron Light Source (NSLS) at Brookhaven National Laboratory (BNL), Upton, NY. Two-dimensional scattering patterns were collected on Fujitsu image plates and then read by a Fujitsu BAS 2000 image plate reader. The wavelength of x-ray beam used was 0.1307 nm with a beam diameter of 0.3 mm. Silver behenate was used to calibrate the sample to detector distance. Polar software was used to reduce the data to one-dimensional intensity, I vs. wave vector, q plots. It is noted here that the peak positions are not expected to be different for the two setups but the detector resolution being higher for the BNL set up resulted in sharper peaks even for the same samples. This was particularly advantageous because for cases when two peaks positions are close, a higher resolution is required to tell them apart. All SAXS profiles were collected at 80 ^{o}C to avoid PEO crystallization if any.

4.3 Results and discussion

For exploring the first strategy to blend different block copolymers, blending of PS-PEO (16-5 kg/mol) with PBd-PEO (11.8-2.9 kg/mol) and different PAA homopolymers is considered. The two BCPs were mixed at various compositions with PAA of molecular weights 8.5, 20 and 44 kg/mol. The rationale behind using bigger PAA chains is that it might reach out better to the two PEO blocks from PS-PEO and PBd-PEO. Figure 4.1 shows the two possible outcomes of such an attempt to blend the

two BCPs and the PAA homopolymer. In one situation, the PAA chains bind the two BCPs and in the other the PAA chains associate with the two BCPs separately resulting in the formation of two co-existing morphologies from the two BCP + homopolymer systems. When PAA results in binding both the BCPs, a jump in d-spacing is expected due to an increased composite molecular weight of the chains. However, when PAA is incorporated separately into the two BCPs, even then an increase in the d-spacing is expected due to the swelling of the PEO domains. This makes the analysis of the SAXS profiles complicated and a high resolution detector is required to identify closely placed peaks. For example, in certain cases, the SAXS profile collected with the SAXS setup described in Chapter 2 showed a gaussian shaped primary peak but the SAXS for the same sample at X27C beamline at BNL showed that there were two peaks placed close to each other.

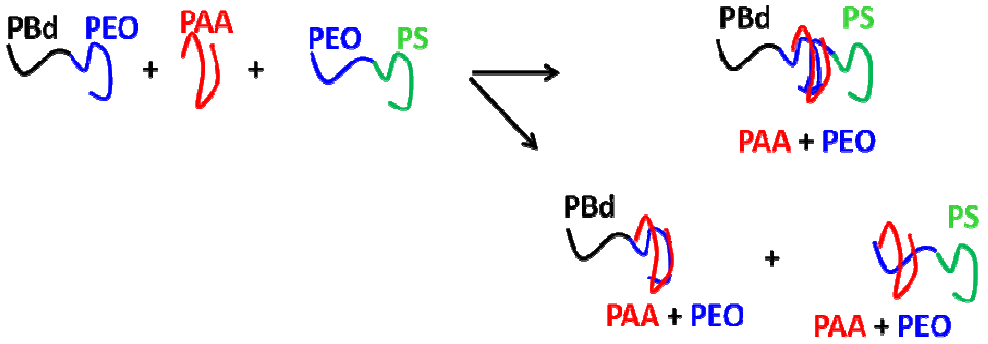

Figure 4.1. Schematic showing two possible outcomes upon blending of PS-PEO, PBd-PEO and PAA. Either a composite morphology would result (top right), or two separate BCP + homopolymer morphologies would co-exist (bottom right)

The solutions containing PS-PEO, PBd-PEO and PAA were formed in two kinds of solvents, namely, pure THF or THF:EtOH = 80:20 by weight to solutions with about 2 % polymers. The solutions were drop casted on glass slides either kept at room

temperature or at 45 ^{o}C. After a few hours of drying, followed by drying under vacuum at 100 ^{o}C, all these samples turned hazy which indicates macrophase separation of the constituents. This is true for various different compositions and PAA chain lengths. Therefore, for this case, it is clear that the formation of a composite morphology did not occur, and most likely, the two BCP + homopolymer systems co-existed.

To cause the homopolymers PS and PBd to blend and not macrophase separate, a decrease in their size would be required to bring the value of the segregation strength (χN) to less than 2 (condition from miscibility from the Flory-Huggins theory). In the present examples the BCPs can be thought of as PS and PBd homopolymers only with PEO at one end. It must be noted that there is no chemical bond junction between the PS and PBd which if were present would prevent their macrophase separation. Therefore, a decrease in the size of the PS and PBd blocks would increase their chance of forming a composite nanostructure as the driving force between PS and PBd to macrophase separate would be smaller and possibly the PAA chains could bind the two PEO blocks. With this rationale, blends of PS-PEO (9.5-5 kg/mol), PBd-PEO (5-2.3 kg/mol) and PAA of various molecular weights were made using a similar procedure to the one described above. Again, the rationale for using PAA of various chain lengths is that above a certain length the PAA chains might be able to reach out and bind the two PEO blocks.

Figure 4.2 shows the scattering profiles obtained for neat PS-PEO (9.5-5 kg/mol) and neat PBd-PEO (5-2.3 kg/mol). The PS-PEO sample was annealed at 120 ^{o}C for 24 hours and the PBd-PEO was annealed at 80 ^{o}C for 24 hours. The scattering profile of PS-PEO shows a primary peak (d-spacing = $2\pi/q^* = 14.6$ nm) but no higher order peaks

indicating that microphase separation between PS and PEO blocks is not strong and a well-ordered morphology is not formed with PS-PEO in the neat form. However, this does not pose a potential problem because in case the PAA is able to bind this pair of PS-PEO and PBd-PEO BCPs, the composite molecular weight would increase and then a strong phase segregation would occur. As shown later, this PS-PEO is able to form well-ordered composite morphologies. The neat PBd-PEO formed a well-ordered hexagonally packed cylindrical morphology with a d-spacing of 13.3 nm.

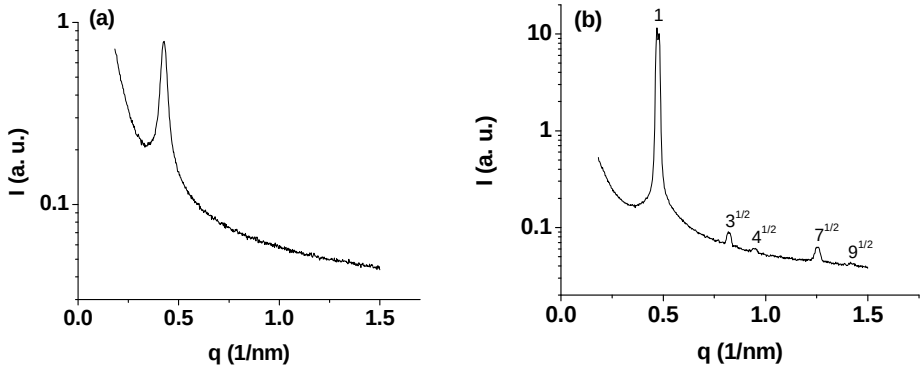

Figure 4.2. SAXS profiles for neat (a) PS-PEO (9.5-5 kg/mol) and (b) neat PBd-PEO (5-2.3 kg/mol).

The composition of the various blends prepared with PS-PEO (9.5-5 kg/mol), PBd-PEO (5-2.3 kg/mol) and PAA of molecular weight 20 kg/mol are shown in Table 4.1 which are named C1 to C6 for simplicity. In these blends, the PAA (20 kg/mol) loading was increased while the two BCPs were added in equal amounts. Sample C1 represents the control sample in which no PAA is added. Table 4.1 also shows the volume fractions of the PS, PBd and PEO + PAA phases. Since PEO blocks are expected to associate with the PAA homopolymer, it is expected that these would form a single phase and therefore their volume fractions are grouped together. The composite

volume fraction of the blends provide an indication of the expected morphology. For example, if the volume fraction for PS, PBd and PEO + PAA phases were equal, lamellar morphology would be expected. To convert the weight percentages to volume percentages, the densities of PS, PBd, PEO and PAA were set to 1.05, 0.895, 1.23 and 1.23 g/cm^3, respectively.

Table 4.1. Compositions of various blends of PS-PEO (9.5-5 kg/mol), PBd-PEO (5-2.3 kg/mol) and PAA of molecular weight 20 kg/mol. The weight ratio of the two BCPs is maintained at unity for all the blends while the percentage of PAA is increased starting from no PAA up to 55 % PAA.

Sample C1		
Weights added		
PAA	0	%
PBd-PEO	0.025	g
PS-PEO	0.025	g
PAA20k	0	g
	volume %	
PBd	39.7	
PS	32.4	
PEO+PAA	27.9	

Sample C2		
Weights added		
PAA	15	%
PBd-PEO	0.0213	g
PS-PEO	0.0213	g
PAA20k	0.0075	g
	volume %	
PBd	34.6	
PS	28.2	
PEO+PAA	37.2	

Sample C3		
Weights added		
PAA	25	%
PBd-PEO	0.0188	g
PS-PEO	0.0188	g
PAA20k	0.0125	g
	volume %	
PBd	31.0	
PS	25.3	
PEO+PAA	43.7	

Sample C4		
Weights added		
PAA	35	%
PBd-PEO	0.0163	g
PS-PEO	0.0163	g
PAA20k	0.0175	g
	volume %	
PBd	27.3	
PS	22.3	
PEO+PAA	50.4	

Sample C5		
Weights added		
PAA	45	%
PBd-PEO	0.0123	g
PS-PEO	0.0152	g
PAA20k	0.0225	g
	volume %	
PBd	21.1	
PS	21.3	
PEO+PAA	57.6	

Sample C6		
Weights added		
PAA	55	%
PBd-PEO	0.01	g
PS-PEO	0.0125	g
PAA20k	0.0275	g
	volume %	
PBd	17.4	
PS	17.8	
PEO+PAA	64.8	

The SAXS profiles obtained for the blends C1 to C6 are shown in Figure 4.3. The SAXS profile for C1 is identical to that of neat PBd-PEO (5-2.3 kg/mol) shown in Figure 4.2. This implies that a composite morphology did not form because there is no increase in the d-spacing. The response of the macrophase separated PS-PEO (9.5-5 kg/mol) is expected to be there as well but it is dominated by the response of PBd-PEO because it has a strong scattering due to strong order (see Figure 4.2). Simply by looking at the SAXS profiles for C2, C3, C5 and C5, it is clear that the blends contain two families of co-existing BCP morphologies since there are two primary peaks present. The formation of two primary peaks indicates that as PAA was added, some of it must have incorporated with PS-PEO and enhanced its segregation. Therefore, while the sample C1 that did not contain any PAA did not show the PS-PEO morphology distinctly, when PAA was added, the PS-PEO + PAA system became strongly segregated and its scattering became comparable to that of the PBd-PEO + PAA system. It is important to note that the segregation of PS block from the PEO block is enhanced when PAA interacts with the PEO block. The sample C6 seems to show only a single primary peak, but the ratio of the peak positions with respect to the primary peak position does not fall in any of the BCP morphologies. Therefore, it seems that there are two co-existing morphologies even in this case and the response of one of the BCP systems dominates and masks the response from the other system present.

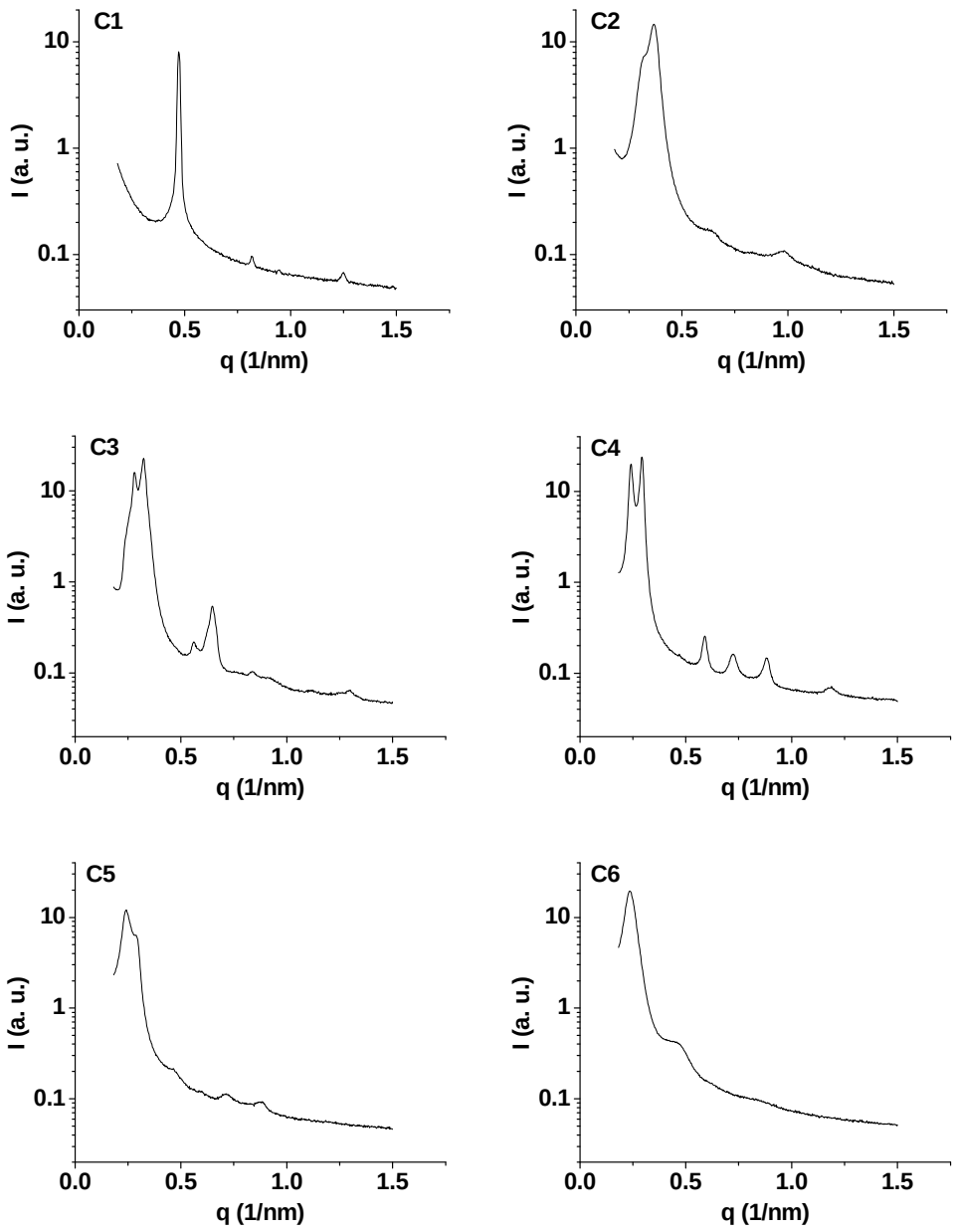

Figure 4.3. SAXS profiles of various blends (C1 to C6) of PS-PEO (9.5-5 kg/mol), PBd-PEO (5-2.3 kg/mol) and PAA of molecular weight 20 kg/mol. The weight ratio of the two BCPs is maintained at unity for all the blends while the percentage of PAA is increased starting from no PAA up to 55 % PAA.

The peak positions for the case of sample C2 to C5 can be mapped on to two different morphologies arising from the two co-existing BCP + PAA systems. For

example, for the case of sample C4, the peaks are observed at q (1/nm) positions of 0.242, 0.293, 0.471, 0.594, 0.726, 0.883, and 1.184. Among these, the peaks at 0.242, 0.471, 0.726, and 1.184 have the peak position ratios of 1, 2, 3, and 5 (with respect to 0.242 which is the primary peak for the first blend system) which indicates the presence of a lamellar morphology. The peaks at 0.293, 0.883, and 1.184 have the peak ratios of 1, 2, 3, and 4 (with respect to 0.293 which is the primary peak for the second blend system) which indicates the presence of another lamellar morphology. The peak at 1.184 falls in both the series and therefore could be a result of superposition of peaks from both the morphologies. Thus, for the case of C4, the PS-PEO + PAA and the PBd-PEO + PAA blends co-exist and form their separate lamellar morphologies. It is also clear that PAA is split between the two BCPs by looking at the shifting trends in the primary peak position. This corresponds to the second option shown in Figure 4.1.

The preference for two co-existing morphologies instead of a single composite morphology from blends of PS-PEO, PBd-PEO and PAA seems more favorable considering the thermodynamics involved. Binding of PAA with the PEO blocks is driven by enthalpically favorable hydrogen bonding interaction. Therefore, both of the two outcomes shown in Figure 4.1 should be equally favorable enthalpically. However, the choice between the two outcomes is governed by the entropic penalties associated with chain stretching. It is easy to visualize that if the PEO blocks from the two different BCPs interact with a single PAA chain in order to form a composite structure, the two PEO blocks and the PAA chains would have to stretch out to reach each other. Coupled with this would be an additional stretching caused the PS and PBd blocks which tend to macrophase separate. However, if the two BCP systems were to phase separate, taking

away their share of PAA, the stretching of the chains would be less and only enough to accommodate the PAA. Therefore, while the enthalpic interactions are equally favorable for the two outcomes, the formation of a composite structure poses a higher entropic penalty than the formation of co-two co-existing morphologies. Likewise, blends with PAA of molecular weight 44 kg/mol also showed two primary peaks. This data is similar to the data for blends with 20 kg/mol PAA and therefore not discussed.

The above study described the results from the first strategy mentioned in the introduction in which a homopolymer was proposed for binding of two different BCPs. In the following the second strategy is explored in which it is proposed to have two BCPs such that one of the blocks on the first BCP can interact via hydrogen bonding with another block on the second BCP, i.e. A-B and C-D (or C-D-C) have been employed such that the block B interacts via hydrogen bonding with block(s) C. In this case, the only way the favorable hydrogen bonding interaction between the B and C block can occur is when the two BCPs form a composite morphology. There is no homopolymer added to provide for favorable enthalpic interaction in the absence of the formation of a composite structure. For this reason, this strategy is more likely to be successful in binding the two BCPs if the interaction between the B and C blocks is strong enough to offset the entropic penalties associated with the chain stretching in forming the composite structure. Additionally, the results are easy to assess because in this case an increase in d-spacing inherently implies binding of the BCPs.

For this case, the two BCPs chosen are PS-PEO (9.5-5 kg/mol) and PBd-PAA (5.8-4 kg/mol) among which the PS-PEO is the same as that used above and its scattering profile is shown in Figure 4.2. The SAXS profile for the neat PBd-PAA is

shown in Figure 4.4 from which it is seen that it forms a lamellar morphology on its own.

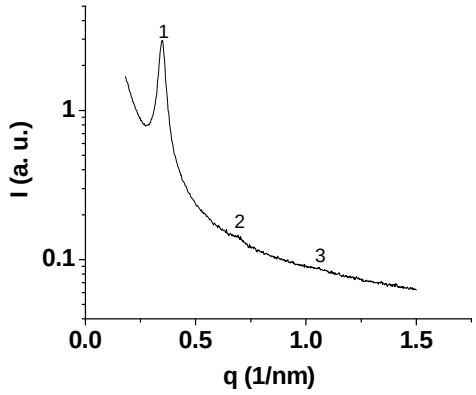

Figure 4.4. SAXS profiles for neat PBd-PAA (5.8-4 kg/mol).

The PS-PEO (9.5-5 kg/mol) and PBd-PAA (5.8-4 kg/mol) BCPs were blended in various compositions to prepare blends A1 to A6 as shown in Table 2.2. The percentage of PS-PEO BCP decreased progressively from A1 to A6. The volume fraction of the PEO + PAA phase remains almost constant while the volume fraction of PS and PBd change from one sample to another. The samples were dissolved in THF:EtOH = 80:20 by weight to form 2 % solutions and then drop casted at room temperature and dried first at room temperature for a few hours followed by drying at 50 ^{o}C under vacuum for 5 hours. Following this, the samples were annealed at 110 ^{o}C for 24 hours under vacuum.

Table 2.2. Blends of PS-PEO (9.5-5 kg/mol) and PBd-PAA (5.8-4 kg/mol). The weights added to form the blends are shown and the corresponding volume fractions for the expected PBd, PS and PEO + PAA phases are shown.

Sample A1		
Weights added		
PBd-PAA	0.005	g
PS-PEO	0.045	g
	volume %	
PBd	7.2	
PS	61.5	
PEO+PAA	31.3	

Sample A2		
Weights added		
PBd-PAA	0.009	g
PS-PEO	0.041	g
	volume %	
PBd	12.9	
PS	55.6	
PEO+PAA	31.5	

Sample A3		
Weights added		
PBd-PAA	0.015	g
PS-PEO	0.035	g
	volume %	
PBd	21.3	
PS	46.9	
PEO+PAA	31.8	

Sample A4		
Weights added		
PBd-PAA	0.025	g
PS-PEO	0.025	g
	volume %	
PBd	34.9	
PS	32.9	
PEO+PAA	32.3	

Sample A5		
Weights added		
PBd-PAA	0.03	g
PS-PEO	0.02	g
	volume %	
PBd	41.4	
PS	26.1	
PEO+PAA	32.5	

Sample A6		
Weights added		
PBd-PAA	0.035	g
PS-PEO	0.015	g
	volume %	
PBd	47.9	
PS	19.4	
PEO+PAA	32.7	

The SAXS profiles obtained for samples A1 to A6 are shown in Figure 4.5. The scattering profile for A1 shows a primary peak at the same position as the neat PS-PEO. This could be an indication that a composite morphology did not form. The morphology formed with A2 is unclear although a peak seems to be present at 0.14 nm^{-1} which corresponds to a d-spacing of about 45 nm. However, there still is a peak at the same position as that for the neat PS-PEO. This response could be due to some PS-PEO molecules that did not interact with the PBd-PAA because of an insufficient amount of PAA to bind all PEO chains. The weak peak at 0.14 nm^{-1} indicates that a portion of these BCPs interacted but did not formed any ordered morphology. The SAXS profile of

A3 shows peaks at q (nm^{-1}) positions of 0.167, 0.349 and 0.444 the ratio of which with respect to the first peak is 1, $4.36^{1/2}$, $7^{1/2}$. The peak position of 0.167 corresponds to a d-spacing of 37.6 nm. Although this increase in d-spacing indicates the formation of a composite structure, it is unclear what the morphology is. A further characterization of this sample with TEM would reveal the structure. The SAXS profiles for samples A4, A5, and A6 clearly show the formation of a composite lamellar morphology with the peak position ratios belonging to the series 1, 2, 3, 4,…. The d-spacing for these samples was found to be 32.2, 31.4 and 31.4 nm respectively. Thus, upon achieving a proper balance between the compositions that provides for sufficient interaction between PEO and PAA blocks, a composite structure results. In this composite morphology, three phases are expected to form from PS, PBd and PEO + PAA chains. This is because PS and PBd are known to be non-interacting (an evidence for this also lies in the failure of the first strategy) and therefore would remain in separate phases, while the PEO + PAA phase also is significantly different from the PS and PBd and therefore should form a separate phase. An increase in the segregation strength of PS-PEO upon addition of PAA as seen earlier supports the rationale that PS should form a phase separate from the PEO + PAA phase.

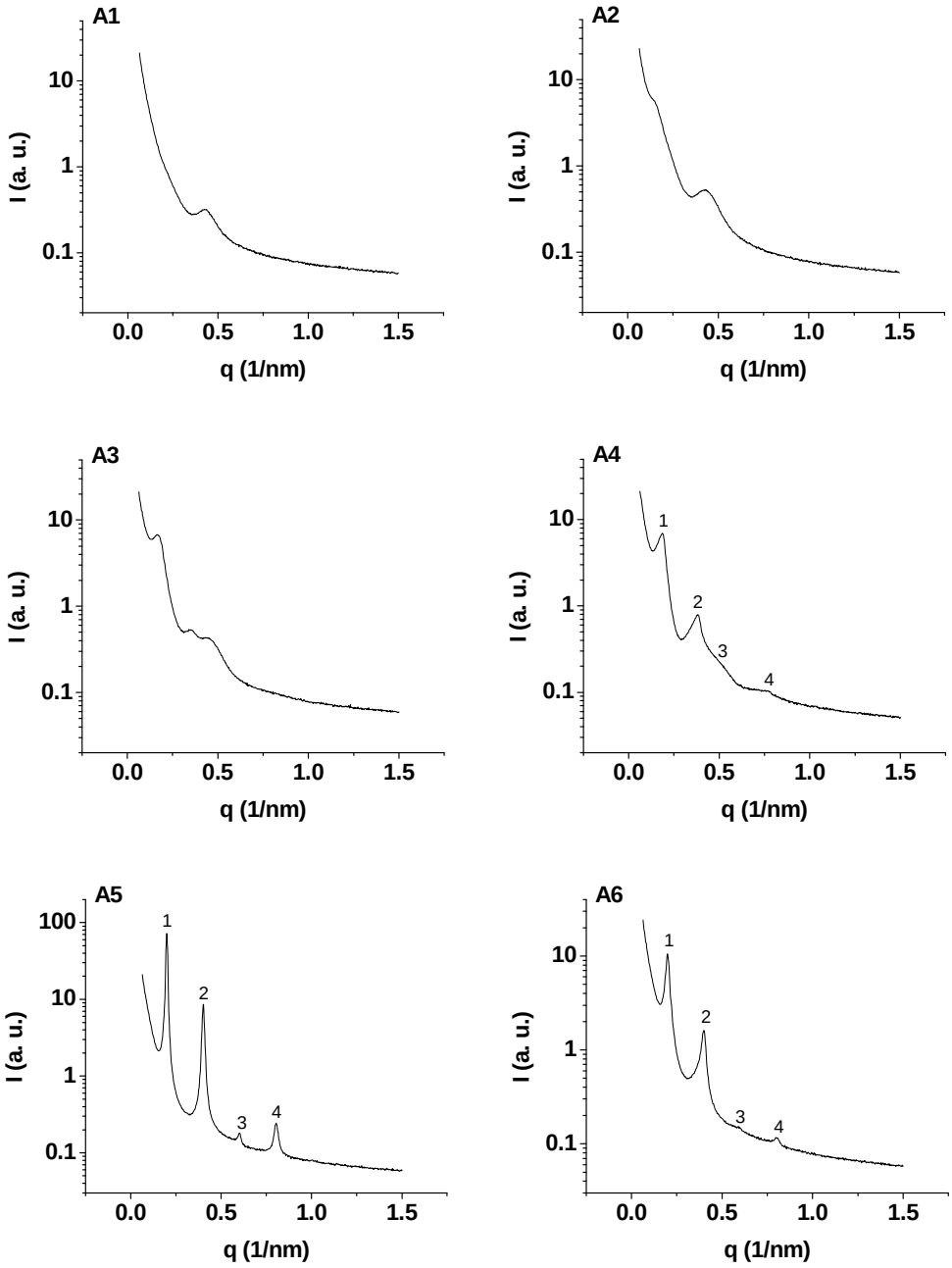

Figure 4.5. SAXS profiles of various blends (A1 to A6) of PS-PEO (9.5-5 kg/mol), PBd-PAA (5.8-4.0 kg/mol).

The volume percent of PS in sample A6 is just 19.4 % while the volume fraction of PBd is 48 %. Even with this high asymmetry in the volume fractions, the blend adopts a lamellar morphology. This is a result of the balance of interaction energies

between various phases and the stretching of chains away from the interfaces. It would be interesting to form blends with even higher amounts of PBd-PAA to find out when the interface gets curved to form PS cylinders and spheres. If indeed that occurs, it is expected that a core-shell morphology would form with PS as the core, PBd as the matrix and the PEO + PAA phase, that has to be in the middle due to chain connectivity on the two sides with PS and PBd, as the shell around the PS cores. This is the case when PS is replaced with a flexible block as seen for sample B2 shown next.

Next, the PS-PEO BCP was replaced with a P105, a PEO-PPO-PEO triblock copolymer. Although P105 is a triblock copolymer, the two PEO blocks would form a single phase without much entropic penalty in looping the PPO chains because PPO is quite flexible at room temperature. The main difference by switching from PS-PEO to PEO-PPO-PEO comes from replacing the PS block with the PPO block. The two blends of P105 and PBd-PAA that were prepared are shown in Table 4.3. The density of PPO was taken as 1 g/cm^3 to estimate the volume fractions while the densities of other components were the same as mentioned earlier. Based on volume fractions, sample B1 and B2 are close to the composition of A4, A5 and A6 but with the PS block replaced with PPO.

The SAXS profiles for samples B1 and B2 are shown in Figure 4.6. The data shown for B1 was collected on the SAXS set up described in Chapter 2 while the data for B2 was collected at BNL just like all the other data shown in this chapter. Due to higher detector resolution at BNL, sharper peaks were formed. Therefore comparison of the width of the peak is not appropriate and only peak positions are considered. It seems that that the sample B1, which is near symmetric volume fractions for the three different

phases, formed a lamellar morphology as the second peak is positioned at double the q value for the primary peak. However, higher order peaks did not form. The relative volume fractions being nearly symmetric, a lamellar morphology is expected. The d-spacing of sample B1 is 23.6 nm which is higher than the d-spacing for neat PBd-PAA (18 nm). Therefore, a composite structure must have formed.

Table 4.3. Blends of P105 (PEO-PPO-PEO, ~6.5 kg/mol, 50 % PEO) and PBd-PAA (5.8-4 kg/mol). The weights added to form the blends are shown and the corresponding volume fractions for the expected PBd, PPO and PEO + PAA phases are shown.

Sample B1		
Weights added		
PBd-PAA	0.025	g
P105	0.025	g
	volume %	
PBd	**34.8**	
PPO	**26.3**	
PEO+PAA	**38.9**	

Sample B2		
Weights added		
PBd-PAA	0.035	g
P105	0.015	g
	volume %	
PBd	**47.9**	
PPO	**15.5**	
PEO+PAA	**36.6**	

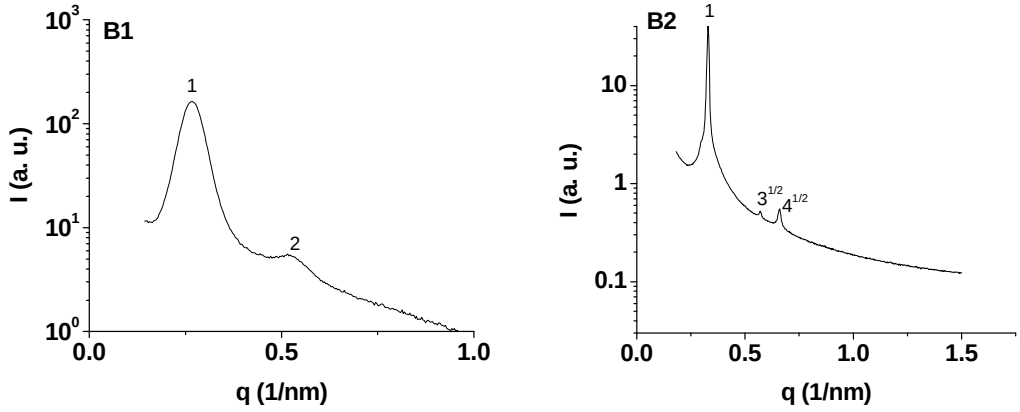

Figure 4.6. SAXS profiles of blends of P105 (PEO-PPO-PEO, ~6.5 kg/mol, 50 % PEO) and PBd-PAA (5.8-4 kg/mol).

The SAXS profile of sample B2 shows a well-ordered hexagonally packed morphology with a d-spacing of 19.2 nm. The neat PBd-PAA forms lamellar morphology as seen in Figure 4.4. Although neat P105 is disordered, it is symmetric in PEO and PPO volume fractions and therefore should also tend to form a lamellar morphology upon ordering (as seen in Chapter 2 where blending of some PAA caused lamellar morphology to form). Based on the volume fraction of various components in sample B2, the formation of a hexagonally packed morphology implies the formation of the structure shown in Figure 4.7. PBd is the majority phase and therefore should form the matrix. PPO is the minority phase and would form cores. Due to chain connectivity of PAA with PBd and PEO with PPO, the PEO + PAA phase should lie in between and therefore form a shell around the PPO cores. Additional characterization such as TEM may be performed to confirm this structure.

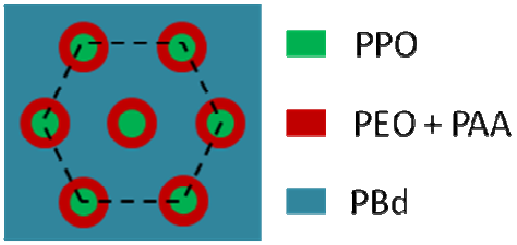

Figure 4.7. Possible structure for the sample B2 that forms a hexagonally packed morphology. PBd is the majority phase and therefore should form the matrix. PPO is the minority phase and would form cores. Due to chain connectivity of PAA with PBd and PEO with PPO, the PEO + PAA phase should lie in between and therefore form a shell around the PPO cores.

4.4 Conclusions

Hydrogen bond interaction between PEO and PAA is utilized to bind two different block copolymers containing only two dissimilar blocks. Thus, the blending of

BCPs containing two chemically dissimilar blocks results in the formation of morphologies more complex than the constituent BCPs can form. Two strategies are attempted to cause the formation of a composite structure by molecular binding of the two different blocks. The first strategy explored is to bind the PEO blocks on two different BCPs with a homopolymer PAA. This strategy fails to result in the formation of a composite structure as the PAA chains associate with the two BCPs to form two separate BCP + homopolymer systems and these co-existing morphologies are identified by the analysis of the SAXS profiles. This behavior is rationalized by considering the entropic penalties associated with chain stretching required in the formation of a composite morphology. To minimize the entropy loss due to the stretching of the chains, two separate BCP + homopolymer systems formed.

The second strategy of choosing the blocks such that they interact among each other successfully results in the formation of composite structures. This strategy is successful because of the absence of any homopolymer that would otherwise interact separately with the blocks. Formation of three-phase lamellar and hexagonally packed morphologies are observed in the resulting blends. While for the case of PS as one of the formed phases, lamellar morphology forms even at asymmetric volume fractions of the three phases, when the PS block is replaced with a flexible PPO block, hexagonally packed morphology is formed. The structure in this hexagonally packed morphology is proposed to be a core-shell type morphology.

CHAPTER 5

PHOTO-INDUCED ORDERING OF BLOCK COPOLYMERS

5.1 Introduction

As introduced in previous chapters, block copolymers (BCPs) exhibit great promise as nanostructured materials and templates because of their ability to spontaneously self-assemble to form well-ordered periodic morphologies with typical domain sizes on the order of 10-50 nm. Many techniques have been devised to manipulate and improve domain order and domain alignment.[103,104] These include chemical[10,105,106] or topographical[11,107] modification of substrates as well as processing methods that include solvent annealing and controlled evaporation of solvent,[108-111] use of neutral surfaces[106,112] or treatment with electric fields.[113] The resulting well-ordered films find utility in device fabrication,[114-117] including their use as lithographic masks or masters for ultra-high density magnetic storage media[11,107,118] or as templates in fabrication of inorganic mesostructured materials[12,13,119] and polymeric nanoporous membranes.[16,120] In this chapter, the design of BCP-additive systems which transition from a disordered state to a well-ordered state via a simple, on-demand photo-induced ordering process is described. Since the process is photo-induced, a photomask can be employed for carrying out photo-induced ordering in a region-selective manner such that only the regions that are exposed to light become ordered while the rest of the film does not show formation of ordered block copolymer morphology. This strategy provides a straight forward, non-intrusive means to form well-ordered chemical and

topographical patterns within arbitrary regions of the target surface. Region-selective nanoscale pattern generation will offer new opportunities for device fabrication. These include the preparation of underlayers for ordering of another block copolymer film or liquid crystal layer, etch masks for subtractive processing of nanopatterned surfaces for use in applications such as nanofluidics and sensors. In the example provided here, the nanostructures formed in the exposed regions bear carboxylic acid groups in one of the domains of the block copolymer structure while the other domain is free of any reactive functionality. The carboxylic acid groups can be used to tether other functional materials such as nanowires,[121,122] biomacromolecules or polymer brushes in a region-selective manner[123] for use in sensors and other nanoscale devices. The contents of this chapter were published recently.[124]

The strategy involves the use of an A-B-A type BCP which is disordered by itself and when blended with an additive, but the additive can be transformed in-situ by exposing the material to light and baking at a moderate temperature. The transformed additive which is analogous to the ones shown in **Chapter 3** (BHCA, CTMA) can drive the ordering of the BCP employed. As described in **Chapter 3**, small BCPs can remain disordered as the product χN sets the lower limit for the formation of an ordered morphology and for the smallest domain spacing and domain size possible, which scale with N for a given BCP. As introduced in the previous chapters, certain disordered BCPs can be ordered by incorporation of a variety of selectively interacting additives like salts, and small organic molecules. Likewise, the previous chapters explored the addition of homopolymers, BCPs and non-polymeric additives that selectively associate through hydrogen bonding with the poly(ethylene oxide) blocks of PEO containing

small and therefore disordered BCPs induces microphase segregation and strong order.[44,125] [63] and polyhedral oligomeric silsesquioxanes functionalized with multiple hydrogen bonding sites at their periphery, can likewise induce order in Pluronic surfactants and other PEO containing block copolymers.

In all the additive-driven assembly approaches used so far, including the ones discussed in the previous chapters, the chemical identity of the additives was pre-programmed to facilitate selective interaction with one of the blocks, thereby enhancing the segregation strength between the blocks and induce ordering. In this chapter, a new paradigm in the design of additive-loaded BCP systems is introduced. Here the blends of the additive and the BCP are initially disordered but can undergo an ordering upon chemical transformation of the additive induced by an external trigger, such as moderate heating in the presence of catalytic amount of a third component (an organic acid) or photogeneration of the catalyst followed by moderate heating. This requires a design in which the additive initially exhibits compatibility via weak interaction with the copolymer such that ordering does not occur. The second requirement is that once the blend is formed, an in situ transformation of the additive should induce sufficiently strong preferential interactions with one of the blocks thereby causing the chemically different blocks of the BCP to phase segregate well enough so that a well-ordered morphology results. Acid catalyzed deprotection of the additive functional groups is used to trigger the in situ transformation of the additive in order to modulate its interaction with the copolymer host. After establishing that these systems undergo an ordering upon additive deprotection, the organic acid catalyst is replaced with a photoacid generator (PAG) to allow creation of acid in light-exposed regions only.

Thus, coupled with the use of a photomask, the photo-induced ordering process enables region-selective control of the ordering in the copolymer film as shown schematically in Figure 5.1. Figure 5.1 also shows the additive employed in its protected and deprotected forms. This protected from of the additive is referred to as MG-TBCM as it belongs to the family of molecular glasses (MGs) based on a calix[4]resorcinarene structure and is protected with tert-butoxycarbonylmethyl (TBCM) groups. Upon baking at moderate temperature in the presence of a strong acid, the TBCM protecting group easily deprotects to form carboxylic acid groups resulting in formation of deprotected MG (i.e. MG-COOH) and therefore this chemistry is used for photoresist applications as well.[126]

Photo-responsiveness has previously been imparted to polymers by chemically grafting photo-sensitive moieties on their chains. These moieties undergo chemical or isomeric transformations when exposed to light of certain wavelengths and affect the polymer backbones to which they are chemically attached. In many instances, the trans-cis and cis-trans isomerization of azobenzene groups upon exposure to ultra violet (UV) light at wavelengths 352 nm and 419 nm respectively have been employed to enable such transformations. For example, exposure to light was shown to influence the orientation of the domains of BCPs with azobenzene moieties grafted on one of its blocks.[127-130] In other work, UV-induced photodimerization of anthracene has also been employed to control micron scale morphology of homopolymer blends.[131] A recent review describes the behavior of block copolymer systems with photosensitive moieties grafted on them.[132] Several examples of photo-induced transitions exist for such block copolymers in solution form, for example, photo-induced sol-gel transitions.[133] In bulk form, such modified block copolymers have been shown to be affected by light and

various studies have been performed on various microphase separated block copolymers to study the effect of exposure to light on morphological transitions. For instance, Xu and coworkers showed how the arrangement of nanoparticles in an ordered BCP is affected by such transitions.[134] In all these cases the block copolymers were already structured and light was used to tailor that structure, for example, alter the domain orientation or enhance their alignment. In contrast, here the focus is on the formation of structure by transitioning from a disordered state to a well-ordered state.

In the above examples interesting UV-induced changes to the structure were observed. However, attempts to cause a photo-induced ordering of such modified BCPs have not yet been very successful in demonstrating a clear transition from a disordered state to a well-ordered state. For example, in one study azobenzene moieties were grafted to the poly(n-butyl methacrylate) block of polystyrene-block-poly(n-butyl methacrylate) BCPs to cause photo-induced trans-cis isomerization of azobenzene with the goal of inducing order in the BCP.[135] The non-irradiated BCPs showed a single glass transition temperature which would be consistent with phase mixed BCPs. The glass transition temperatures of the irradiated BCPs were not shown, so it is not clear from DSC whether a disorder-to-order transition (DOT) occurred upon irradiation. X-ray reflectivity indicated that thin films of such BCPs underwent some photo-induced changes, but the morphology could not be precisely determined.

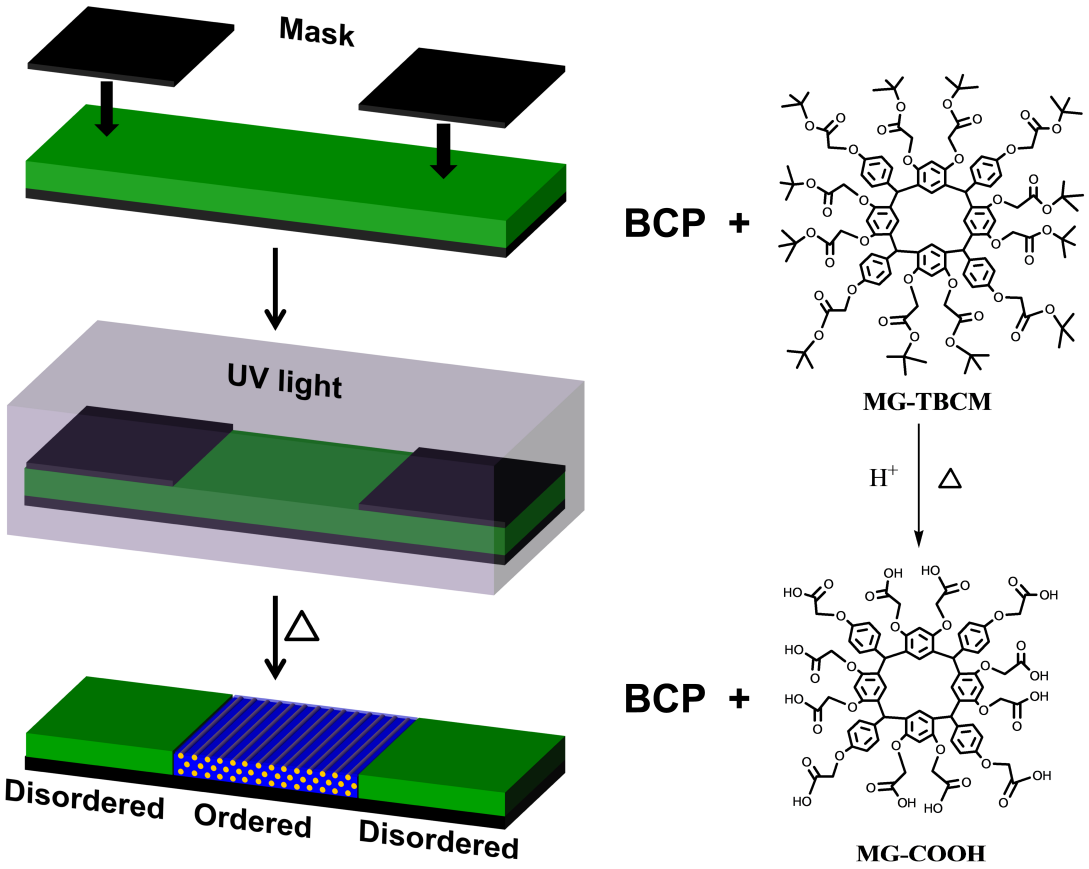

Figure 5.1. Schematic representation of the photo-induced ordering process (left) and the underlying reaction (right). Upon spin coating a blend of F127, MG-TBCM and a photoacid generator, the film is disordered (green). Upon irradiation of the disordered film with UV light through a mask placed on top, a photo-generated acid is liberated in the exposed regions, which drives the chemical transformation of MG-TBCM to MG-COOH (reaction on right) upon baking while the unexposed regions remain unchanged. MG-COOH interacts strongly via hydrogen bonding with PEO resulting in spontaneous formation of microstructure due to disorder-to-order transition of F127 as PPO microphase separates as cylinders (orange) from the PEO + MG-COOH + photoacid phase which form the matrix (blue).

In contrast to the yet explored method of chemical grafting of photo-responsive moieties to impart photo-responsiveness to the block copolymers, here a different and simpler chemistry and governing physics is employed to formulate highly photo-sensitive disordered block copolymer systems. This strategy relies upon simply blending

disordered block copolymers with a photo-sensitive additive and catalytic amounts of a third ingredient to formulate disordered blends. The MG additive employed in this work was originally designed as stand-alone chemically amplified photoresist and can be efficiently deprotected to yield the –COOH functionality upon UV exposure using PAGs.[126] This photosensitivity is exploited here for the realization of photo-induced ordering to form well-ordered nanoscale features. Thus, the synthetic efforts are significantly minimized because the host BCP does not require grafting of photo-responsive moieties. MGs with similar aromatic cores bearing other protecting groups are also being explored as chemically amplified high resolution photoresists on account of their small molecular size.[136,137]

A Pluronic triblock copolymer, F127 (EO_{96}-PO_{62}-EO_{96}, ~12 kg/mol), which has a DOT temperature of approximately 8 ^{o}C[48] is chosen as a representative example of a disordered BCP. While the TBCM groups provide weak interaction with F127 ensuring miscibility, the carboxylic acid groups can interact strongly with PEO blocks via hydrogen bonding. Thus, the chemical transformation from MG-TBCM to MG-COOH gives rise to strong interactions that induce ordering of F127 leading to formation of well-ordered morphology.

5.2 Experimental

5.2.1 Materials

Pluronic triblock copolymer F127 (PEO_{96}-PPO_{62}-PEO_{96}, ~12 kg/mol) was donated by BASF and p-toluenesulfonic acid (PTSA) was obtained from Acros

Chemicals. Triphenylsulfonium triflate (TPST), 5,5'-Carbonylbis-(trimellitic acid) (CTMA), 4-hydroxybenzaldehyde, resorcinol, and tert-butyl bromoacetate were purchased from Sigma-Aldrich and used without further purification. N,N-dimethylformamide, ethanol and ethyl acetate were purchased from Sigma-Aldrich and used without further drying.

5.2.2 Synthetic procedure for MG-TBCM

The synthesis of the phenolic version of the molecular glass was carried out by Jin-Kyun Lee at Cornell University. These phenolic version was protected with TBCM groups with the help of Evan L. Schwartz. Some of the characterization of the synthesized MG-TBCM was performed by Evan which were also confirmed at UMass. Details of the synthesis and characterization are described elsewhere.[124]

5.2.3 Sample preparation for small angle x-ray scattering and for differential scanning calorimetry

Samples of neat F127 and its blend with CTMA were made by dissolving their appropriate amounts in DMF by heating at 60 ^{o}C with occasional stirring. These solutions were vacuum dried on glass slides for two days in a vacuum oven set at 75 ^{o}C.

Samples of neat F127 and its blends with MG-TBCM and/or PTSA were made by dissolving the solids into a cosolvent containing ethanol and ethyl acetate in weight ratio of 1:1. These solutions were kept on a hot plate for 24 h at 75 ^{o}C and then drop casted on glass slides kept on hot plate at 80 ^{o}C. The glass slides were kept on the hot plate for about 5 hours to ensure complete deprotection after which they were vacuum dried at 70 ^{o}C for one day.

Binary blend compositions are reported as weight ratio of additive to F127. For example, a blend referred to as 30/70 contains 30% additive and 70% F127. For ternary blends to which MG-TBCM, F127 and PTSA or TPST were added, blend compositions are represented as x/y/z. Here, x and y denote the ratio of MG-TBCM and F127 and z/100 denotes the amount of PTSA or TPST added per gram of the MG-TBCM/F127 blend. For example, a 40/60/5 blend of MG-TBCM, F127 and PTSA implies a 40/60 blend of MG-TBCM and F127 to which 0.05 g of PTSA was added per gram of the 40/60 blend.

5.2.4 Small angle x-ray scattering

The procedure and the setup described in Chapter 2 were also used for these measurements.

5.2.5 Differential scanning calorimetry

The procedure and the setup described in Chapter 3 were also used for these measurements.

5.2.6 Sample preparation for scanning force microscopy

For spin coating thin films for photo-induced ordering and scanning force microscopy (SFM) characterization, solutions (5 wt. % solids) of MG-TBCM with F127 and TPST were made by dissolving appropriate amounts of solids into ethanol-ethyl acetate (1:1 by weight) cosolvent. These solutions were kept on a hot plate at 60 ^{o}C for 2 hours to dissolve the contents. The solutions were filtered through 0.2 micron PTFE

filters and spin coated at 2000 RPM on silicon wafers cleaned with carbon dioxide snowjet followed by an oxygen plasma treatment. The spin coated films were placed immediately on a hot plate set at 80 ^{o}C kept underneath a 254 nm wavelength UV lamp and some portions of the films were covered by aluminum foil to mask off exposure to UV light. The films were kept on the hot plate for a total of 3 minutes and the UV lamp was switched on to expose the unmasked portion of the film to UV light in the middle one minute of the 3 minute heating cycle. At the end of 3 minutes the wafers were removed from the hot plate and the exposed and unexposed regions were characterized at room temperature by SFM.

5.2.7 Scanning force microscopy

SFM was carried out on a Veeco Dimension 3100 scope with a Nanoscope III controller operated in tapping mode to acquire the phase and height images.

5.3 Results and Discussion

Differential scanning calorimetry (DSC) measurements were performed to ascertain compatibility of the protected and deprotected forms of the additive in the blends and to compare the interaction of MG-TBCM and MG-COOH with F127. The vertically shifted thermograms are shown in Figure 5.2. The melting endotherms are ascribed to the melting of PEO crystallites within F127, as PPO does not crystallize. Also shown are the values of the melting temperatures as represented by the endotherm peak positions and the melting enthalpy normalized to the amount of PEO present in the blend. The addition of a strong acid, p-toluenesulfonic acid (PTSA), or MG-TBCM to

F127 caused the melting point and melting enthalpy to decrease indicating the compatibility of both PTSA and MG-TBCM with F127. When both PTSA and MG-TBCM were added simultaneously, which results in deprotection of MG-TCBM, PEO crystallization was completely inhibited. This is attributed to the strong interaction of MG-COOH with PEO chains of F127 via hydrogen bonding. Thus, the compatibility of F127 with the additive in both protected and deprotected forms was verified. Further, when these blends were drop casted from their respective solutions on glass slides at 80 ^{o}C, which is the temperature at which photo-induced ordering experiments were conducted (discussed later) and is above the melting point of PEO crystallites, all the blends were found to be clear, which indicates formation of homogenous blends without macrophase separation.

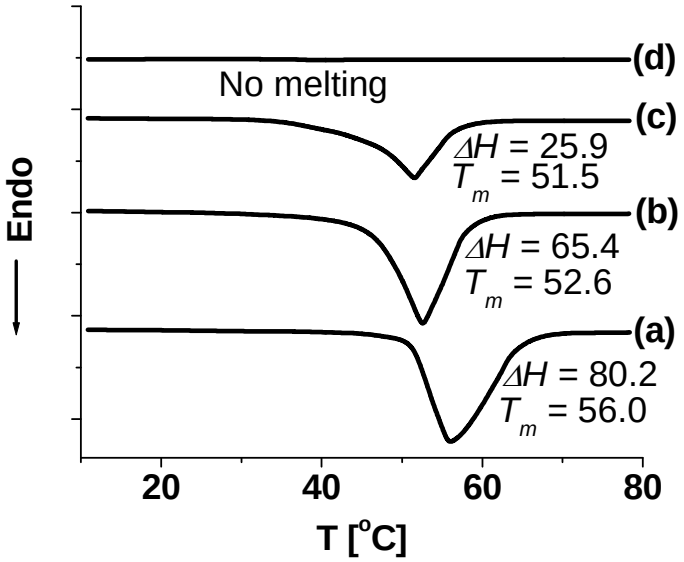

Figure 5.2. DSC thermograms of (a) neat F127, (b) 5/95 blend of PTSA/F127, (c) 40/60 blend of MG-TBCM/F127, (d) 40/60/5 blend of MG-TBCM/F127/PTSA (MG-TBCM here is actually converted to MG-COOH). The thermograms have been shifted vertically to avoid overlap. The melting temperature (^{o}C) and melting enthalpy J/(g of PEO) are mentioned beside each curve where melting was seen.

First, small angle x-ray scattering (SAXS) is used to study the phase behavior of blends F127 with the additive 5,5'-carbonylbis-(trimellitic acid) (CTMA), which is similar in functionality to the molecular glass in its deprotected form, MG-COOH. Figure 5.3 shows that the incorporation of CTMA in F127 induces ordering resulting in the formation of well-ordered hexagonally packed cylindrical morphology. The SAXS profile of neat F127 at 80 ^{o}C shows a broad peak, which is a typical signature of disordered BCPs arising due to correlation hole effects or compositional fluctuations.[6,47] A similar broad peak was observed to form for F108 in Chapter 2. However, as CTMA can hydrogen bond with the PEO blocks of F127, incorporation of 30 % CTMA causes its ordering as indicated by the sharpening of first peak and appearance of multiple higher order peaks, the positions of which indicate formation of cylindrical morphology (peak position ratios 1, √3, √4, √7). It is also of interest to note the effect of strong interactions on the morphology at 22 ^{o}C, which is below the melting temperature of PEO crystallites. The SAXS profiles obtained after maintaining the samples at room temperature for 24 hours are also shown in Figure 5.3. Neat F127 shows lamellar morphology (peak position ratios 1, 2, 3…) which is not due to an ordered BCP morphology but rather is due to crystallization of PEO below its melting point of 56 ^{o}C.[138] In comparison, the room temperature SAXS profile of F127 loaded with 30 % CTMA did not show evidence of PEO crystallization and the BCP morphology was maintained upon cooling. Thus, strong interaction of the PEO chains with CTMA inhibits crystallization of PEO and sustains the block copolymer morphology. The behavior of the blend of CTMA with F127 provides an indication about the expected

phase behavior for the case of blends of F127 with the MG in deprotected form i.e. MG-COOH.

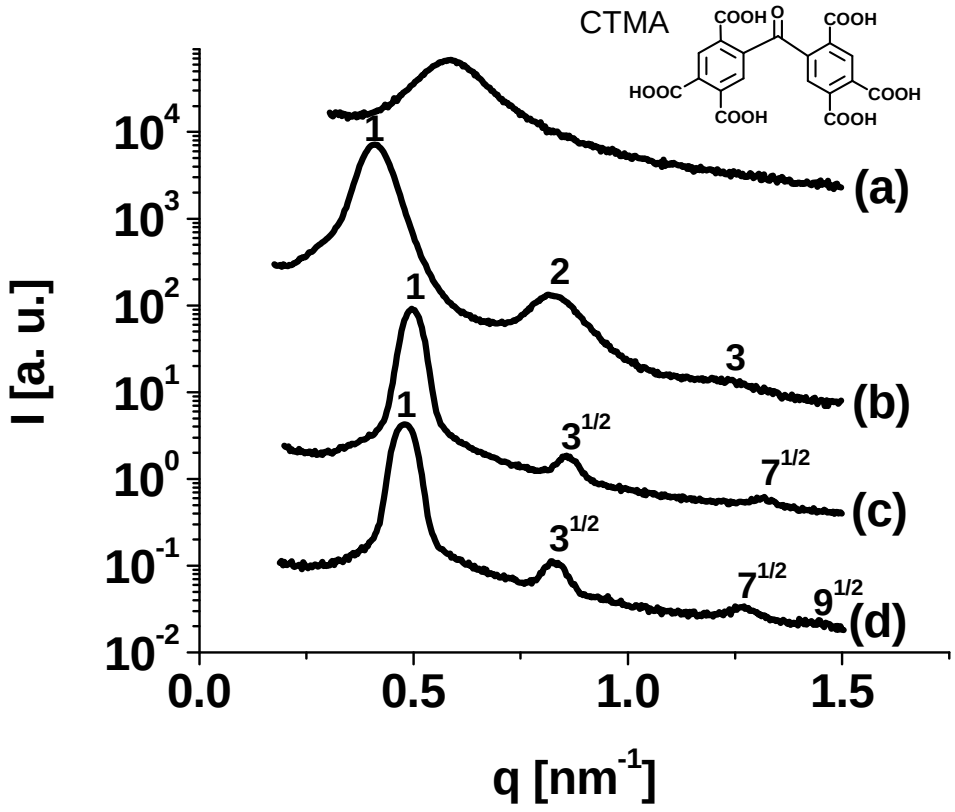

Figure 5.3. SAXS profiles of (a) neat F127 at 80 ^{o}C, (b) neat F127 at 22 ^{o}C, (c) 30/70 blend of CTMA/F127 at 80 ^{o}C, (d) 30/70 blend of CTMA/F127 at 22 ^{o}C

Next, the phase behavior of blends of F127 and MG-TBCM with and without the addition of PTSA is compared in Figure 5.4. The blend composition was varied between 20 % MG-TBCM to 50 % MG-TBCM. The MG-TBCM in the samples to which PTSA is added deprotects to form MG-COOH. At a range of composition between 20 % to 40 % MG-TBCM, the blends containing no PTSA were found to be disordered while the blends containing PTSA showed well-defined primary peaks with

multiple higher orders of reflection. The results indicate formation of a well-ordered hexagonally packed cylindrical morphology with an interplanar spacing ($d = 2\pi/q^*$) of about 13.0 nm. This is an important aspect in this work. MG-COOH represents an additive structure which is capable of ordering F127. At 50 % loading of MG-TBCM with PTSA, the primary peak of the scattering profile broadened, which indicates a loss of a well-ordered structure most likely due to a loss in the positional correlation of the PPO domains. The full width at half maximum intensity (FWHM) for the scattering profiles of neat F127 (FWHM=0.18) and F127/PTSA blend (FWHM=0.12) were estimated as discussed previously.[63] While the correlation hole peak for the F127/ PTSA blend exhibits a FWMH that is slightly narrower than that of neat F127, it is apparent that the F127/PTSA blend remains phase mixed indicating weak interaction between F127 and PTSA. Likewise, the disordered state of MG-TBCM/F127 blends indicates weak interaction. This indicates that the ordering of F127 in the presence of the deprotected additive was a result of hydrogen bonding interactions between the carboxylic acid groups of MG-COOH and PEO chains rather than simply due to interaction of PTSA with PEO.

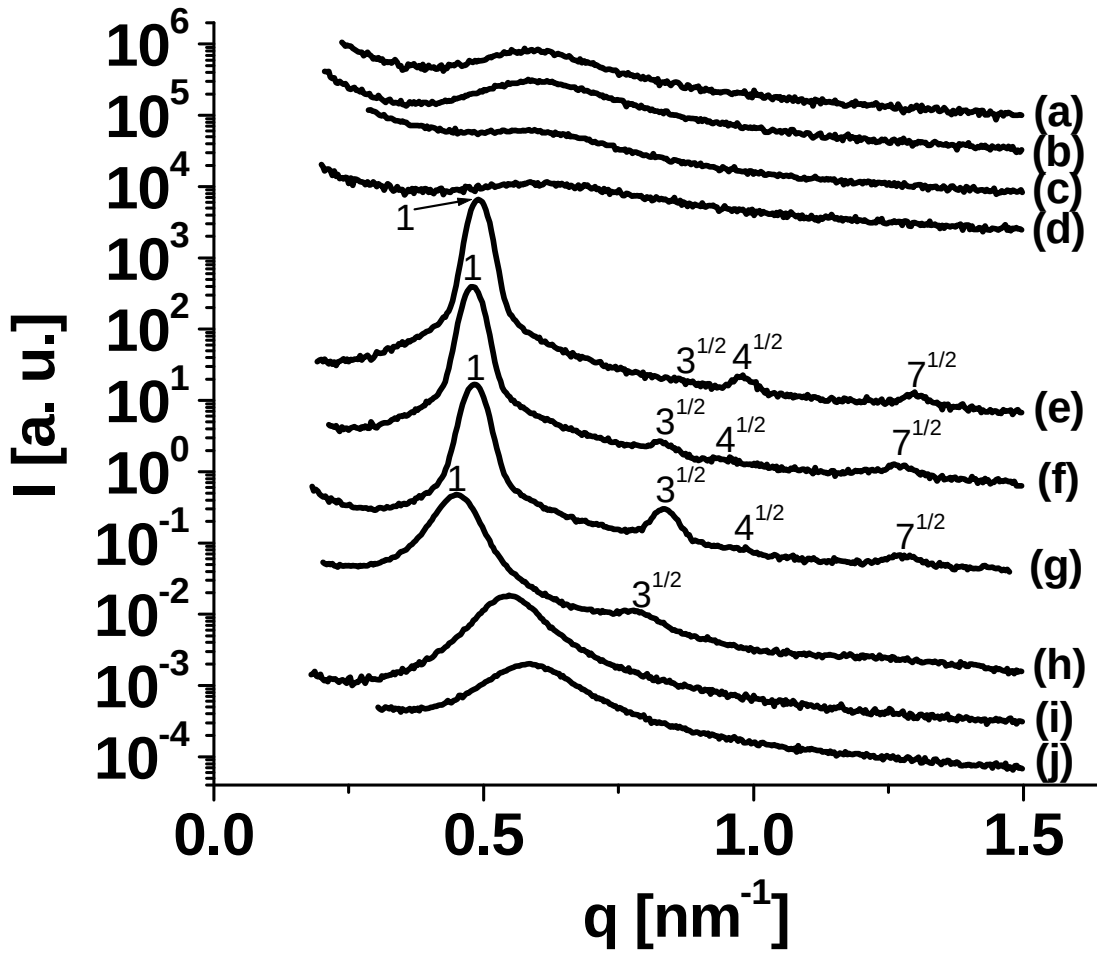

Figure 5.4. SAXS profiles of neat F127 and its blends with PTSA and/or MG-TBCM at varying compositions at 80 °C: (a) 20/80 MG-TBCM/F127, (b) 30/70 MG-TBCM/F127, (c) 40/60 MG-TBCM/F127, (d) 50/50 MG-TBCM/F127, (e) 20/80/5 MG-TBCM/F127/PTSA, (f) 30/70/5 MG-TBCM/F127/PTSA, (g) 40/60/5 MG-TBCM/F127/PTSA, (h) 50/50/5 MG-TBCM/F127/PTSA, (i) 5/95 PTSA/F127, (j) neat F127. Ratio of higher order peak positions with that of primary peaks indicate hexagonally packed cylindrical morphology for samples that contained both MG-TBCM and PTSA (e, f, g, and h).

The SAXS and DSC measurements described above confirm that a DOT can be induced in F127 by transitioning from weak to strong interactions between the additive and the BCP. With the governing chemistry and physics in place, the formulation of the BCP system that undergoes photo-induced ordering follows a simple switch of the

strong acid, PTSA with a PAG, triphenylsulfonium triflate (TPST). Photo-induced ordering experiments were carried out on spin coated films and scanning force microscopy (SFM) was used to characterize the resulting morphology. The 40 % MG-TBCM blend was chosen as the system to demonstrate photo-induced ordering, as this system in deprotected form shows the formation of well-ordered morphology and complete inhibition of PEO crystallization. Films of F127 with 40 % MG-TBCM and 5 wt. % TPST were spin coated onto cleaned Si wafers. As explained in detail in the sample preparation section, the films were baked at 80 ^{o}C for 3 minutes, during which a portion was exposed to UV light (254 nm wavelength) for one minute to cause liberation of a strong photoacid, which deprotects MG-TBCM to MG-COOH. The solvents employed and the cleaved leaving group byproducts are volatile and leave the films upon spin coating and baking, leaving behind F127, MG-COOH and the generated acid in the exposed regions. From previous work it is known that the photoacid[12,13,119] and additives similar to MG-COOH[63] are selective for the PEO phase as depicted in Figure 5.1. High loadings of the additives bearing hydrogen bond donating groups are possible due to strong interactions between additive and the PEO chain segments, which are hydrogen bond acceptors.[63] Figure 5.5 shows representative SFM images of unexposed and exposed regions. The roughness of the film observed in unexposed region is attributed to crystallization of PEO. The regions that were exposed to UV light showed a finger-print pattern which indicates formation of well-ordered cylindrical morphology. Since both height and phase images reveal the morphology, it is clear that the photo-induced ordering process caused formation of both topographical and chemical patterns. Additionally, the exposed regions did not show any signs of PEO

crystallization which agrees with the findings in Figure 5.3 where the crystallization of PEO was found to be inhibited due to strong interactions with carboxylic acid groups. Appendix 5.1 at the end of this chapter shows the thicknesses of protected and deprotected films and confirms complete deprotection of MG-TBCM throughout the thickness of the film in the exposed regions. While the films shown in Figure 5.5 exhibit thicknesses that are greater than a single domain spacing, the concept can be extended to single-domain thickness masks. We recently demonstrated that single-domain thickness masks with cylindrical morphologies and high etch selectivity can be prepared by blending F127 with multi-ring aromatic additives bearing multiple phenol groups at their periphery. The phenol groups serve as hydrogen bond donors and drive assembly through interactions with the ether oxygen of the PEO segments in a similar manner as the deprotected molecular glass additives described here.[139] Photo-induced ordering in single and multi-domain thickness films could further be combined with the existing techniques that allow precise control over the orientational and translational placement of the BCP domains over large areas to realize long-range order in the exposed regions of the films.[103,104] However, for certain applications, for example, fabrication of mesoporous materials using the BCP film as a template, thick films are required and the BCP template does not necessarily require long-range order.[12] One undesirable aspect of the present system as employed here is the roughness in the unexposed regions of the film, which could be an issue for some thin film applications. There are several alternative approaches. These include reversing the volume fractions in the current block copolymer such that PEO is the minor component and PEO crystallization is confined or using films of smaller thicknesses, equivalent to a single domain or a few

layers, to limit the volume of PEO crystallization. Ultimately, one could also apply the concepts described here to systems in which the hydrogen bond acceptor block is amorphous.

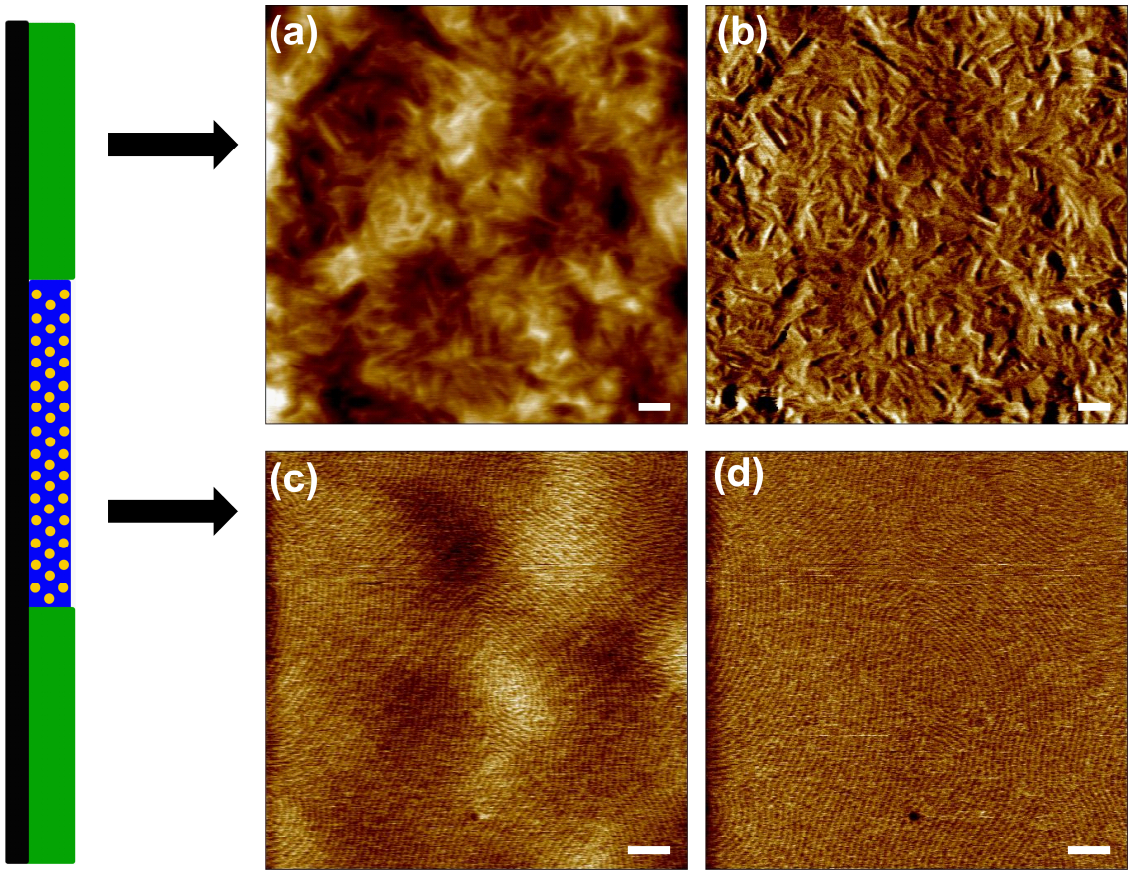

Figure 5.5. SFM images of unexposed and exposed regions of the film. (a) Height image of the unexposed region (z range = 10 nm), (b) Phase image of the unexposed region (z range = 22^{o}), (c) Height image of the exposed region (z range = 4 nm), (d) phase image of the exposed region (z range = 9^{o}). Unexposed regions are rough due to formation of PEO crystallites while the exposed regions form well-ordered cylindrical morphology showing features in height and phase images thus indicating formation of chemical and topographical BCP pattern. Scale bars = 150 nm.

One additional advantage of this approach over the method of chemical grafting of photo-responsive moieties on block copolymer chains is that the wavelength of UV light can be selected for the PAG employed. Therefore, simply by employing PAGs that can be activated to generate photoacid at different wavelengths, an array of materials that order when exposed to different wavelengths of light could be formulated with the same material. Also, since the intensity of light governs liberation of photoacid from PAGs, generation of 3D microstructures containing ordered domains within an otherwise disordered film could be envisioned by performing a controlled 3D exposure through 3D fabrication techniques such as holographic lithography.[140,141] The use of an ordered underlying BCP film as a pattern for manipulating the structure of a BCP film on top as demonstrated by Nealey and coworkers[106] could also benefit from this photo-induced ordering strategy because the order in the underlying layer - and consequently the alignment and ordering in the top layer - could now be directed only in regions desired merely by exposing the bilayer films to UV and moderate heating, thus providing a lever to control regions where the top film is modified.

Although F127 was chosen as the disordered BCP, this design of photo-induced ordering system depends upon the hydrogen bonding interaction of PEO blocks with the additive and therefore it is likely that this strategy could be extended to other PEO containing BCPs as well as to BCPs containing other hydrogen-bonding blocks. For example, as shown in Figure 5.6, in the presence of PTSA, MG-TBCM was found to induce ordering of various other PEO containing BCPs. This additive driven approach is particularly advantageous towards enabling easy scale up because the BCPs themselves do not require any special synthetic procedures to enable photosensitivity. Thus, the

ability to independently synthesize the additives and independently choose a relevant BCP and a PAG simplifies the design and yet adds versatility towards the design of BCP systems that undergo photo-induced ordering to form various morphologies when exposed to UV light of a desired wavelength. We are currently extending this strategy to define sub-micron and nanoscale patterned regions of ordered structures, which are of interest for current and future block copolymer device applications.

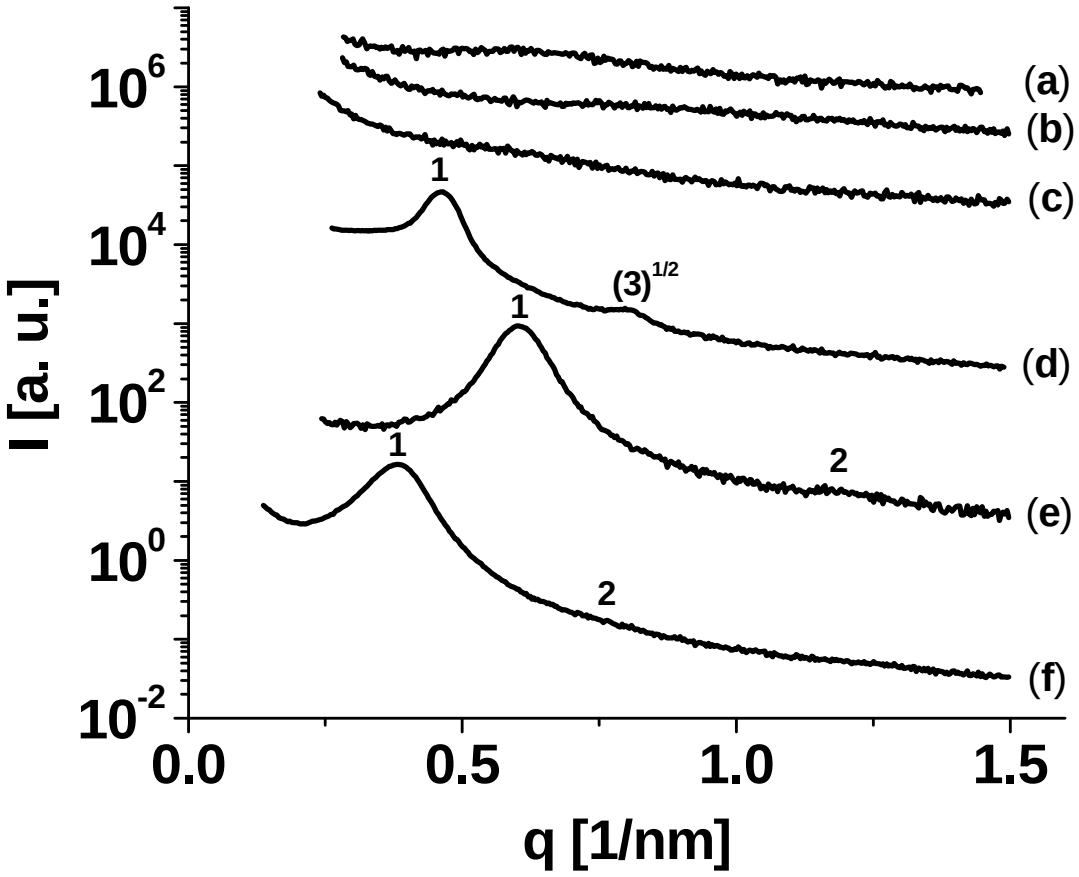

Figure 5.6. SAXS profiles of blends of various PEO containing block copolymers with MG-TBCM with and without PTSA: (a) 40/60 blend of MG-TBCM and F108, (b) 40/60 blend of MG-TBCM and P105, (c) 40/60 blend of MG-TBCM and PS-PEO, (d) 40/60/5 blend of MG-TBCM, F108 and PTSA, (e) 40/60/5 blend of MG-TBCM, P105 and PTSA, and (f) 40/60/5 blend of MG-TBCM, PS-PEO and PTSA.

5.4 Conclusions

Design strategy of blends of block copolymers and a photosensitive additive is shown to undergo photo-induced ordering using a standard UV exposure and moderate baking. The strategy proposes a new concept of dual nature of the additive such that in one form it interacts weakly with the BCP and blends with it but in the other form it interacts strongly with one of the blocks to drive phase segregation of the disordered BCP. The transition can be induced by heating in the presence of acid, which in turn can be formed with the help of a photoacid generator to impart photo-sensitive mode of transition. Since UV light is used as a trigger to generate the photoacid, it is easy to control the regions where the material is exposed to light to form a photoacid. In the subsequent baking step the regions containing acid forms an ordered morphology because of the acid catalyzed transformation of the additive molecules to a strongly interacting form. Thus, this study allows traversing between two largely different states on the BCP phase diagram in a simple and non-intrusive manner.

Appendix 5.1. Measurement of film thickness before and after deprotection

Although both F127 and the molecular glass have good transparency for 254 nm UV light employed, the loss in thickness upon deprotection would confirm that the UV light penetrated through the entire film in the exposed regions and caused complete deprotection of MG-TBCM. Thicknesses of the protected and deprotected films were obtained by spectroscopic ellipsometry using GES-5 spectroscopic ellipsometer (SOPRA, λ=300-800 nm). The refractive index of the polymer film was obtained using a Cauchy dispersion relationship.[142] These films were prepared using the same procedure from the solution that was also spin coated to carry out photo-induced ordering experiments and SFM characterization. Therefore the thickness of the protected and deprotected films correspond to the thickness of the unexposed and exposed regions respectively.

The thickness of the film upon spin coating and baking for three minutes at 80 ^{o}C without exposure to UV light was found to be 240.6 ± 0.6 nm (refractive index = 1.5). However, due to deprotection of MG-TBCM, the thickness of the film which was exposed to UV for a minute during the three minutes of baking at 80 ^{o}C was found to be 192.7 ± 1.9 nm (refractive index = 1.53). The theoretical loss in thickness upon complete deprotection of MG-TBCM throughout the thickness of the film in the exposed region is ~12%. The thickness loss of 19.9% here accounts for complete deprotection of MG-TBCM as well as strong interactions that occur in the exposed regions due to hydrogen bonding interactions that should cause a slight increase in film

density. Thus, the cylindrical morphology observed on the top surface of the film must propogate through the entire thickness of the film in the exposed regions.

CHAPTER 6

ADDITIVE-LOADED EUV PHOTORESISTS: PERFORMANCE ENHANCEMENT AND THE UNDERLYING PHYSICS

6.1 Introduction

Photoresist solutions typically contain a polymer and other minor components and are spin-coated to form photoresist films on substrates. When a photoresist film is exposed to ultra violet (UV) light and baked, it undergoes a change in its solubility in developer solutions when. Therefore, region-selective exposure of a photoresist film through a mask bearing holes in a desired pattern and consequent development can result in formation of patterned polymer films such that the polymer is present in some areas and absent in other areas. Figure 6.1 shows a schematic of this process. Patterned films made in this way enable a variety of region-selective treatments to the underlying substrate including etching and metal deposition. After such a process, the photoresist film is usually removed to obtain patterned underlying substrates. This process of using photoresists to pattern the underlying substrates is called photolithography. The devices and other structures on semiconductor chips are made layer-by-layer building upon silicon wafers. In the state-of-the-art chip fabrication, a single chip may require up to thirty photolithography steps.

The pattern on the substrate follows from the pattern of the polymer film and therefore the quality of patterns on polymer film affects the quality of patterns on substrate. Therefore improvements in photolithography translate directly into improvement in desired structures on each layer and hence improvements in

performance of the entire semiconductor chip. The most challenging photolithography steps are the ones in which smaller features are made and the present research aims to develop materials that cater to this requirement. Wallraff and Hinsberg provided a good review on using lithographic techniques for the formation of nanoscopic features.[143]

The aim of using photoresists is to end up forming patterned polymer film on substrates and employ it for certain region-selective processing of the substrate. As shown in Figure 6.1, there are two kinds of photoresists, namely, positive photoresists or negative photoresists both of which result in patterned polymer films. Positive photoresists contain a photosensitive pendant group also known as chemical protection group and a photoacid generator dissolved in a solvent. Upon exposure to UV light, the photoacid generator liberates a photoacid which is a strong organic acid capable of deprotecting (i.e. converting chemically) the protected groups to polar groups such as phenols and carboxylic acids. The deprotected polymer is chemically different and therefore can be dissolved away using a basic developer solution while the protected polymer remains undissolved. Thus patterned polymer films are formed (Figure 6.1 (d)). Often, a small quantity of a base (called base quencher) is added to the formulation so that the photoacid liberated in the exposed regions that diffuse into the unexposed regions are neutralized before they can cause the deprotection reaction in the unexposed regions. The name “positive” comes from the fact that for positive photoresists the regions that are exposed are the ones that are developed off and the unexposed regions remain behind.

In certain cases, the unexposed portions of positive photoresists, or the exposed portions of negative photoresists, are also slightly soluble in the developer solution

used. This is undesired and would result in a reduction in the thickness of the patterned polymer films obtained. Additionally, it could also lead to blurring of the edges of the patterns obtained. The loss in thickness upon development of the unexposed regions of a photoresist film is termed dark loss.

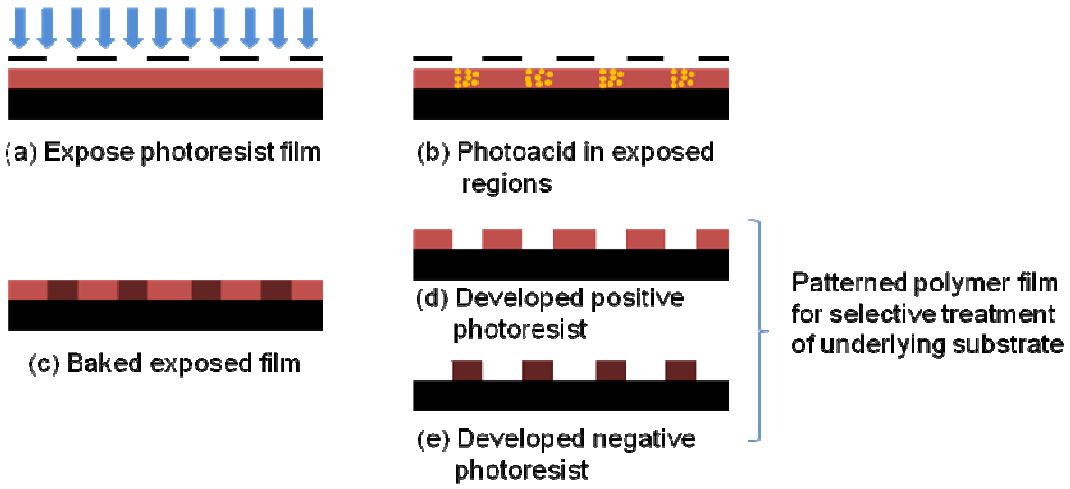

Figure 6.1. Schematic showing photolithography (a) shows exposure of film to UV using a mask, (b) shows generation of photoacid in the exposed regions, (c) shows change in material in exposed region as a result of acid catalyzed reaction upon baking, (d) shows patterned photoresist film formed after developing positive photoresists, (e) shows patterned polymer film after developing negative photoresists

In the case of negative photoresists, a crosslinkable polymer is mixed with a crosslinker and a photoacid generator. Here UV light causes photoacid generation which upon baking causes acid catalyzed crosslinking of the polymer rendering it insoluble. The polymer in the unexposed region dissolves away in the developer leaving behind a patterned polymer film (Figure 6.1 (e)). Thus for the case of negative photoresists, the regions that are exposed are the ones that are remain behind and the unexposed regions are washed away during development. While most of the work discussed in this chapter

deals with positive photoresists, Appendix 6.1 discusses the possibility of formulating highly etch-resistant negative photoresists. Due to the current practical constraints in the choice of the developer solution, this system was simply shown to function at micron scale patterning but was not developed any further to explore the sub-100 nm patterning capabilities.

The ability to continually reduce the size of features on a semiconductor chip has allowed the industry to maintain pace with Moore's predictions which proposed that the number density of transitors on an integrated circuit would double every two years. These developments were made possible by improvements in optical exposure systems which allowed higher exposure resolutions as well as improvements in photolithographic materials for their suitability with the wavelength of light used. Over the years, to achieve better resolution the wavelength of UV light employed for exposing photoresists was stepped down from 436 nm (Hg G-line) to 365 nm (Hg I-line) to 248 nm (KrF) to 193 nm (ArF), A decrease in wavelength has allowed achieving better resolution and spurred development of photoresist materials that are suitable to the wavelength employed. Development of photolithographic materials for extreme UV (EUV) at an exposure wavelength of 13.5 nm is presently an area of active research and is also the focus of this work.

With the processing conditions optimized, the photolithographic performance depends largely upon the photoresist materials. One of the main challenges is to restrict the penetration of the photoacid in exposed regions of the photoresist film to unexposed regions. While baking is required to drive the acid catalyzed deprotection or crosslinking reactions, the process of baking also enhances the penetration of photoacid

into unexposed regions because diffusivity of photoacid increases as the temperature of the film increases. Such diffusion makes photoacid available in unexposed regions where deprotection reaction can occur which causes blurring of the edges of the polymer pattern obtained after development. Blurring of the edges is measured in terms of line edge roughness (LER) which is the roughness of the edges (edges of the patterns in the patterned photoresist films) which should ideally be perfectly smooth. This diffusion is also responsible for limiting the size of smallest features (critical dimension, CD) possible with a particular photoresist. Photoacid diffusion through various photoresists has also been measured experimentally through various techniques like ion conductivity measurements,[144] photometric methods using a pH sensitive dye[145] and x-ray and neutron reflectivity.[146]

The incorporation of silica and other nanoparticles in negative resists has been shown to increase image resolution, but the mechanisms and structure-property relationships have not been characterized or optimized.[147,148] However, in the absence of strong interactions with the polymer matrix, the additives aggregated towards the surface of the film[149-151] which is undesired. In this work, the aim is to identify mechanisms behind additive-induced enhancements in resolution for copolymers of hydroxystyrene (HOST) and tert-butyl acrylate (tBA) (ESCAP resist), a positive photoresist, and apply this knowledge to the development of multi-functional additives that can enhance extreme ultra violet (EUV) photolithographic performance. In this work, molecular glass additives have been employed.

There are several challenges that need to be met for forming a suitable photoresist formulation. First, the miscibility of additives with the polymeric photoresist must be ensured before and after deprotection. Since the polymer undergoes a significant change in its functionality and therefore its hydrophilicity, the additives must be designed to undergo a similar change to ensure compatibility in both forms. Failure to achieve this compatibility would lead to additive aggregation and consequently, inhomogeneous film properties which would be detrimental to the photolithographic performance. Therefore, chemically protected additives that blend with the protected polymer resist have been incorporated. These additives undergo deprotection along with the polymer resist to generate strongly interacting groups in the exposed regions as shown in Figure 6.2. This scheme ensures compatibility of the additive with the polymer before and after deprotection.

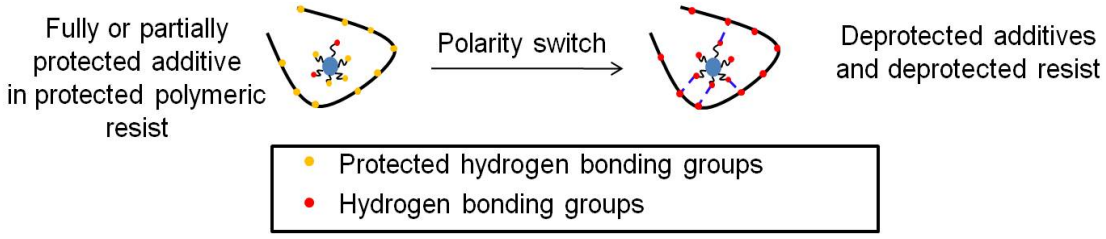

Figure 6.2. Scheme for ensuring compatibility of additives with the polymeric photoresist both before and after deprotection. Fully or partially protected additives are blended with protected photoresists. Upon deprotection of the polymer photoresist, the groups on the additives also undergo deprotection to form groups that can interact via strong hydrogen bonds with the polymer backbone and cause physical crosslinking.

There are several groups that can be used to protect the additives. Among these, both tert-butoxycarbonyl (tBOC) group and tert-butoxycarbonylmethyl (tBCM) groups

have been shown to cause the compatibility of additives with ESCAP resists.[152] While the tBCM group was found to promote compatibility better than tBOC group, it is not known whether upon deprotection, the phenol groups (formed from tBOC) or carboxylic acid groups (formed from tBCM) groups interact more strongly with the deprotected ESCAP resist. Here by choosing simple model systems, this aspect is explored as discussed later.

Next, the processing conditions for the photolithography experiments - especially the post-exposure baking temperature and duration - are also a significant factor in the ultimate performance. For these, the properties of the film like its glass transition temperatures as well as temperature required to drive deprotection reaction must be considered and the post-exposure baking step must be optimized accordingly. The diffusion length of a small molecule through a polymer matrix depends upon the temperature and time. The diffusion of the photoacid (a small molecule) through the polymer + additive matrix is expected to occur much faster as the baking temperature exceeds the glass transition temperature, a baking temperature as low as possible should be applied which maintaining the deprotection reaction kinetics which is faster at high temperature.

Additives of different sizes, architecture and number of functional groups are expected to pack differently within the polymer matrix. Although these aspects are complex, the consequences of incorporating additives into polymers are represented simplistically in Figure 6.3 by simply considering a difference in the size of the additive molecules. For cases when the additive disperses well in the polymer, there can be four different situations. When the additives molecules are very small, they are expected to

plasticize the polymer (Figure 6.3 (a)) which would be detrimental to the photoresist performance. On the other extreme, when the additive molecules are very large, they would phase separate from the polymer due to the excessive chain stretching required to accommodate the additives (Figure 6.3 (d)). Figure 6.3 (c) represents a situation in which the additive molecule is still larger than desired and it simply pushes out the the polymer chains. In such a situation, the photoacid would still be able to diffuse through the polymer matrix which is free of the additive. Figure 6.3 (b) represents the desired case in which the additive molecules blend well with the polymer so that they can serve as effective physical barrier to photoacid diffusion. Thus, since the photoacid molecule has to diffuse through this blend, different additives are expected to affect the acid diffusion differently. With an aim to identify the additive that reduces the acid diffusion the most, the photolithographic performance of the blends of ESCAP resist with the additives must be evaluated based on the additive molecule characteristics. Therefore, this study was conducted by choosing a series of molecular glass additives to identify the additive parameters that lead to better of their blends with the ESCAP resist.

The type of photoacid generator and the base quencher used also affects the resist performance. As discussed through this chapter, in this work, we choose two kinds of photoacid generator and two kinds of base quenchers to evaluate the effect of these minor components.

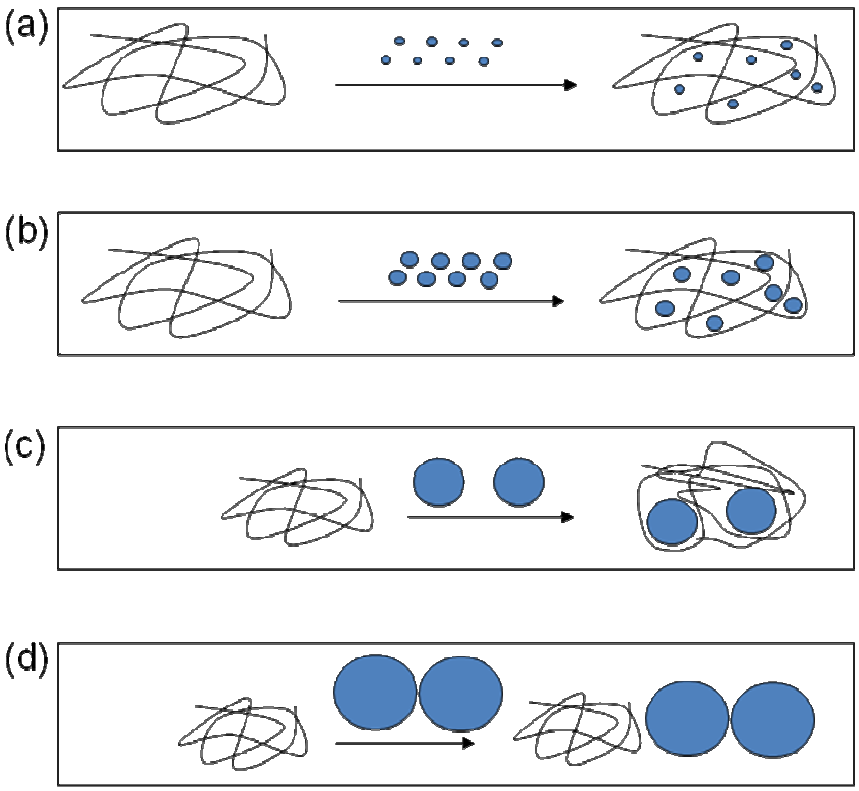

Figure 6.3. (a) Plasticization upon addition of small additives, (b) Molecular mixing where additive blends well with the polymer and can obstruct photoacid diffusion (antiplasticization) (c) Molecular mixing but large additives do not pack efficiently in polymer matrix (d) Entropy driven phase separation of large additives

As mentioned earlier, it is proposed that the incorporation of nanoparticles within amorphous resists leads to a decrease in photoacid mobility by causing a reduction in the free volume. We further propose that improvements in line edge roughness (LER) can be realized through incorporating additives that exhibit strong, non-covalent, multipoint interactions with the resist chain segments that yield reductions in photoacid diffusion due to a slowdown in the resist chain mobility and reduction in the overall free volume of the as-applied resist. Several molecular glasses (MGs) protected with tert-butoxylcarbonylmethyl (tBCM) groups were employed as

additives for incorporation in the ESCAP resist. The tBCM groups deprotect to form carboxylic acids that are capable of hydrogen bonding with the ESCAP resist. While all MGs decrease the dark loss by inhibiting solubility as also observed by Ito, Ueda and coworkers,[152] the results in this chapter indicate that MG additives deliver an additionally reduce photoacid diffusivity, which is important to achieving lower critical dimension (CD). Further, our results indicate that optimization of the additive molecular structure, size, and composition can improve CD and LER. Acid diffusion length measurements using the method of bilayers developed at the Polymers Division of National Institute of Standards and Technology (NIST)[146] also show differences in the acid diffusion lengths for photoresist blends with different MGs additives.

A successful blend of a polymer resist and MG has excellent film-forming attributes and sufficient glass transition temperature (T_g), which are difficult to achieve in neat small molecule resists.[152] In addition, the incorporation of additives allows for reductions in dark loss, and more importantly for reductions in photoacid diffusivity to achieve better resolution.

The ESCAP-based phenolic photoresists are being explored with EUV exposure wavelengths for obtaining features in the sub-50 nm range.[153] The high dissolution rate of neat ESCAP-based photoresists in the standard tetramethylammonium hydroxide (0.26 N aqueous solution) developer is undesired. The incorporation of dissolution inhibitors has been explored to reduce the associated dark loss. MGs with acid labile groups were blended into the ESCAP resists to significantly retard the dissolution rate of the ESCAP resist and thus prevent dark loss, as elaborated by Ito and co-workers.[152] It was found that blends of an ESCAP resist (molar ratio HOST:tBA = 70:30) with

protected MGs show good contrast. Further, 40 nm imaging resolution of blends of such MGs with a ketal resist system (KRS) was demonstrated using e-beam lithography. Here we explore the behavior of an ESCAP-based resist containing a molar fraction of 20 % styrene copolymerized with HOST and tBA under EUV photolithography. Further, we explore some fundamental properties with respect to the size and architecture of the protected MGs, which provide insights into optimized MGs that would yield enhanced performance.

The MGs employed in this work show miscibility with ESCAP resist and inhibit solubility similar to the MGs used in the study by Ito and coworkers.[152] When molecular additives are incorporated into polymers, changes in its thermal properties can be expected. Where the interaction is not strong, plasticization typically occurs, which is reflected in a reduction in the T_g. This reduction in T_g typically follows the Fox equation, which states that the T_g of the blends is the weighted average of the T_g of individual components. However, with favorable interaction and additive molecules commensurate with the size of the voids in the polymer matrix, the T_g of the blend system can show positive deviations from the Fox Equation. These positive deviations are an indication of how well the additive molecule incorporates within the polymer free volume. Therefore, some MGs might serve as better physical barriers to photoacid diffusion than others. We first study this behavior of various MGs when blended with an ESCAP-based photoresist and then explore these systems in further detail for their photolithographic performance.

While both tert-butoxycarbonyl (tBOC) group and tBCM groups have been explored as the acid-labile groups on the MGs, the work by Ito and co-workers indicated

that tBCM groups cause a more favorable interaction with the hydroxystyrene segments of ESCAP resists.[152] Thus the tBCM group is expected to better promote miscibility of MGs in ESCAP resist than tBOC group. However, to reduce photoacid migration from exposed to unexposed regions, a decrease in the photoacid diffusivity in exposed regions of the film is also desired, since it is expected to reduce acid crossover to the unexposed regions. A stronger interaction between the additive and the polymer matrix after deprotection is expected to cause the formation of a stronger physical network that should be more effective in reducing the photoacid diffusivity. Therefore, the choice between tBOC and tBCM is also influenced by the strength of the interaction of the deprotected groups, namely phenols or carboxylic acids. The group that interacts more strongly with the polymer matrix is more favorable. Here we have compared the strength of the interaction between model deprotected polymer and deprotected additives to rationalize the choice of tBCM as the protecting group from the standpoint of reduced photoacid diffusion. As indicated schematically in Figure 6.4, in protected form the additives should serve as a physical barrier to photoacid diffusion, and in the exposed and deprotected region, the diffusivity should decrease further due to physical networking via hydrogen bonding.

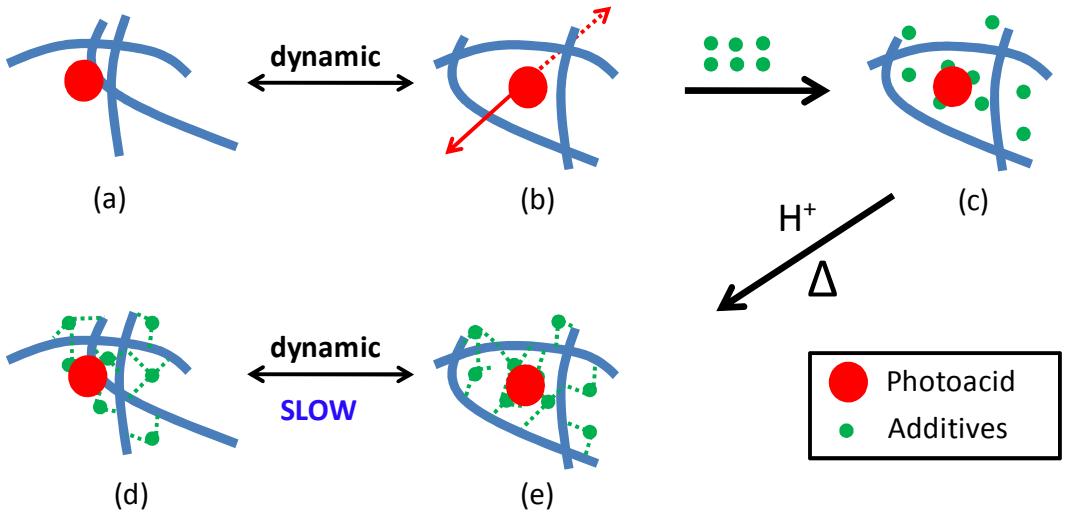

Figure 6.4. (a) and (b) depict the generation of jump volume due to segmental motion or side chain rearrangements of the photoresist polymer and the photoacid molecule diffusing through the created jump volume (shown by red arrows). (c) shows how additives can pack within the polymer matrix to obstruct the photoacid molecule, reducing its diffusivity. (d) and (e) depict the generation of strong interaction between the additive and the polymer segments due to the formation of hydrogen bonding groups on the additive upon deprotection. This strong interaction is expected to result in the formation of physical crosslinking which is expected to slow down the polymer dynamics and consequently the diffusion of photoacid.

The molecule shape and core size of the MGs that were incorporated in the ESCAP-based resist were varied to find out what structures lead to optimized performance of the photoresist blends. The structure of the MGs and the ESCAP resist used is shown in Figure 6.5. The ESCAP resist used here is different from the one used earlier by Ito and coworkers; a third co-monomer, styrene is copolymerized, at a molar fraction of 20 %, along with HOST and tBA. The styrene is expected to reduce the dissolution rate of the protected polymer in the developer. Even so, as seen later, the polymer film without MGs suffered a significant dark loss, which disappeared when MGs were incorporated at sufficient loading.

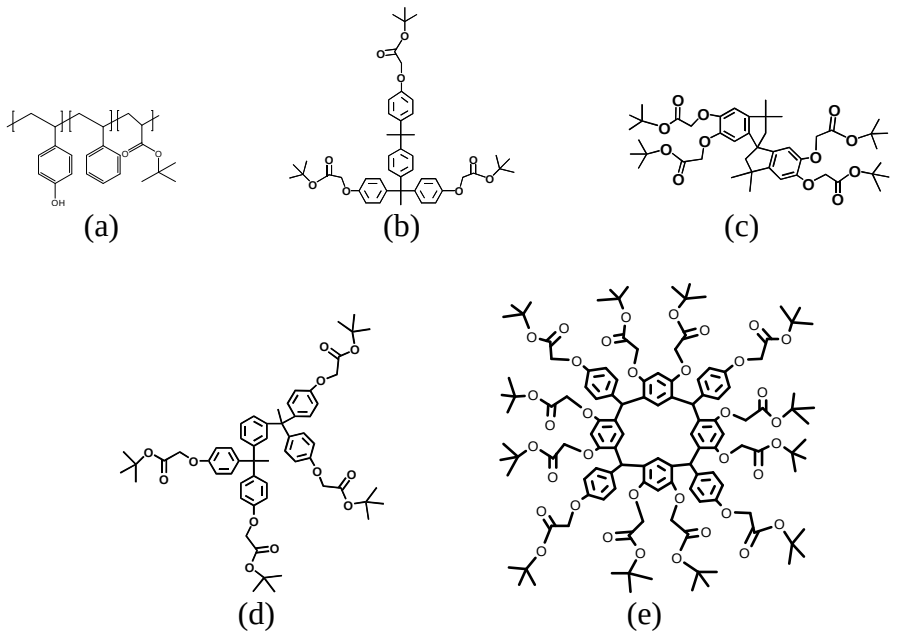

Figure 6.5. Structures of the polymer resist and the MGs employed in this work: (a) ESCAP photoresist (molar ratio of HOST:PS:tBA = 65:20:15, weight average molecular mass M_w = 10 kg/mol), (b) MG1-tBCM, (c) MG2-tBCM, (d) MG3-tBCM, (e) MG4-tBCM

6.2 Experimental

6.2.1 Materials

The ESCAP photoresist (molar ratio of HOST:PS:tBA = 65:20:15, M_w = 10 kg/mol) was provided by Electronic Materials Division of the Dow Chemical Company. The phenolic versions of the MGs MG1-tBCM and MG2-tBCM, namely MG1OH and MG2OH were purchased from TCI America and the MGs MG3OH and MG4OH were synthesized by Ying Lin at University of Massachusetts Amherst. The synthesis of these additives is described elsewhere.[154] The photoacid generators triphenylsulfonium triflate (TPST) and Iodonium Nonaflate (NonI) and the base quenchers trioctylamine (TOA)

and triethanolamine (TEA) and the solvents, propylene glycol monomethyl ether acetate (PGMEA) and ethyl acetate (EtAc) were purchased from Sigma Aldrich.

6.2.2 Description of photoresist formulations

The MGs and ESCAP resist were blended with a photoacid generator (PAG), either TPST or NonI, and a base quencher, either TOA or TEA, was added. The amounts of the PAG and base quencher were based on the total photoresist blend (i.e., ESCAP resist and the MG). For example, a mass fraction of x % TPST implies addition of 0.01x g of TPST per gram of the blend. These were dissolved in PGMEA with a mass fraction of 10 % EtAc for formulations that contained NonI PAG.

6.2.3 Description of photolithographic characterization

Photolithography was performed using the SEMATECH's EUV MET at Albany (quadrapole illumination, partial coherence = 0.4/0.68). Contrast curves and focus exposure matrix were obtained for the formulations. A post-apply bake (PAB) and post-exposure bake (PEB) of 1 min was carried out at different temperatures ranging between 70 ^{o}C and 115 ^{o}C. The imaged films were developed for 30 s using the standard tetramethylammonium hydroxide (TMAH) developer (0.26 N aqueous solution).

6.3 Results and discussion

6.3.1 Determination of functionality desired on the additive molecules

In protected form, both tBOC and tBCM groups can facilitate incorporation of MGs into ESCAP resists.[152] However, deprotected additives and deprotected polymer

should interact strongly so as to enable formation of a physical hydrogen-bonded network to slow down the diffusion of the photoacid and thus prevent its encroachment into unexposed regions during PEB.

We first explored representative model deprotected photoresist blends to determine the preferred functionality on the protected MG, i.e., tBOC or tBCM. PHOST was chosen as a model deprotected photoresist, and benzene-1,2,3,4,5,6-hexol (HHB) and benzene-1,2,3,4,5,6-hexacarboxylic acid (BHCA) were chosen as model deprotected additives. The structures of HHB and BHCA are shown in Figure 6.6. These additives at mass fractions of 15 % and 30 % in PHOST were dissolved in DMF and spin-coated on silicon wafers. X-ray reflectivity of the films obtained was performed at the Polymer Division, NIST.[10] The program Reflfit was used for the data analysis to obtain the film thicknesses and critical angles (first dip in the reflectivity profiles) by fitting the reflectivity profiles using a single film model. [11]

(a) (b)

Figure 6.6. Structure of hydrogen bonding additives incorporated in PHOST: a) benzene-1,2,3,4,5,6-hexacarboxylic acid (BHCA)and b) benzene-1,2,3,4,5,6-hexol (HHB)

The electronic density of the films, ρ_e can be determined from the critical angle θ_c by the following expressions:

$$Q_c^{\,2} = 6\pi r_0 \rho_e,$$

$$Q_c = (4\pi/\lambda)\sin\theta_c,$$

where λ is the X-ray wavelength and r_0 the classical electron radius. The mass density can be calculated by electronic density for films of known composition by using the following expression (see Appendix 6.2 for derivation):

$$\rho_e = N_A \rho_m \sum_{j=compounds} \frac{W_j}{100} \left(\frac{\sum_{i=elements} n_i Z_i}{\sum_{i=elements} n_i A_i} \right)$$

where,

j = each compound in the mixture

W_j = weight percent of j^{th} compound in the mixture

n_i = number of atoms of element i in j^{th} compound

Z_i = atomic number of the element i in j^{th} compound

A_i = atomic weight of the element i in j^{th} compound

The film thickness, critical angle, and film density changes upon incorporation of HHB and BHCA at mass fractions of 15 % and 30 % in PHOST (M_w = 20 kg/mol) are shown in Table 6.1. BHCA causes the film density to increase more than HHB, which indicates its stronger interaction with the PHOST matrix (assuming the same density of amorphous forms of HHB and BHCA). Therefore, the MGs in this study were protected with tBCM groups. For a more relevant comparison, the obtained film densities must be compared with weighted average densities obtained by using the densities of amorphous forms of HHB and BHCA and the density of PHOST. That comparison would show how much of the density change is due to interactions between the additives and PHOST. However, since HHB and BHCA are crystalline in their neat forms, their amorphous densities are not reported. Therefore, if it is assumed that the amorphous densities of HHB and BHCA are the same, the data shown in Table 6.1 indicates stronger interaction between BHCA and PHOST than between HHB and PHOST.

Table 6.1. Increase in density upon incorporation of HHB and BHCA at different mass fractions into PHOST. The error bars of the thickness t and Q_c^2 are from the Reflfit program. [11]

Sample	t (nm) (±0.1)	Q_c^2 (A^{-2}) (±5x10^{-6})	ρ_m ($g.cm^{-3}$)	% density increase
PHOST	95.1	0.000538	1.18	
PHOST 15 % HHB	78.8	0.000547	1.21	2.2
PHOST 30 % HHB	68.1	0.000549	1.22	3.0
PHOST 15 % BHCA	98.2	0.000553	1.24	4.7
PHOST 30 % BHCA	78.4	0.000558	1.24	5.2

Although, in this chapter the results with molecular glass additives is presented, preliminary studies were also conducted with various POSS based additives to identify what functionalities and what molecular architectures might be suitable for implementation of the desired strategy. Appendix 6.1 shows the results of that study which clearly indicates the role of multi-point and strong interactions between the additive and the photoresist polymer towards achieving good compatibility. Additionally, it is noted here that since POSS is an inorganic moiety, it can impart significant etch resistance to photoresist films which might be advantageous for the current demands of sub-50 nm photoresist films.

6.3.2 Glass transition temperatures (T_gs) of candidate resist systems

The process conditions of photoresists and their ultimate performance is significantly influenced by their T_g. As the temperature of the photoresist increases above the T_g, the polymer relaxation processes speed up exponentially with temperature,

which causes a corresponding exponential increase in the diffusivity of small molecules through amorphous polymers.[155] Therefore, to keep the photoacid diffusion under control, the PEB temperature is generally kept below the T_g. However, the chemical deprotection kinetics slows down at lower temperatures; therefore, photoresist films with sufficiently high T_g (higher than usual PEB temperatures) are advantageous. The retardation in the chemical deprotection kinetics sets a lower limit on the PEB temperature. Considering these factors, the use of ESCAP resist is advantageous due to its high T_g.

Figure 6.7 shows the T_gs of neat MGs and neat polymer resist and their blends with a mass fraction of 30 % MGs. The measured neat component T_gs were also used to estimate the T_gs of the blends based on the Fox equation, which provides weighted average values. This comparison indicates which shapes and sizes of additive molecules allow a more favorable packing in the polymer matrix. Among the four MG additives, the blend containing MG1-tBCM shows the maximum deviation in T_g from the Fox equation (+12.3 ^oC), indicating the most efficient packing. MG2-tBCM shows a positive deviation of 9.8 ^oC, MG3-tBCM shows a higher positive deviation of 11.2 ^oC, and MG4-tBCM shows the least deviation of 3.3 ^oC. Since the functionality of the additives is the same, it is highly likely that molecules with elongated structures cause a higher positive deviation due to efficient packing within the polymer matrix. In such cases, the additives would serve as effective physical barriers to the diffusion of other small molecules (like photoacid generator) through the polymer matrix. The EUV photolithographic performance of neat ESCAP and its blends at a mass fraction of 30 % MG1-tBCM and MG4-tBCM are shown later.

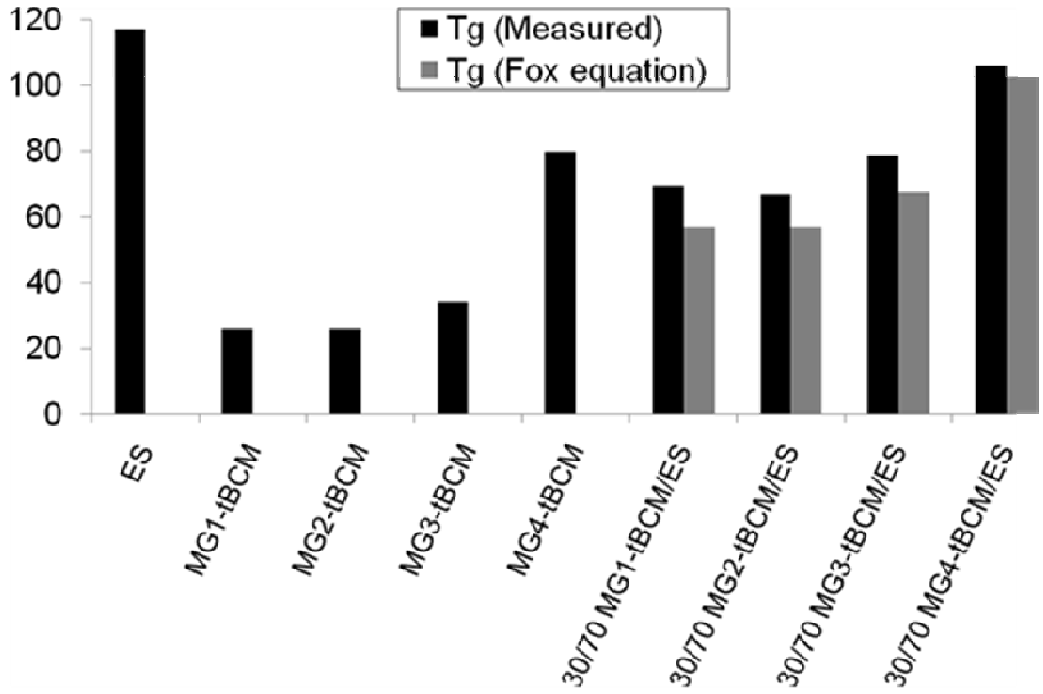

Figure 6.7. Glass transition temperatures (°C) of neat ESCAP (ES), neat molecular glasses, and their blends at a mass fraction of 30 % MGs in ESCAP. Comparison with estimates using the Fox equation is also shown for the blends. DSC thermograms were measured between -40 °C and 120 °C (at a ramp rate of 10 °C/min) and the T_g observed during the second heating cycle is reported.

6.3.3 EUV photolithographic performance

In the initial trials, TPST and TOA were chosen as the PAG and the base quencher. The performance of formulations with and without MGs was evaluated to determine a suitable composition of the MGs. Figure 6.8 shows the contrast curves obtained for ESCAP resist without any MG additive and ESCAP with MG3-tBCM and MG4-tBCM at various compositions. Each formulation contained a mass percent of 5 % TPST (except B at 4%) and 0.15 % TOA based on the blend. The contrast curve for ESCAP without any MG shows high dissolution at very small doses, which corresponds

to the dissolution of the unexposed resist. In contrast, the thickness loss at very small doses is significantly minimized with MG additives at a mass fraction of 20 %, and the loss is negligible at a mass fraction of 40 %. This finding is in agreement with the earlier finding of the dissolution inhibition effect of similar MG additives.[152]

Figure 6.8 also shows the imaging performance (at an 80 nm line/space (L/S) feature size) of these formulations to gain further insight into the changes as a result of loading the MGs. These patterns were obtained with films about 85 nm in thickness. From the scanning electron microscopy (SEM) images, it is clear that while MG4-tBCM loadings at mass fractions of 20 % and 40 % are suitable, 60 % loading results in poor imaging even though the contrast curve for 60 % loading seems to indicate good resist behavior. Likewise, MG3-tBCM loadings at mass fractions of 20 % and 40 % resulted in similarly good patterns. Therefore, for further trials, the loading of MGs was set to a mass fraction of 30 %.

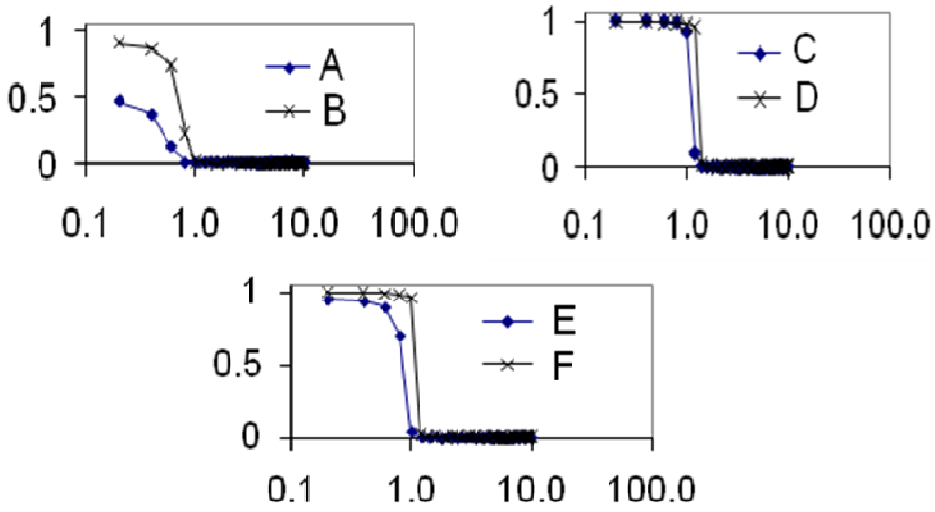

(a)

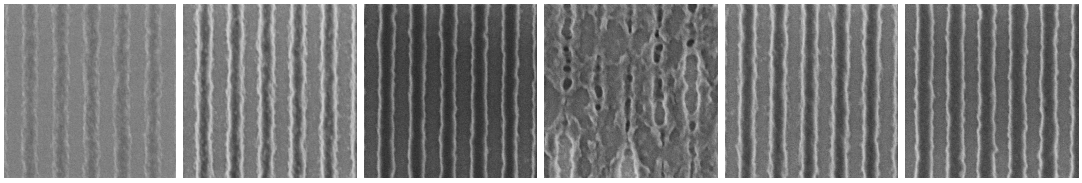

A B C D E F

(b)

Figure 6.8. a) Contrast curves (normalized thickness remaining vs. Log (dose, mJ/cm^2)) of ESCAP and its blends with MG3-tBCM and MG4-tBCM at various loadings in terms of mass ratio: A) ESCAP, B) 20/80 MG4-tBCM/ESCAP, C) 40/60 MG4-tBCM/ESCAP, D) 60/40 MG4-tBCM/ESCAP, E) 20/80 MG3-tBCM/ESCAP, F) 40/60 MG3-tBCM/ESCAP. Each formulation contained a mass percent of 5 % TPST (except B at 4%) and 0.15 % TOA based on the blend. b) SEM micrographs of patterns at 80 nm L/S obtained for the six formulations with films about 85 nm in thickness. The corresponding doses in mJ/cm^2 were A) 1.7, B) 2.2 C) 2.6, D) 3.3, E) 1.8, and F) 2.2.

Low dose requirements at TOA mass percent of just 0.15 % suggest a potential of even better resolution with higher base quencher loading. Figure 6.9 shows the result when the base quencher loading is increased by tenfold. With the formulation with a mass percent of 30 % MG1-tBCM 40 nm lines were obtained, whereas the formulation without any MG barely formed features in a 60 nm L/S patterning. This indicates that adding MGs not only inhibits solubility but also results in higher resolution probably due to a reduction in the photoacid diffusivity as we have observed in another set of experiments.[45] The sensitivity of these formulations decreased as is evident from the increased dose requirements for patterning.

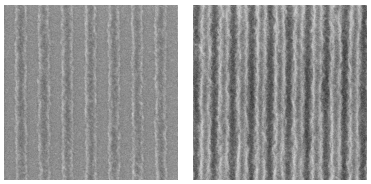

G H

Figure 6.9. SEM micrographs of patterns obtained from G) ESCAP at 60 nm L/S at a dose of 17.5 mJ/cm^2, H) 30/70 (mass ratio) MG1-tBCM/ESCAP at 40 nm L/S at a dose of 18.7 mJ/cm^2 with films of about 85 nm in thickness.

Next, the effects of changing the PAG from TPST to NonI and the base quencher from TOA to TEA are explored. NonI forms larger photoacid counterion which is known to have a slower diffusion.[156] TEA bears hydroxyl groups, therefore it can form hydrogen bonding with the resist material and thus disperses better in the photoresist film. Figure 6.10 shows the contrast curves and patterning results obtained with a mass percent of 30 % MG1-tBCM in the ESCAP resist at a fixed (and optimized) loading of NonI at a mass fraction of 8.5 %. Two TEA loadings at mass percentages of 0.63 % and 0.93 % are used. For comparison, the pattern obtained for a mass percent of 30 % MG4-tBCM in ESCAP (formulation K) is also shown. Clearly, the performance with MG1-tBCM is better than that with MG4-tBCM.

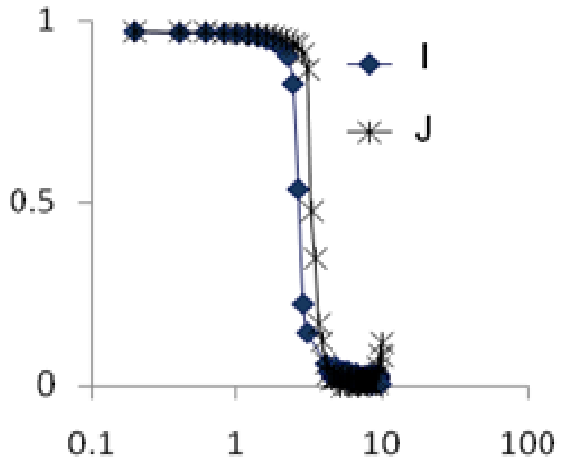

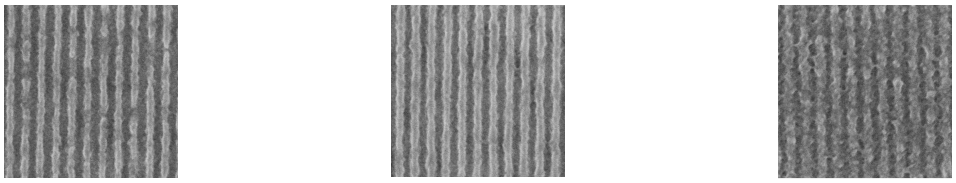

I J K

Figure 6.10. Left) Contrast curves (normalized thickness remaining vs. Log (dose, mJ/cm^2) and right) SEM micrographs of patterns obtained at 30 nm L/S: I) 30/70 (mass ratio) MG1-tBCM/ESCAP, NonI at a mass percent of 8.5 %, TEA at 0.63 %, dose = 6.6 mJ/cm^2, J) 30/70 (mass ratio) MG1-tBCM/ESCAP, NonI at a mass fraction of 8.5 %, TEA at 0.93 %, dose = 8.8 mJ/cm^2 at a film thickness of 60 nm, K) 30/70 (mass ratio) MG4-tBCM/ESCAP, NonI at a mass fraction of 8.5 %, TEA at 0.93 %, dose = 6.3 mJ/cm^2 at a film thickness of 60 nm.

Figure 6.11 shows the line widths at various focus for formulations I and J. The constant line width over a range of 500 nm depth-of-focus is sufficient to provide good processing latitude for such formulations.

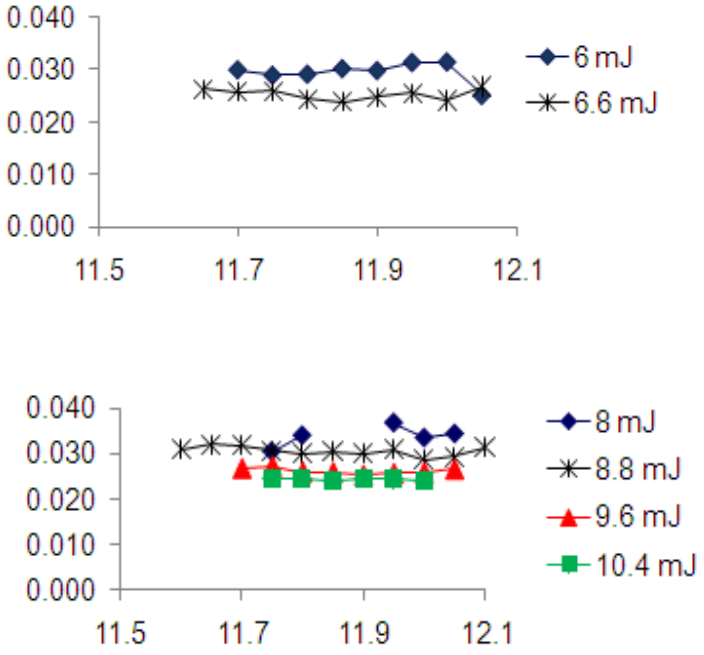

Figure 6.11. Line width (μm, y-axis) at varying focus (μm, x-axis) for formulations I (top) and J (bottom) at various doses (the doses in the legend are per cm^2 area of the photoresist film).

6.3.4 Characterization of acid diffusion length by bilayer experiments

Figure 6.12 shows the scheme for bilayer fabrication and its processing to measure the acid diffusion lengths as developed by researchers at Polymers Division at NIST.[146] For the bilayer fabrication, the photoresist through which acid diffusion length is desired to be measured is spin-coated on a silicon wafer. This is called the bottom layer. On top of this film, an acid feeder layer (top layer) containing a PAG is required. However, this layer cannot be spin-coated on top because the solvent contained in the spin coating process would dissolve the bottom film as well. Therefore, an alternate route was taken to fabricate the bilayer. The top film was coated on a PDMS (Sylgard 184) pad made on silicon wafer. For this, the Sylgard 184 resin and the crosslinker were mixed thoroughly, degassed under vacuum at room temperature and poured over hexamethyldisilazane (HMDS) treated silicon wafers that was then kept in an oven preheated to 70 ^oC for two hours to crosslink the Sylgard 184 resin. The PDMS pad (~5 mm thick) was cut around the wafer edge and peeled off from the wafer. The side of the PDMS pad that was in contact with the wafer is smooth. This side was treated with oxygen plasma which then allowed spreading of the spinning solvent on it. The top film was spin coated on the PDMS pad. The film on the PDMS pad was put down on the bottom layer and pressed carefully to remove the air in between. The wafer was then put on a hotplate at 100 ^oC and the PDMS pad was pressed for 30 seconds. The wafer was then removed and kept on a cold metal plate to let it cool following which the PDMS

pad was peeled off. The top layer sticks to the bottom layer and does not come off with the PDMS pad. Thus a bilayer is obtained on top of a silicon wafer. In this bilayer, the top layer contains a PAG and the bottom layer contains the photoresist through which acid diffusion is desired to be measured. However, the bottom layer does not contain any PAG.

These bilayers were processed by exposing them to UV light for 30 seconds to liberate the photoacid from the PAG. Then the wafers were baked at a desired PEB temperature of either 80 ^{o}C or 100 ^{o}C to cause the photoacid produced to diffuse into the bottom layer and cause the deprotection reaction as it proceeds to do so. During the baking step, the entire top film would be deprotected. In addition, the length up to which the photoacid would diffuse into the bottom layer would be deprotected. The films were then developed with the standard tetramethylammonium hydroxide solution (0. 26 N) for 30 seconds. The thickness of the initial bottom layer and the remaining bottom layer was measured using x-ray reflectivity as described before and the results obtained are shown in Table 6.2.

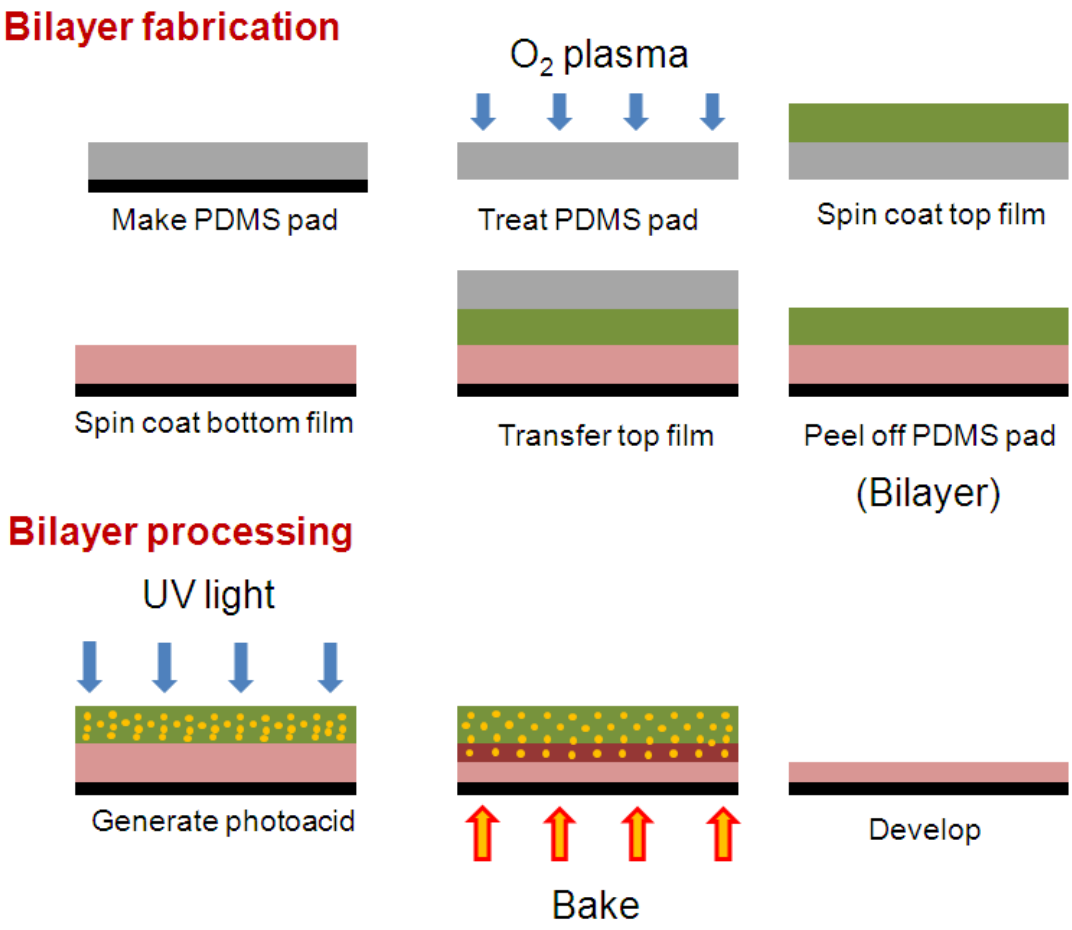

Figure 6.12. The method of bilayer fabrication and processing for estimation of acid diffusion length for various photoresist formulations

Table 6.2. Results of acid diffusion length measurements for the ESCAP resist blended with MG1-tBCM and MG4-tBCM at 30 % loading. Top layer of the bilayer film was made from ESCAP resist (ES) with 8.5 % NonI and 1 % TEA loading while the bottom layers contained 1 % TEA as well.

Samples	Thickness (nm)			
Bottom Layer	Bottom layer	Developed without exposure	After Bilayer processing at PEB = 80 °C	After Bilayer processing at PEB = 100 °C
30% MG1-tBCM in ES	122.6	122.1	118	95.5
30% MG4-tBCM in ES	124.9	124.2	95.8	87.5

From Table 6.2 a comparison of the bottom layer thickness with the thickness remaining after developing without exposure indicates that at 30 % loading, both MG1-tBCM and MG4-tBCM provide excellent solubility inhibition as there is no significant loss in film thickness upon developing without exposure. The bilayer experiments were performed at two post-exposure bake (PEB) temperatures (80 °C and 100 °C). For both MG1-tBCM and MG4-tBCM blends, as the PEB temperature increases, the remaining bottom layer thickness decreases as expected due to higher diffusivity of the photoacid at higher temperature. However, the thickness loss is greater at both temperatures for MG4-tBCM than for MG1-tBCM blends which indicates that MG1-tBCM can slow down the photoacid diffusion more than MG4-tBCM. This is in agreement with the better performance for the case of MG1-tBCM additive as seen earlier.

6.4 Conclusions

The addition of various tBCM-protected MGs to ESCAP resists were found to inhibit solubility as well as promote better imaging contrast and resolution. The structure of the MG was found to influence the thermal properties of the photoresist formulations, which in turn influences molecular packing and acid diffusion length.

MG1-tBCM showed the highest positive deviation while MG4-tBCM showed the minimum positive deviation in T_g from the Fox equation. Correspondingly, the photolithographic performance was found to be better with the MG1-tBCM-loaded ESCAP resist than with the same resist loaded with MG4-tBCM. A resolution of 25 nm to 30 nm was achieved using EUV photolithography at a dose of 8.8 mJ/cm^2 or less and depth of focus of more than 500 nm.

Appendix 6.1. Incorporation of POSS based additives in model deprotected photoresist and the possibility of a negative photoresist with high etch resistance

Two different POSS-based additives (Figure 6.13) were first evaluated for their compatibility with PHOST. Both, diol and trisilanol groups should interact via hydrogen bonding with the phenol groups of PHOST. However, as shown in Figure 6.14, these interactions were not sufficient to make these additives compatible with PHOST and phase separation of the additive from PHOST occured.

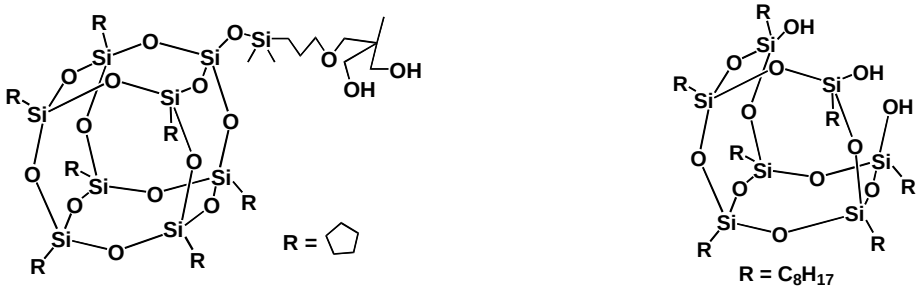

(a) **(b)**

Figure 6.13. Structures of POSS-based additives (a) diol functionalized POSS, (b) trisilanol POSS

Next, POSS cages functionalized with carboxylic acid groups, POSS octa maleamic acid (POSS-OAA) was dissolved with PHOST and spin-coated. This resulted in the formation of smooth films indicating compatibility of POSS-OAA with PHOST. As shown in Table 6.3, a systematic increase in the film density as measured by XRR indicates miscibility of POSS-OAA up to 40 % loading. This systematic increase in the density of the films indicates good compatibility of POSS-OAA with PHOST.

Therefore, as found in previous chapters, multi-point strong interactions were found to be effective in causing high loadings of the additives into homopolymers.

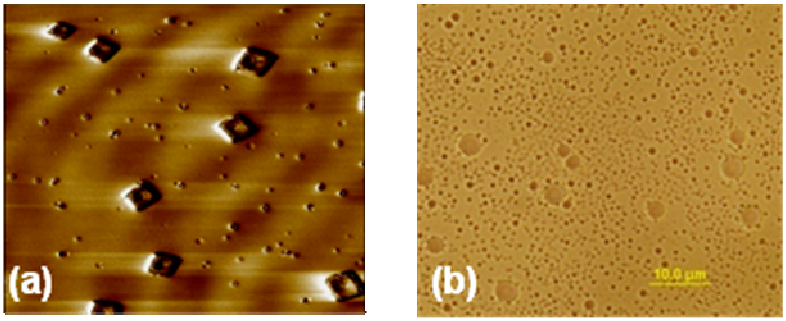

Figure 6.14. Images showing systems where POSS molecules did not interact strongly enough and therefore phase separated from PHOST (a) AFM image (10x10 micron) of diol-POSS with PHOST, (b) Optical image of trisilanol-POSS with PHOST

The compatibility of POSS-OAA with PHOST also indicates the suitability of tBCM group as the protection group on the additive because its deprotection leads to the formation of carboxylic acid groups.

Table 6.3. Density of neat PHOST and its blend with POSS-OAA obtained by reflectivity

Sample	Film thickness (nm)	ρ_m (g/cm^3)
PHOST	95	1.076
PHOST + 20 % POSS-OAA	85	1.137
PHOST + 40 % POSS-OAA	80	1.171

Phenolic groups can be used as negative photoresists in the presence of a suitable crosslinker.[136,157] Since, POSS additives contain a significant inorganic content, the miscibility of POSS-OAA into PHOST provides a means to increase the etch

resistance of negative phenolic resists. It was verified using micron scale photolithography that blends of PHOST and POSS-OAA when mixed with a crosslinker and PAG form negative resists. Here tetramethoxymethylglycouril (TMMGU) was used as a crosslinker and TPST was used as the PAG. A representative example is shown in Figure 6.15. However, the incorporation of POSS-OAA makes the polymer film too acidic and hence too soluble in the standard tetramethylammonium hydroxide solutions (0.26 N) and only weaker solutions could be employed which are currently unacceptable to industry. Therefore, this formulation was not developed any further.

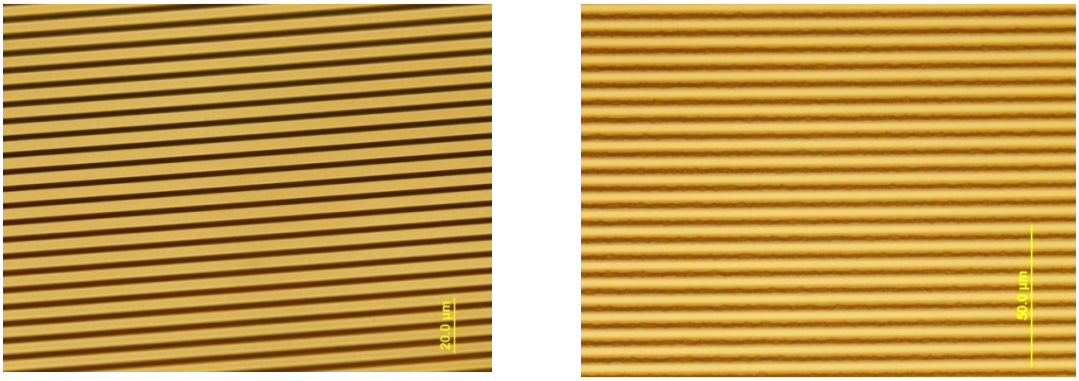

(a) (b)

Figure 6.15. Micron scale photolithography of blend of PHOST with POSS-OAA: PHOST (20 kg/mol): POSS-OAA=80:20, 20.7 % TMMGU, 10 % TPST. (a) Mask, (b) polymer film after developing in 0.1 N tetramethylammonium hydroxide solution. The exposure was carried out in a contact printing mode in which the mask was placed on the top of the photoresist film during exposure.

Appendix 6.2. Derivation of the formula to convert electronic density to mass density

The formula to convert electronic density into mass density was derived as follows. Suppose the film was made of two compounds A_xB_y and C_pD_q with a mass fraction of M % of the first compound and N % of the second compound such that M + N = 100.

If we assume there is 1 gram of the material, the volume of this 1 gram = $1/\rho_m$ (cm^3)

Moles of the two compounds in 1 gram of the mixture would be

Moles of A_xB_y = $\frac{M}{100(xA_A + yA_B)}$ (i.e. weight in grams divided by the molecular weight)

Moles of C_pD_q = $\frac{N}{100(pA_C + qA_D)}$

So the total number of electrons in 1 gram would be

Number of electrons in 1 gram of the mixture = $\frac{MN_A}{100}\frac{(xZ_A + yZ_B)}{(xA_A + yA_B)} + \frac{NN_A}{100}\frac{(pZ_C + qZ_D)}{(pA_C + qA_D)}$

Therefore, the electron density is

$$\rho_e = \frac{Number\ of\ electrons\ in\ 1\ gram}{Volume\ of\ 1\ gram} = \rho_m\left[\frac{MN_A}{100}\frac{(xZ_A + yZ_B)}{(xA_A + yA_B)} + \frac{NN_A}{100}\frac{(pZ_C + qZ_D)}{(pA_C + qA_D)}\right]$$

Or,

$$\rho_e = N_A\rho_m\left[\frac{M(xZ_A + yZ_B)}{100(xA_A + yA_B)} + \frac{N(pZ_c + qZ_D)}{100(pA_C + qA_D)}\right] \quad \text{(i.e. equation 2)}$$

Or in the generalized form:

$$\rho_e = N_A \rho_m \sum_{j=compounds} \frac{W_j}{100} \left(\frac{\sum_{i=elements} n_i Z_i}{\sum_{i=elements} n_i A_i} \right)$$

where,

j = each compound in the mixture

W_j = weight percent of j^{th} compound in the mixture

n_i = number of atoms of element i in j^{th} compound

Z_i = atomic number of the element i in j^{th} compound

A_i = atomic weight of the element i in j^{th} compound

CHAPTER 7

FINAL COMMENTS AND OUTLOOK

In this work, the design of additives that enable their high loadings in block copolymers (BCPs) and homopolymers via hydrogen bonding has been considered. Homopolymers and non-polymeric additives were incorporated at high loadings in BCPs containing poly(ethylene oxide) (PEO) as one of the blocks. Here, the PEO chain segments served as hydrogen bond acceptors while the carboxylic acid, phenol and amine groups on the additives served as hydrogen bond donating groups. In some cases, the additive contained more than one of these functional groups providing routes for phase selective reactions. The possibility of high and selective loading of additives in one of the phases of the ordered BCP composite was utilized in one case (polyhedral oligomeric silsesquioxane based additive) for the formation of a network structure between adjoining additive cores to derive mesoporous silica with its structure templated by the block copolymer. This concept of hydrogen bonding was also extended to blend different block copolymers bearing hydrogen bonding blocks. While only a few examples for each type of additives were explored, the examples presented demonstate the generality of the concept and its potential for extensions for incorporation of other kinds of additives. Additionally, the design of additives that allow high loadings via selective hydrogen bonding with one of the blocks of the block copolymers should also be applicable in general to homopolymers that could serve as hydrogen bond acceptors examples of which include PEO, poly(vinyl pyridine), and poly(hydroxystyrene).

In most of the examples, small, disordered BCPs were employed and ordering was induced upon incorporation of additives. In all these examples and in other examples of additive-driven assembly of BCPs in the literature, the additives bear functionalities that enable their selective interaction with the BCP. This selective interaction enhances the segregation strength and induces order of disordered BCPs. In this work, a new concept of duality in the nature of additives is demonstrated such that the additive can exist in two different forms, one of which is only weakly interacting with the block copolymer and is unable to induce order. Upon in situ conversion of the additive to the other form, strong and selective interactions between the additive and a block of the BCP results in ordering. This in situ conversion of the additive was caused by the presence of a strong acid that can be produced using a photoacid generator when exposed to ultra violet light. Thus, block copolymer - additive systems were formulated that can undergo a photo-induced ordering to result in the formation of nanostructures when exposed to ultraviolet light and baked moderately. Underlying this strategy is the ability to transition a weakly interacting additive to its strongly interacting form. This strategy provides an on-demand, non-intrusive route for formation of well-ordered nanostructures in arbitrarily defined regions of an otherwise disordered material. Although the concept is demonstrated to work, the choice of the BCP (Pluronic F127) was found to have its disadvantages: the interface between the ordered and disordered regions was quite broad and the disordered regions were rough due to polymer crystallization. The primary reason for the broad interface is that exposures were carried out merely by covering the one portion of the films with aluminum foils. Use of a photomask used for photolithography would result in the formation of a shaper

interface. However, the blocks of the BCP used in the present work have low glass transition temperatures and therefore are expected to allow excessive photoacid diffusion resulting in the broadening of the interface between the exposed and unexposed regions. The diffusion of the photoacid from exposed to unexposed regions could be controlled by using a BCP with PEO as the minority block and the majority block with higher glass transition temperature than PPO. Choosing PEO as the minority block would also confine the crystallization of PEO to its domains which is expected to allow a reduction in the roughness of the unexposed regions of the film. Finally, since light is used as the trigger to order the film, with these improvements, it should be possible to pattern the exposed and unexposed regions at nanoscale dimensions. These improvements are currently ongoing with an aim to develop this strategy to obtain BCP-additive systems capable of high-resolution patterning.

The concepts of hydrogen bonding between additives and the polymer backbone was also explored for developing additive-loaded photoresists for next generation extreme ultra violet (EUV) photolithography applications. Here, the strategy explored was to cause the formation of a physical network of the additives and the polymer with an aim to slow down the diffusion of photoacid leading to better photolithographic performance. This work lead to development of photoresist formulations capable of forming features with resolution as small as 25 nm.

BIBLIOGRAPHY

1. Kotsilkova, R., Fragiadakis, D., and Pissis, P., Reinforcement effect of carbon nanofillers in an epoxy resin system: Rheology, molecular dynamics, and mechanical studies. *Journal of Polymer Science Part B-Polymer Physics* **43,** 522-533 (2005).

2. Du, M. L., Guo, B. C., Liu, M. X., and Jia, D. M., Formation of reinforcing inorganic network in polymer via hydrogen bonding self-assembly process. *Polymer Journal* **39,** 208-212 (2007).

3. Rebouillat, S., Peng, J. C. M., and Donnet, J. B., Surface structure of Kevlar (R) fiber studied by atomic force microscopy and inverse gas chromatography. *Polymer* **40,** 7341-7350 (1999).

4. Jeong, U. et al., Phase behavior of mixtures of block copolymer and homopolymers in thin films and bulk. *Macromolecules* **36,** 3626-3634 (2003).

5. Bates, F. S. and Fredrickson, G. H., Block copolymers - Designer soft materials. *Physics Today* **52,** 32-38 (1999).

6. Leibler, L., Theory of Microphase Separation in Block Co-Polymers. *Macromolecules* **13,** 1602-1617 (1980).

7. Bates, F. S. and Fredrickson, G. H., Block Copolymer Thermodynamics: Theory and Experiment. *Annual Reviews Physical Chemistry* **41,** 525-557 (1990).

8. La, Y. H. et al., Pixelated chemically amplified resists: Investigation of material structure on the spatial distribution of photoacids and line edge roughness. *Journal of Vacuum Science & Technology B* **25,** 2508-2513 (2007).

9. Park, S. et al., Macroscopic 10-Terabit-per-Square- Inch Arrays from Block Copolymers with Lateral Order. *Science* **323,** 1030-1033 (2009).

10. Ruiz, R. et al., Density multiplication and improved lithography by directed block copolymer assembly. *Science* **321,** 936-939 (2008).

11. Bita, I. et al., Graphoepitaxy of self-assembled block copolymers on two-dimensional periodic patterned templates. *Science* **321,** 939-943 (2008).

12. Pai, R. A. et al., Mesoporous silicates prepared using preorganized templates in supercritical fluids. *Science* **303,** 507-510 (2004).

13. Tirumala, V. R. et al., Mesoporous silica films with long-range order prepared from strongly segregated block copolymer/homopolymer blend templates. *Chem. Mater.* **19,** 5868-5874 (2007).

14. Nagarajan, S. et al., An efficient route to mesoporous silica films with perpendicular nanochannels. *Advanced Materials* **20,** 246-+ (2008).

15. Hillmyer, M. A., in *Block Copolymers Ii* (Springer-Verlag Berlin, Berlin, 2005), Vol. 190, pp. 137-181.

16. Kang, M. and Moon, B., Synthesis of Photocleavable Poly(styrene-block-ethylene oxide) and Its Self-Assembly into Nanoporous Thin Films. *Macromolecules* **42,** 455-458 (2009).

17. Luchnikov, V. et al., Moire patterns in superimposed nanoporous thin films derived from block-copolymer assemblies. *Nano Letters* **7,** 3628-3632 (2007).

18. Misner, M. J., Skaff, H., Emrick, T., and Russell, T. P., Directed deposition of nanoparticles using diblock copolymer templates. *Advanced Materials* **15,** 221-+ (2003).

19. Sohn, B. H. and Cohen, R. E., Silver nanocluster formation within microphase-separated block copolymers. *Acta Polymerica* **47,** 340-343 (1996).

20. Barber, R. P., Gomez, R. D., Herman, W. N., and Romero, D. B., Organic photovoltaic devices based on a block copolymer/fullerene blend. *Organic Electronics* **7,** 508-513 (2006).

21. Barrau, S. et al., Self-assembling of novel fullerene-grafted donor-acceptor rod-coil block copolymers. *Macromolecules* **41,** 2701-2710 (2008).

22. Yang, C., Lee, J. K., Heeger, A. J., and Wudl, F., Well-defined donor-acceptor rod-coil diblock copolymers based on P3HT containing C-60: the morphology and role as a surfactant in bulk-heterojunction solar cells. *J. Mater. Chem.* **19,** 5416-5423 (2009).

23. Fink, Y. et al., presented at the Workshop on Electromagnetic Crystal Structures, Laguna Beach, California, 1999 (unpublished).

24. Urbas, A. et al., Tunable block copolymer/homopolymer photonic crystals. *Advanced Materials* **12,** 812-814 (2000).

25. Urbas, A., Fink, Y., and Thomas, E. L., One-dimensionally periodic dielectric reflectors from self-assembled block copolymer-homopolymer blends. *Macromolecules* **32,** 4748-4750 (1999).

26. Kim, H. C., Park, S. M., and Hinsberg, W. D., Block Copolymer Based Nanostructures: Materials, Processes, and Applications to Electronics. *Chemical Reviews* **110,** 146-177.

27. Bockstaller, M. R., Mickiewicz, R. A., and Thomas, E. L., Block copolymer nanocomposites: Perspectives for tailored functional materials. *Advanced Materials* **17,** 1331-1349 (2005).

28. Mayes, A. M. and Delacruz, M. O., Microphase separation in multiblock copolymer melts. *Journal of Chemical Physics* **91,** 7228-7235 (1989).

29. Matsen, M. W. and Thompson, R. B., Equilibrium behavior of symmetric ABA triblock copolymer melts. *Journal of Chemical Physics* **111,** 7139-7146 (1999).

30. Black, C. T., Self-aligned self assembly of multi-nanowire silicon field effect transistors. *Applied Physics Letters* **87,** (2005).

31. Black, C. T. et al., Integration of self-assembled diblock copolymers for semiconductor capacitor fabrication. *Applied Physics Letters* **79,** 409-411 (2001).

32. Black, C. T. et al., High-capacity, self-assembled metal-oxide-semiconductor decoupling capacitors. *IEEE Electron Device Lett.* **25,** 622-624 (2004).

33. Chang, L.-W. and Wong, H.-S. P., *Proc. SPIE* **6156,** (2006).

34. Li, W. K. and Yang, S., Creation of sub-20-nm contact using diblock copolymer on a 300 mm wafer for complementary metal oxide semiconductor applications. *Journal of Vacuum Science & Technology B* **25,** 1982-1984 (2007).

35. Chen, H. T. et al., Accessibility of cylindrical channels within patterned mesoporous silica films using nanoparticle diffusion. *J. Mater. Chem.* **19,** 70-74 (2009).

36. Tirumala, V. R. et al., Well ordered polymer melts from blends of disordered triblock copolymer surfactants and functional homopolymers. *Advanced Materials* **20,** 1603-+ (2008).

37. Ruzette, A. V. G., Soo, P. P., Sadoway, D. R., and Mayes, A. M., Melt-formable block copolymer electrolytes for lithium rechargeable batteries. *Journal of the Electrochemical Society* **148,** A537-A543 (2001).

38. Chen, J., Frisbie, C. D., and Bates, F. S., Lithium Perchlorate-Doped Poly(styrene-b-ethylene oxide-b-styrene) Lamellae-Forming Triblock Copolymer as High Capacitance, Smooth, Thin Film Dielectric. *Journal of Physical Chemistry C* **113,** 3903-3908 (2009).

39. Epps, T. H., Bailey, T. S., Pham, H. D., and Bates, F. S., Phase behavior of lithium perchlorate-doped poly (styrene-b-isoprene-b-ethylene oxide) triblock copolymers. *Chemistry of Materials* **14,** 1706-1714 (2002).

40. Epps, T. H., Bailey, T. S., Waletzko, R., and Bates, F. S., Phase behavior and block sequence effects in lithium perchlorate-doped poly(isoprene-b-styrene-b-ethylene oxide) and poly(styrene-b-isoprene-b-ethylene oxide) triblock copolymers. *Macromolecules* **36,** 2873-2881 (2003).

41. Hashimoto, T., Tanaka, H., and Hasegawa, H., Ordered Structure in Mixtures of a Block Copolymer and Homopolymers .2. Effects of Molecular-Weights of Homopolymers. *Macromolecules* **23,** 4378-4386 (1990).

42. Tanaka, H., Hasegawa, H., and Hashimoto, T., Ordered Structure in Mixtures of a Block Copolymer and Homopolymers .1. Solubilization of Low-Molecular-Weight Homopolymers. *Macromolecules* **24,** 240-251 (1991).

43. Lowenhaupt, B., Steurer, A., Hellmann, G. P., and Gallot, Y., Microphases and Macrophases in Polymer Blends with a Diblock Copolymer. *Macromolecules* **27,** 908-916 (1994).

44. Tirumala, V. R. et al., Well-ordered polymer melts with 5 nm lamellar domains from blends of a disordered block copolymer and a selectively associating homopolymer of low or high molar mass. *Macromolecules* **41,** 7978-7985 (2008).

45. Manuscript in preparation.

46. Kline, S. R., Reduction and analysis of SANS and USANS data using IGOR Pro. *Journal of Applied Crystallography* **39,** 895-900 (2006).

47. Zhang, F. J. and Stuhn, B., Composition fluctuation and domain spacing of low molar weight PEO-PPO-PEO triblock copolymers in the melt, during crystallization and in the solid state. *Colloid and Polymer Science* **284,** 823-833 (2006).

48. Patrick, J. et al., First observation of an ordered microphase in melts of poly(oxyethylene)-poly(oxypropylene) block copolymers. *Physical Chemistry Chemical Physics* **2,** 1503-1507 (2000).

49. Balazs, A. C., Emrick, T., and Russell, T. P., Nanoparticle polymer composites: Where two small worlds meet. *Science* **314,** 1107-1110 (2006).

50. Zhao, Y., Hashimoto, T., and Douglas, J. F., Frustrating the lamellar ordering transition of polystyrene-block-polyisoprene with a C-60 additive. *Journal of Chemical Physics* **130,** (2009).

51. van Zoelen, W. and ten Brinke, G., Thin films of complexed block copolymers. *Soft Matter* **5,** 1568-1582 (2009).

52. Bondzic, S. et al., Self-assembly of supramolecules consisting of octyl gallate hydrogen bonded to polyisoprene-block-poly(vinylpyridine) diblock copolymers. *Macromolecules* **37,** 9517-9524 (2004).

53. Tung, S. H., Kalarickal, N. C., Mays, J. W., and Xu, T., Hierarchical assemblies of block-copolymer-based supramolecules in thin films. *Macromolecules* **41,** 6453-6462 (2008).

54. van Zoelen, W. et al., Phase behavior of solvent vapor annealed thin films of PS-b-P4VP(PDP) supramolecules. *Macromolecules* **41,** 3199-3208 (2008).

55. Ruokolainen, J. et al., Switching supramolecular polymeric materials with multiple length scales. *Science* **280,** 557-560 (1998).

56. Ruokolainen, J. et al., Supramolecular routes to hierarchical structures: Comb-coil diblock copolymers organized with two length scales. *Macromolecules* **32,** 1152-1158 (1999).

57. Singh, M. et al., Effect of molecular weight on the mechanical and electrical properties of block copolymer electrolytes. *Macromolecules* **40,** 4578-4585 (2007).

58. Hawker, C. J. and Russell, T. P., Block copolymer lithography: Merging "bottom-up" with "top-down" processes. *MRS Bulletin* **30,** 952-966 (2005).

59. Sidorenko, A., Tokarev, I., Minko, S., and Stamm, M., Ordered reactive nanomembranes/nanotemplates from thin films of block copolymer supramolecular assembly. *Journal of the American Chemical Society* **125,** 12211-12216 (2003).

60. Kondyurin, A. et al., Nanostructured carbonized thin films produced by plasma immersion ion implantation of block-copolymer assemblies. *Plasma Processes and Polymers* **5,** 155-160 (2008).

61. Zschech, D. et al., Transfer of sub-30-nm patterns from templates based on supramolecular assemblies. *Macromolecules* **40,** 7752-7754 (2007).

62. Tokarev, I. et al., Microphase separation in thin films of poly(styrene-block-4-vinylpyridine) copolymer-2-(4 '-hydroxybenzeneazo)benzoic acid assembly. *Macromolecules* **38,** 507-516 (2005).

63. Daga, V. K. and Watkins, J. J., Hydrogen-Bond-Mediated Phase Behavior of Complexes of Small Molecule Additives with Poly(ethylene oxide-b-propylene oxide-b-ethylene oxide) Triblock Copolymer Surfactants. *Macromolecules* **43,** 9990-9997 (2010).

64. Warren, S. C. et al., Ordered mesoporous materials from metal nanoparticle-block copolymer self-assembly. *Science* **320,** 1748-1752 (2008).

65. Maurer, J. J., Eustace, D. J., and Ratcliffe, C. T., Thermal characterization of Poly(acrylic acid). *Macromolecules* **20,** 196-202 (1987).

66. The GaussAmp function of Origin software, $I = I_o + Ae^{-(q-q^*)^2/2w^2}$ was used to fit the primary peak to obtain *w*. Here, *I* and I_o represent the intensity along the curve and base intensity respectively and *q** represents the position of maximum *I* (i.e. peak position) and FWHM, w_1 was found as $w_1 = 2w\sqrt{\ln 4}$.

67. Lai, C. J., Russel, W. B., and Register, R. A., Scaling of domain spacing in concentrated solutions of block copolymers in selective solvents. *Macromolecules* **35,** 4044-4049 (2002).

68. The volume fraction vs. interplanar spacing (ϕ_p, *d*) data for the three additives was fitted to the equation $d=A\phi_p^{-\beta}$ to find the three β values. *A* represents the hypothetical value of *d* for neat F108 because neat F108 is disordered. However, since the value of *A* should be the same in all the three cases, *A* was not fitted but a value for it was determined such that the value of *S* - the sum of the sums of square of residuals for each data set - was minimized. Mathematically, *S* is denoted as $S = \sum_{All\ Additives} \sum_{Each\ Additive} \left(Aw_p^{-\beta} - d\right)^2$. The inner summation represents the residuals for each additive's data set (i.e. the difference between calculated and experimental values of *d*) while the outer summation represents summation of residuals obtained for data sets of each additive.

69. Hashimoto, T., Shibayama, M., and Kawai, H., Ordered structure in block polymer-solutions. 4. Scaling rules on size of fluctuations with block molecular - weight, concentration, and temperature in segregation and homogenous regimes. *Macromolecules* **16,** 1093-1101 (1983).

70. Mamodia, M., Panday, A., Gido, S. P., and Lesser, A. J., Effect of microdomain structure and process conditions on the mechanical Behavior of cylindrical block copolymer systems. *Macromolecules* **40,** 7320-7328 (2007).

71. Shibayama, M., Hashimoto, T., and Kawai, H., Ordered structure in block polymer-solutions. 1. Selective solvents. *Macromolecules* **16,** 16-28 (1983).

72. Daga, V. K. and Watkins, J. J., *Macromolecules (DOI: 10.1021/ma101694n)* (2010).

73. Boontongkong, Y. and Cohen, R. E., Cavitated block copolymer micellar thin films: Lateral arrays of open nanoreactors. *Macromolecules* **35,** 3647-3652 (2002).

74. Cummins, C. C., Schrock, R. R., and Cohen, R. E., Synthesis of ZNS and CDS within ROMP block copolymer microdomains. *Chemistry of Materials* **4,** 27-30 (1992).

75. Joly, S. et al., Multilayer nanoreactors for metallic and semiconducting particles. *Langmuir* **16,** 1354-1359 (2000).

76. Saito, R., Okamura, S., and Ishizu, K., Introduction of colloidal silver into a poly(2-vinyl pyridine) microdomain of microphase separated poly(styrene-b-2-vinyl pyridine) film. *Polymer* **33,** 1099-1101 (1992).

77. Sohn, B. H. and Seo, B. H., Fabrication of the multilayered nanostructure of alternating polymers and gold nanoparticles with thin films of self-assembling diblock copolymers. *Chemistry of Materials* **13,** 1752-1757 (2001).

78. Hirai, T. et al., One-Step Direct-Patterning Template Utilizing Self-Assembly of POSS-Containing Block Copolymers. *Advanced Materials* **21,** 4334-+ (2009).

79. Chandler, C. M. et al., *On incorporation of molecular glasses in Pluronic BCPs (submitted)* (2011).

80. Park, S. C. et al., Controlled ordering of block copolymer thin films by the addition of hydrophilic nanoparticles. *Macromolecules* **40,** 8119-8124 (2007).

81. Jeong, U. et al., Enhancement in the orientation of the microdomain in block copolymer thin films upon the addition of homopolymer. *Advanced Materials* **16,** 533-+ (2004).

82. Lin, Y. et al., Self-directed self-assembly of nanoparticle/copolymer mixtures. *Nature* **434,** 55-59 (2005).

83. Wang, J. Y., Chen, W., Sievert, J. D., and Russell, T. P., Lamellae orientation in block copolymer films with ionic complexes. *Langmuir* **24,** 3545-3550 (2008).

84. Moon, J. H., Seo, J. S., Xu, Y. G., and Yang, S., Direct fabrication of 3D silica-like microstructures from epoxy-functionalized polyhedral oligomeric silsesquioxane (POSS). *J. Mater. Chem.* **19,** 4687-4691 (2009).

85. Lynd, N. A., Meuler, A. J., and Hillmyer, M. A., Polydispersity and block copolymer self-assembly. *Progress in Polymer Science* **33,** 875-893 (2008).

86. By neutron scattering, we have found this to be the case for PEO-PPO-PEO triblock copolymers blended with poly(acrylic acid) in which just next to the PPO domains, there is a thin PEO layer that contains smaller amount of PAA than the rest of the PEO domain, (shown in Chapter 2)

87. Mihailov, M., Bogdanov, B., and Davarska, G., X-ray-diffraction analysis of high molecular weight poly(ethylene oxide) films moulded at different temperatures. *Acta Polymerica* **36,** 481-483 (1985).

88. Fina, A. et al., Polyhedral oligomeric silsesquioxanes (POSS) thermal degradation. *Thermochimica Acta* **440,** 36-42 (2006).

89. Mabry, J. M., Vij, A., Iacono, S. T., and Viers, B. D., Fluorinated polyhedral oligomeric silsesquioxanes (F-POSS). *Angewandte Chemie-International Edition* **47,** 4137-4140 (2008).

90. Mehta, N. B., Phillips, A. P., Lui, F. F., and Brooks, R. E., Maleamic and citraconamic acids, methyl esters, and imides. *Journal of Organic Chemistry* **25,** 1012-1015 (1960).

91. Coleman, L. E., Bork, J. F., and Dunn, H., Reaction of primary aliphatic amines with maleic anhydride. *Journal of Organic Chemistry* **24,** 135-136 (1959).

92. Hanes, J., Chiba, M., and Langer, R., Synthesis and characterization of degradable anhydride-co-imide terpolymers containing trimellitylimido-L-tyrosine: Novel polymers for drug delivery. *Macromolecules* **29,** 5279-5287 (1996).

93. Vasquez-A, M. A. et al., FTIR and photoluminescence studies of porous silicon layers oxidized in controlled water vapor conditions. *Revista Mexicana De Fisica* **53,** 431-435 (2007).

94. Silverstein, R. M., Webster, F. X., and Kiemle, D. J., *Spectrometric identification of organic compounds*. (John Wiley & Sons, Inc., 2005).

95. Kumar, B. and Rodrigues, S. J., Poly(ethylene oxide)-based composite electrolytes crystalline reversible arrow amorphous transition. *Journal of the Electrochemical Society* **148,** A1336-A1340 (2001).

96. Kumar, B., Rodrigues, S. J., and Koka, S., The crystalline to amorphous transition in PEO-based composite electrolytes: role of lithium salts. *Electrochimica Acta* **47,** 4125-4131 (2002).

97. Kumar, B., Rodrigues, S. J., and Scanlon, L. G., Ionic conductivity of polymer-ceramic composites. *Journal of the Electrochemical Society* **148,** A1191-A1195 (2001).

98. Nookala, M., Kumar, B., and Rodrigues, S., Ionic conductivity and ambient temperature Li electrode reaction in composite polymer electrolytes containing nanosize alumina. *Journal of Power Sources* **111,** 165-172 (2002).

99. Gomez, E. D. et al., Effect of Ion Distribution on Conductivity of Block Copolymer Electrolytes. *Nano Letters* **9,** 1212-1216 (2009).

100. Panday, A. et al., Effect of Molecular Weight and Salt Concentration on Conductivity of Block Copolymer Electrolytes. *Macromolecules* **42,** 4632-4637 (2009).

101. Asari, T., Matsuo, S., Takano, A., and Matsushita, Y., Three-phase hierarchical structures from AB/CD diblock copolymer blends with complemental hydrogen bonding interaction. *Macromolecules* **38,** 8811-8815 (2005).

102. Tang, C. B. et al., Evolution of block copolymer lithography to highly ordered square arrays. *Science* **322,** 429-432 (2008).

103. Albert, J. N. L. and Epps, T. H., Self-assembly of block copolymer thin films. *Mater. Today* **13,** 24-33.

104. Marencic, A. P. and Register, R. A., in *Annual Review of Chemical and Biomolecular Engineering, Vol 1* (2010), Vol. 1, pp. 277-297.

105. Stoykovich, M. P. et al., Directed assembly of block copolymer blends into nonregular device-oriented structures. *Science* **308,** 1442-1446 (2005).

106. Park, S. M. et al., Combinatorial generation and replication-directed assembly of complex and varied geometries with thin films of diblock copolymers. *Langmuir* **23,** 9037-9045 (2007).

107. Park, S. et al., Macroscopic 10-terabit-per-square-inch arrays from block copolymers with lateral order. *Science* **323,** 1030-1033 (2009).

108. Kim, S. H. et al., Highly oriented and ordered arrays from block copolymers via solvent evaporation. *Adv. Mater.* **16,** 226-231 (2004).

109. Kim, G. and Libera, M., Morphological development in solvent-cast polystyrene-polybutadiene-polystyrene (SBS) triblock copolymer thin films. *Macromolecules* **31,** 2569-2577 (1998).

110. Kimura, M. et al., Long-range ordering of diblock copolymers induced by droplet pinning. *Langmuir* **19,** 9910-9913 (2003).

111. Park, S. et al., Lateral ordering of cylindrical microdomains under solvent vapor. *Macromolecules* **42,** 1278-1284 (2009).

112. Han, E. et al., Effect of composition of substrate-modifying random copolymers on the orientation of symmetric and asymmetric diblock copolymer domains. *Macromolecules* **41,** 9090-9097 (2008).

113. Morkved, T. L. et al., Local control of microdomain orientation in diblock copolymer thin films with electric fields. *Science* **273,** 931-933 (1996).

114. Park, M. et al., Block copolymer lithography: Periodic arrays of similar to 10(11) holes in 1 square centimeter. *Science* **276,** 1401-1404 (1997).

115. Stoykovich, M. P. and Nealey, P. F., Block copolymers and conventional lithography. *Mater. Today* **9,** 20-29 (2006).

116. Harrison, C. et al., Lithography with a mask of block copolymer microstructures. *J. Vac. Sci. Technol., B* **16,** 544-552 (1998).

117. Jung, Y. S., Jung, W., Tuller, H. L., and Ross, C. A., Nanowire conductive polymer gas sensor patterned using self-assembled block copolymer lithography. *Nano Lett.* **8,** 3776-3780 (2008).

118. Cheng, J. Y. et al., Formation of a cobalt magnetic dot array via block copolymer lithography. *Adv. Mater.* **13,** 1174-1178 (2001).

119. Nagarajan, S. et al., An efficient route to mesoporous silica films with perpendicular nanochannels. *Adv. Mater.* **20,** 246-251 (2008).

120. Jackson, E. A. and Hillmyer, M. A., Nanoporous Membranes Derived from Block Copolymers: From Drug Delivery to Water Filtration. *Acs Nano* **4,** 3548-3553 (2010).

121. Cui, Y., Wei, Q. Q., Park, H. K., and Lieber, C. M., Nanowire nanosensors for highly sensitive and selective detection of biological and chemical species. *Science* **293,** 1289-1292 (2001).

122. Timko, B. P. et al., Design and Implementation of Functional Nanoelectronic Interfaces With Biomolecules, Cells, and Tissue Using Nanowire Device Arrays. *Ieee Transactions on Nanotechnology* **9,** 269-280.

123. Aydin, D. et al., Polymeric Substrates with Tunable Elasticity and Nanoscopically Controlled Biomolecule Presentation. *Langmuir* **26,** 15472-15480.

124. Daga, V. K. et al., Photoinduced Ordering of Block Copolymers. *Nano Lett.* **11,** 1153-1160.

125. Tirumala, V. R. et al., Well ordered polymer melts from blends of disordered triblock copolymer surfactants and functional homopolymers. *Adv. Mater.* **20,** 1603-1608 (2008).

126. Iimori, H., Shibasaki, Y., Ueda, M., and Ishii, H., A new positive-working alkaline developable photoresist based on partially O-tert-

butoxycarbonylmethylated-tetra-C-methylcalix[4]resorcinarene and a photoacid generator. *J. Photopolym. Sci. Technol.* **16,** 685-689 (2003).

127. Rosenhauer, R. et al., Light-induced orientation of liquid crystalline terpolymers containing azobenzene and dye moieties. *Macromolecules* **38,** 2213-2222 (2005).

128. Yu, H. F., Iyoda, T., and Ikeda, T., Photoinduced alignment of nanocylinders by supramolecular cooperative motions. *Journal of the American Chemical Society* **128,** 11010-11011 (2006).

129. Morikawa, Y., Kondo, T., Nagano, S., and Seki, T., Photoinduced 3D ordering and patterning of microphase-separated nanostructure in polystyrene-based block copolymer. *Chem. Mater.* **19,** 1540-1542 (2007).

130. Morikawa, Y. et al., Optical alignment and patterning of nanoscale microdomains in a block copolymer thin film. *Adv. Mater.* **18,** 883-886 (2006).

131. Tran-Cong-Miyata, Q. et al., Controlling the morphology of polymer blends using periodic irradiation. *Nat. Mater.* **3,** 448-451 (2004).

132. Schumers, J. M., Fustin, C. A., and Gohy, J. F., Light-Responsive Block Copolymers. *Macromol. Rapid Commun.* **31,** 1588-1607.

133. Zheng, P. J. et al., Photoregulated sol-gel transition of novel azobenzene-functionalized hydroxypropyl methylcellulose and its alpha-cyclodextrin complexes. *Macromol. Rapid Commun.* **25,** 678-682 (2004).

134. Zhao, Y. et al., Small-molecule-directed nanoparticle assembly towards stimuli-responsive nanocomposites. *Nat. Mater.* **8,** 979-985 (2009).

135. Huang, C. F. et al., Synthesis of Photoisomerizable Block Copolymers by Atom Transfer Radical Polymerization. *Macromolecular Chemistry and Physics* **210,** 1484-1492 (2009).

136. Dai, J. Y. et al., Molecular glass resists for high-resolution patterning. *Chem. Mater.* **18,** 3404-3411 (2006).

137. De Silva, A., Felix, N. M., and Ober, C. K., Molecular glass resists as high-resolution patterning materials. *Adv. Mater.* **20,** 3355-3361 (2008).

138. Innocenzi, P., Malfatti, L., Piccinini, M., and Marcelli, A., Evaporation-induced crystallization of pluronic F127 studied in situ by time-resolved infrared spectroscopy. *J. Phys. Chem. A* **114,** 304-308 (2010).

139. Chandler, C. M. et al., Sub-10 nm Self-Assembly of Molecular Glass Photoresists Using Commodity, Non-Ionic Block Copolymer Surfactants. *submitted to Chem. of Mater*. (2010).

140. Moon, J. H., Ford, J., and Yang, S., Fabricating three-dimensional polymeric photonic structures by multi-beam interference lithography. *Polym. Adv. Technol.* **17,** 83-93 (2006).

141. Jang, J. H. et al., 3D micro- and nanostructures via interference lithography. *Adv. Funct. Mater.* **17,** 3027-3041 (2007).

142. Tompkins, H. and McGahan, W., *Spectroscopic Ellipsometry and Reflectometry: A User's Guide*. (Wiley, New York, 1999).

143. Wallraff, G. M. and Hinsberg, W. D., Lithographic imaging techniques for the formation of nanoscopic features. *Chemical Reviews* **99,** 1801-1821 (1999).

144. Fedynyshyn, T. H., Thackeray, J. W., Georger, J. H., and Denison, M. D., Effect of acid diffusion on performance in positive deep ultravoilet resists. *Journal of Vacuum Science & Technology B* **12,** 3888-3894 (1994).

145. Richter, E., Hien, S., and Sebald, M., Acid diffusion analysis in the chemically amplified CARL resist. *Microelectronic Engineering* **53,** 479-483 (2000).

146. Lin, E. K. et al., Direct measurement of the reaction front in chemically amplified photoresists. *Science* **297,** 372-375 (2002).

147. Gonsalves, K. E., Merhari, L., Wu, H. P., and Hu, Y. Q., Organic-inorganic nanocomposites: Unique resists for nanolithography. *Advanced Materials* **13,** 703-714 (2001).

148. Merhari, L. et al., Nanocomposite resist systems for next generation lithography. *Microelectronic Engineering* **63,** 391-403 (2002).

149. Wu, H. P., Hu, Y. Q., Gonsalves, K. E., and Yacaman, M. J., Incorporation of polyhedral oligosilsesquioxane in chemically amplified resists to improve their reactive ion etching resistance. *Journal of Vacuum Science & Technology B* **19,** 851-855 (2001).

150. Tegou, E., Bellas, V., Gogolides, E., and Argitis, P., Polyhedral oligomeric silsesquioxane (POSS) acrylate copolymers for microfabrication: properties and formulation of resist materials. *Microelectronic Engineering* **73-74,** 238-243 (2004).

151. Tegou, E. et al., Polyhedral oligomeric silsesquioxane (POSS) based resists: Material design challenges and lithographic evaluation at 157 nm. *Chemistry of Materials* **16,** 2567-2577 (2004).

152. Ito, H. et al., Characterization and lithographic application of calix[4]resorcinarene derivatives. *Chemistry of Materials* **20,** 341-356 (2008).

153. Ito, H., in *Microlithography - Molecular Imprinting* (2005), Vol. 172, pp. 37-245.

154. Daga, V. K. et al., Additive-loaded EUV photoresists: performance enhancement and the underlying physics. *SPIE Digital Library and SPIE Proceedings*, Extreme Ultraviolet (EUV) Lithography II, (2011).

155. Vrentas, J. S. and Duda, J. L., Diffusion of small molecules in amorphous polymers. *Macromolecules* **9,** 785-790 (1976).

156. Vogt, B. D. et al., Measurements of the reaction-diffusion front of model chemically amplified photoresists with varying photoacid size. *Macromolecules* **39,** 8311-8317 (2006).

157. De Silva, A. et al., Study of the structure-properties relationship of phenolic molecular glass resists for next generation photolithography. *Chemistry of Materials* **20,** 1606-1613 (2008).